Licentiate Thesis

Single molecule studies of DNA in fluidic systems

Department of Physics, Faculty of Engineering, Lund University
SE-221 00 Lund, Sweden

LUND
UNIVERSITY

Author:
Camilla Freitag

Supervisors:
Jonas Tegenfeldt
Annette Granéli

May 17, 2013

Abstract

Mutations in the DNA sequence are associated with many severe diseases (such as Schizophrenia, Duchenne muscular disease and Huntington chorea), raising the need to develop cheap, fast and reliable methods to decode a DNA sequence. In addition, DNA interacting proteins are responsible for replication, gene expression and regulation, genome rearrangements as well as DNA repair. Understanding these interactions are therefore highly important to fully understand the complexity of biological organisms as well as identifying epigenetic disorders.

The uniform stretching of DNA molecules confined in nano-channels have been utilized to achieve high-resolution mapping patterns or barcodes along single DNA molecules. Melting mapping have become popular to obtain a barcode pattern. However, this approach still possesses problems with reproducibility. Something that is a prerequisite for identification of bacteria and microorganisms with melting mapping. Furthermore, the large size of whole chromosomes makes them difficult to image efficiently with the linear channel designs used today, which limits the biological relevance of this technique.

DNA arrays within micro-channels gives a high throughput and can be used to study DNA-protein interactions and DNA behavior. However, todays channel designs only allows for investigations with a single buffer condition for each experiment.

Within the scope of this work the reproducibility of melting mapping was increased by optimizing the DNA molecules occupation time in the nano-channel system and thereby their time at a higher temperature. We show that the melting pattern develops during the first 10 min at a raised temperature, after which an equilibrium state is reached. The efficiency for imaging whole chromosomes was increased by folding the nano-channels into a meandering pattern that enabled DNA molecules in the Mbp range to be imaged within a single field of view. As a proof of principle we show an entire chromosome (5.7 Mbp) from *S.pombe* imaged within a single field of view. A barcode pattern was experimentally created along the elongated chromosomes and used to identify repetitive parts along the DNA chains.

In addition, we have combined Y-shaped micro-channels and DNA arrays to create a versatile tool able to detect concentration thresholds with the help of a concentration gradient along the width of the measurement channel. As a proof of principle our tool was here used to probe the concentration dependent binding behavior of Rad51 to DNA. At the concentrations used in this study no positive cooperative binding could be detected.

Keywords: DNA, mapping, melting, fluorescent imaging, microfluidics, nanofluidics, Rad51, DNA array

Appended Papers

Paper I:

Mapping of intact chromosomes in meandering nano-channels
C. Freitag, J. Fritzsche, F. Persson, T. Ambjörnsson, C. Noble, M. Reiter-Schad, K. U. Mir, A.Granéli and J. O. Tegenfeldt.
Manuscript

Paper II:

Time dependence of DNA melting mapping
C. Freitag, J. Fritzsche, F.Persson, T. Ambjörnsson, C. Noble, M. Reiter-Schad, K. U. Mir, A.Granéli and J. O. Tegenfeldt
Manuscript

Paper III:

Probing concentration-dependent behavior of DNA-binding proteins on a single molecule level illustrated by repair protein Rad51
K. Frykholm, **C. Freitag**, F. Persson, J. O. Tegenfeldt and A. Granéli
Manuscript

My contribution to the appended papers

Paper I: I performed all the experiments and was involved in the chip production and planning. The theoretical matching was performed by Tobias Ambjörnsson, Charleston Noble and Michaela Reiter-Schad. I was involved in the writing process together with my co-authors.

Paper II: I performed all the experiments and was involved in the planning and analysis. The theoretical matching was performed by Tobias Ambjörnsson, Charleston Noble and Michaela Reiter-Schad. I was involved in the writing process together with my co-authors.

Paper III: I performed the theoretical calculations of the concentration profile and helped with the experiments.

Contents

Acknowledgments

First, I would like to thank my main supervisor Jonas Tegenfeldt for giving me the opportunity to work with this alluring project in the borderline between physics, chemistry and biology. A very special thanks goes to my other supervisor Annette Graneli for taking me under her wings when I needed it the most. Without her help and support this thesis would most likely not have been completed. Fredrik Persson deserves a big thanks for all the practical help in the lab as well as the support and friendship during the first years of my time as a PhD student. Also, I would very much like to thank Joachim Fritzsche for manufacturing the fused silica chips for my meander experiments, but even more for the encouragement and friendship he has given me that I hope will last for many years ahead. Furthermore, I am thankful to my former group members Erik, Katarina and Fredrik for all the fruitful discussions about everything from science to ice-cream and for providing an interesting working environment. In addition, I would like to show my gratitude to Karolin Frykholm for showing me a new world of PDMS, microfluidics, lipids and proteins during my transfer into a new filed.

I would like to thank every one at level 8 physics for the many fascinating conversations during lunch and "fika". Special thanks to Jan-Åke for the many great lunches we have shared and to Johan for being a good friend and for helping me with the photos for this thesis.

I am also very grateful for all the support I have received from my friends outside work. Here I would especially like to thank Emma and Oskar for all "therapy sessions" and for providing most needed sanctuaries where work could be forgotten and my energy levels refilled.

Last but not least I would like to send my thoughts of gratitude to my family for everything they have done and all the love we have shared. Within my family Björn deserves a special thank you for always being there to take care and listen to me when I needed it and for all practical help he has provided for my work.

Nomenclature

AFM	Atomic force microscopy
BME	β - mercaptoethanol
DNA	Deoxyribonucleic acid
dsDNA	Double-stranded DNA
FISH	Fluorescence in situ hybridization
FRAP	Fluorescence recovery after photobleaching
LOC	Lab-on-a-chip
PCR	Polymerase chain reaction
PDMS	Polydimethylsiloxane
SLB	Supported phospholipid bilayers
SNP	Single-nucleotide polymorphism
ssDNA	Single-stranded DNA
TBE	Tris-Borate-EDTA

1 Introduction

In his famous talk "*There's Plenty of Room at the Bottom*" on December 29 1959, Richard Feynman was the first to introduce the idea of using nanotechnology for studies in biophysics. Biophysics refers to the interdisciplinary science that combines physics and biology [1]. Within biophysics often instruments developed within the physics community are used to gain a better understanding of the physical principles of biological systems. Commonly used instruments within the field of biophysics can be divided into the two areas of manipulation and imaging. Instruments used for imaging are for example x-ray crystallography, nuclear magnetic resonance (NMR) spectroscopy, electron microscopy and fluorescent imaging techniques (such as total internal reflection fluorescence microscopy (TIRFM), fluorescence resonance energy transfer (FRET), confocal microscopy and epi-fluorescence). In the area of manipulating biological samples atomic force microscopy (AFM), optical and magnetic tweezers and micro- and nano-fluidics are popular. With the help of those instruments the permeability of skin, physical properties of cells and cell membranes, interactions between cells and bio molecules as well as the behavior of single biomolecules have been studied.

Nanotechnology is named after the prefix "nano" that means one billionth and describes the field where objects in the size range of one-billionth meter are manipulated to create useful devices. With a range of inventions including faster-burning rocket fuel additives, new cancer treatments, biosensors, new drug delivery systems, neuro-electronic interfaces and electrical components used in for example smart phones nanotechnology has exploded during the last decade [2]. Furthermore, through the development of new techniques, nanotechnology have opened the doors for new ways to study single cells or biomolecules.

Single cell or molecule studies eliminates the sample averaging that is inherent in all bulk-phase biochemical assays. Since every cell or molecule is individually investigated rare subpopulations, variations in genotype or molecular states can be identified [3, 4]. In addition, single molecule studies are ideal for investigating the activity, dynamics and response to environmental changes of systems that can not be synchronized, such as molecular motors walking around within a cell [4].

The field of single molecule studies can roughly be divided into fluorescence microscopy and force spectroscopy. Force spectroscopy is based on measuring the response to an applied force. The force is usually created by pulling at one or both ends of the biomolecule with the help of for example optical traps, magnetic traps or AFM. These

methods can for example be used to detect the response of a DNA (deoxyribonucleic acid) molecule to changes in its surrounding environment or binding of a protein in real time. Fluorescence imaging has the ability to continuously visualize and record dynamic processes and has for example been used to directly follow the binding dynamics of DNA binding proteins and the movement of membrane proteins within the lipid membrane on a single molecule level.

The ability to study the behavior of single biomolecules in real time makes it possible to detect reaction intermediates that are too short-lived to be detected in an ensemble of asynchronous reactions [3]. Furthermore, fluorescence imaging opens up for the possibility to investigate how the concentration affects the dynamics or behavior of a biomolecule.

Since the 1940s when it was realized that DNA carries the heredity information it has been intensely studied. However, it was not until 1953 when James Watson, Francis Crick, Maurice Wilkins and Rosalind Franklin discovered the structure of DNA that the mystery about how this information was stored and transferred to the next generation could be solved [5]. Understanding of the structure also provided some clues about how DNA could encode the information for making proteins [6]. This discovery had a huge impact on medicine and lead to a nobel price for James Watson, Francis Crick and Maurice Wilkins in 1962. Today we know that an error in the genetic code can lead to severe diseases (such as schizophrenia, mental retardation [7], Duchenne muscular disease and Huntington chorea) or in worst cases death. Therefore huge efforts have been put into understanding the behavior of the DNA molecule as well as develop methods to decode its information. Furthermore, an insight into the human genome sequence allows for a better understanding of our heredity and opens up for personalized medicine. Sequencing the human genome was considered so essential that in 1989 a publicly founded consortium started a project called the Human Genome Project (HGP) [8]. Included in the aim of this project was to determine the sequence of the complete human genome, identify the approximately 20,000-25,000 genes within the human genome as well as store this information in databases and improve the tools used for data analysis [9]. During this project a mixture of DNA from a number of anonymous donors was used, although later the genome from a single individual has also been sequenced [10].

Proteins are the worker molecules within the cells and are involved in most biological functions. One category of proteins interact with the DNA chain and are responsible for DNA replication, gene expression and regulation, genome rearrangements as well as DNA repair. Studying protein DNA interactions underlying these processes is therefore alluring both from the biological and biophysical point of view. A better understanding of these interactions can potentially be used to identify and cure epigenetic disorders.

Lab-On-a-Chip (LOC) systems have lately become popular within biophysics community. A LOC system is a device that contains one or more laboratory functions on a single chip. Within the LOC systems a sub field of handling single biomolecules (and especially DNA) in micro- and nano-channels have emerged.

Nano-channels have been used for polymer physics [11–14], to study the binding of the lac repressor to DNA [15] and to study the effect of dextran nano-particles on single DNA molecules [16]. The high interest for using nano-channels to study single DNA molecules arises form the uniform stretching that scales linearly with the contour length of the elongated molecules [11] as well as the possibility to a high throughput by using a design

including a tight array of nano-channels. The uniform stretching provides a correlation between features spatial position along the polymer and their position within the genome. Recently nano-channels was utilized to achieve high-resolution mapping patterns (or barcodes) along DNA molecules [17–21]. The experimentally produced barcodes can be matched to theoretically calculated barcodes, which opens the doors for this method to be used for identification of different organisms and large genomic rearrangements. Among the various mapping techniques the method based on local melting of DNA molecules stained with a dye that only fluoresces when bound to dsDNA has become a popular (i.e melting mapping). This way of creating a mapping pattern along a DNA molecule shows large potential due to its relative simplicity and lack of inherent benefit from prior knowledge of the sequence to be investigated, which accompanies many other mapping methods. However, it still possesses problems with reproducibility, an obstacle that needs to be overcome before it can be made commercially available.

Although, nano-channel systems exhibit a large potential the channel design used today suffers from one mayor drawback, namely the limitation in the size of a DNA chains that can be imaged within a field of view during fluorescence imaging. Only relatively short (in the kbp range) DNA strands can be easily imaged with the straight channel design used today. Since most genome sizes are in the Mbp range, the short imaging sizes limits the usefulness for biologically relevant problems.

Areas of use for micro-channels includes cell sorting [22], DNA mapping [23], electrophoretic separation of DNA molecules [24] as well as separation and accumulation of membrane bound proteins [25]. Furthermore, the laminar flow within a micro-channel have been utilized to align and elongate hundreds of DNA molecules within a field of view [26]. Thereby the throughput is increased compared to many other single DNA molecule methods. Its usefulness has been shown through investigations of protein-DNA interactions as well as measurements of the physical properties of DNA molecules in different surroundings [27–29]. However, this technique suffers from a major drawback, namely that todays channel designs only allows for investigations with a single buffer condition for each experiment.

In this work micro- and nano-channels were used to manipulate single DNA molecules which were imaged with fluorescence microscopy. The work had three main focuses. First, increasing the length of DNA molecules manipulated and imaged in a system of micro- and nano-channels. The nano-channels used to elongate the DNA molecules were folded into a meandering pattern in order to reduce the number of frames needed to image large genomes. DNA molecules in the Mbp range were with ease imaged within a single filed of view with this new design. We have thereby increased the biological relevance for DNA molecules elongated and visualized inside nano-channels. We showed the clinical and biological relevance by creating a barcode along the elongated molecules. The barcode can be used to locate repetitive regions along the chromosome, or identify large genomic rearrangements.

The second focus was to optimize melting mapping. As a step towards commercialization the time spent by the DNA molecule in confinement and thereby at a raised temperature was optimized.

Thirdly, we integrated DNA-arrays into Y-shaped micro-channels to create a versatile tool for high throughput single molecule studies of DNA behavior and protein-DNA interactions. The Y-shape of the micro-channel allows for a stable concentration gradient across the measurement channel as well as rapid exchange of buffer. In combination with

fluorescence imaging it can be used to monitor reaction dynamics and heterogeneity as well as discover of rare events and threshold behaviors. In this work the binding behavior of Rad51 to DNA was probed with this tool.

2
DNA - The Molecule

2.1 Chemical structure and information storage

The dsDNA molecule is often described as having the structure of a twisted ladder (see figure 2.1B). In the case of the DNA molecule the ladder is composed of two long polynucleotide chains connected by hydrogen bonds. Each nucleotide in the chain consists of a nitrogen-containing base and a phosphate group bound to the five carbon sugar deoxyribose. The backbone of a DNA molecule is composed of alternating sugar and phosphate groups, covalently bound to each other. The two backbones are twisted around each other to create a helix with a minor and a major groove running along the length of the molecule. In DNA the four bases are Adenine (A), Thymine (T), Guanine (G) and Cytosine (C), these creates the steps of the ladder (0.34 nm apart) by binding to each other with hydrogen bonds (figure 2.1) [30].

However, these bases do not pair with each other randomly. Adenine always pair to Thymine with two hydrogen bonds whereas Guanine always pair to Cytosine with three hydrogen bonds. Through this arrangement a purine is always paired with a pyrimidine giving the energetically most favorable structure, as well as setting the basics for the information storage properties of DNA molecules. This specific paring leads to two strands with complementary sequences of nucleotides, and is therefore called comple-

Table 2.1: Sizes of genomes from different organisms.

Type	**Organism**	**Genome size**	**Comments**
Fish	Protopterus aethiopicus (Marbled lungfish)	119 Gb [31]	Largest vertebrate genome known
Mammal	Tympanoctomys barrerae (Red viscacha rat)	7.5 Gb [31]	Largest mammal genome known
Mammal	Homo sapiens (Human)	3.2 Gb	
Nematode	Pratylenchus coffeae	20 Mb [31]	Smallest multicellular animal genome known
Yeast	Saccaromyces Cereviseae	12.1 Mb [32]	
Bacteria	Escherichia coli	4.6 Mb [33]	
Virus	Phage λ	48 kb	

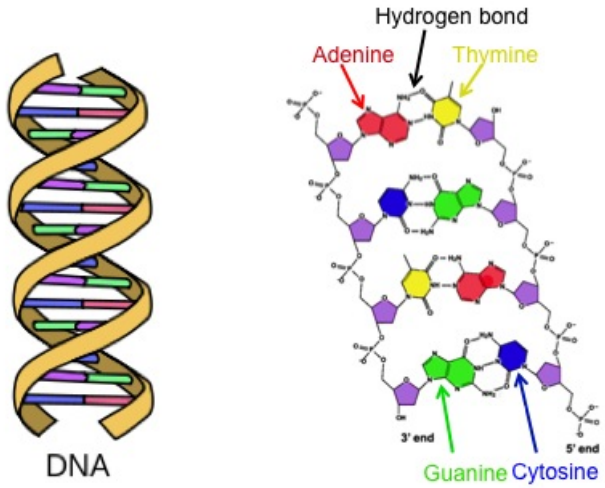

Figure 2.1: Structure of the DNA molecule. LEFT A schematic illustration of the double helical structure of a DNA molecule. RIGHT Chemical structure of a DNA molecule with the different bases and the backbone high-lighted with different colors. Note that Cytosine and Guanine are connected by three hydrogen bonds, while Adenine and Tymine are only connected by two hydrogen bonds.

mentary base-paring. The complementarity enables DNA to encode information in the order, or sequence, of the nucleotide bases along each strand in the same way as the order of the letters encodes the information in this thesis. Just as books differ from each other through the order of the letters, organisms differ from one another because of the different nucleotide sequences along their DNA molecules. The complete information stored by the DNA (i.e. the genome) is in eukaryotic cells packaged into chromosomes, whereas bacterias usually carry their genes on a single circular DNA molecule [6]. The human genome is divided into 46 chromosomes available in the cell nuclei in every cell of the body. Different organisms have different sized genomes (table 2.1), but the genome size is not directly correlated to the complexity of the organism.

2.2 From DNA to proteins

The information stored along the DNA molecules is used to create RNA (ribonucleic acid) and proteins molecules 2.2. However, only some parts of the genome (the genes) are used for constructing proteins. The rest is called non-coding or "junk-DNA". Each gene carries the information to create a specific protein, but the function of the non-coding DNA is to this day not clear, hence the name.

Proteins are long unbranched polymers just as DNA molecules, although the monomer units are not nucleotides but amino acids. In comparison to the four different nucleotides that are the building blocks of DNA, there is in total 20 different amino-acids available for protein fabrication [6]. The large number of different building blocks opens up for a wide range of physical and chemical properties for different proteins. Due to the large variations in physical and chemical properties proteins are involved in processes ranging from oxygen transportation to the copying of DNA.

When a certain protein is needed in the cell, the gene encoding that particular protein

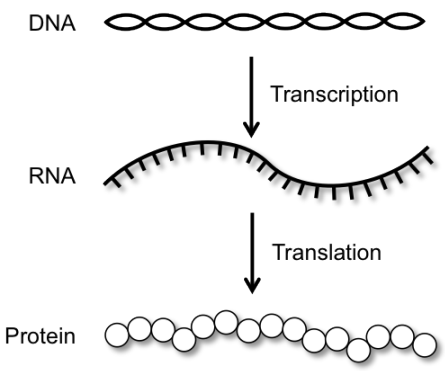

Figure 2.2: Central dogma of biology schematically illustrated.

is first copied into a RNA in a process called transcription. The sequence of nucleic acids along the RNA chain is complementary to the nucleotide sequence along the DNA strand being used as a template. The resulting RNA chain can then be used as a template for protein production in a process called translation, where three consecutive bases along the RNA chain encodes for one amino-acid. In this way the base-pair sequence along the DNA is transferred to a specific amino-acid sequence. Each protein has a unique amino-acid sequence that helps determine how the protein is folded into its 3D shape, which in turn determines its function [6].

A change in the amino-acid sequence can potentially lead to an erroneous folding, which can render the protein un functional. If the change in the code is created during the transcription or translation it will not have a huge impact because it will be localized to a single cell and only occur during a short period of time before the proteins and RNA molecules are replaced. If however the mistake lies within the DNA code (the long term storage of the information) the error will occur in every protein made from that gene and can lead to severe complications for the organism carrying the erroneous (mutated) DNA. The mutations can be both due to a change in a single base-pair (i.e. single-nucleotide polymorphism (SNP)) or large genomic rearrangements such as translocations, inversions, duplications and deletions. An error in the DNA code can lead to genetic diseases such as mental retardation, schizophrenia and cancer [7].

2.3 DNA repair

Inside the cell nucleus the genome is constantly under attack from a range of chemical species as well as UV-radiation [30]. Breaks in the DNA threaten the genome integrity and can potentially lead to cell cycle arrest or even apoptosis. Furthermore, many types of cancer arises due to failure to correctly repair DNA breaks [30]. Both single-stranded and double-stranded breaks occurs but the double-stranded breaks are more critical to the cell. Due to the high risks accompanying DNA breaks, cells have developed pathways to accurately detect and repair damaged DNA [30].

2.3.1 Repairing double stranded breaks

For double-strand repair two pathways are used by to eukaryotic organisms: end-joining and homologous recombination [34]. During the end-joining, two free DNA ends are

paired and merged. No verification of correct pairing occurs during end joining and it therefore has a higher mutation rate than homologous recombination, which use a homologous sister chromatid to verify the repair and is therefore almost error free [34]. Homologous recombination is initiated by a modification of the broken ends to create 3'-terminated single-strand DNA (ssDNA) overhangs. These single stranded parts works as substrates for strand-exchange proteins (such as Rad51 in eukaryotes and RecA in bacteria). Upon binding Rad51/RecA creates a nucleoprotein filament that assists in locating the homologous sequence to the broken part. After localization of the homologous sequence, strand invasion occurs to form a joint molecule. Using the homologous chain as a template branch migration and replication occur until the two strands are completely extended. In the final step the created junctions are enzymatically resolved to release the repaired DNA [35].

2.3.2 RAD51

Human Rad51 is a DNA-dependent ATPase comprised of 339aa, that has attracted interest due to its main role of initiating strand exchange during homologous recombination in eukaryotes. In other organisms these functions are performed by similar proteins and together they create the RecA/Rad51/Dmc1/RadA superfamily of DNA recombinases [29]. Rad51 have been shown to bind to both single- and double-stranded DNA with comparable affinities and eject DNA dyes upon binding [36]. It forms a continuos right-handed helical filament that extends the DNA chain by approximately 50% compared to normal B-form DNA [28].

2.4 Physics of a DNA molecule

A naked DNA chain can be modeled as a semi-flexible polymer [37, 38]. A semi-flexible polymer is bendable over much longer length scales than the size of a single monomer unit, which in the case of DNA is the nucleotide. The length over which they are rigid is called the persistence length, meaning a polymer with a length shorter than the persistence length behaves as a rigid rod. The persistence length of a DNA molecule varies depending on the surrounding buffer conditions, but within standard buffer conditions used during DNA studies (~ 0.1 M NaCl) it has a persistence length of 50 nm [39].

Although it is energetically favorable for a semi-flexible polymer to be completely straight there are entropic forces that drive a DNA molecule to coil up in order to increase the number of possible conformations and thereby increase its entropy (figure 2.3A). This sets the basis of DNA behavior both in confinement and free in solution. Free in solution the self-avoidance of the chain due to for example electrostatic interactions sets a limit to the coiling and the DNA molecule will create a lose coil often referred to as a Flory coil with a radius of gyration (the average root-mean-square distance of a segment from the center of mass of the molecule) described by equation 2.1.

$$R_F \backsimeq (\mathrm{w_{eff}} 2P)^{1/5} L_C^{3/5} \tag{2.1}$$

where $\mathrm{w_{eff}}$ is the effective width of the polymer when the self-avoiding effects are taken into account, P is the persistence length and L_C is the contour length of the DNA [37].

2.4.1 Confined DNA

Even though entropic forces are still acting to coil the DNA chain, a DNA molecule in a space smaller than its radius of gyration will be forced to deform and elongate. If a nano-channel is used for the confinement (as in this work) the elongation is dependent on the channel diameter, D. The stretching mechanism can be divided into two regimes. The first regime, called the de Gennes regime, considers channels with diameters in the range $P < D < R_g$. The second regime, called the Odijk regime, considers channels with a diameter smaller than the persistence length of DNA.

In the de Gennes regime the extension of a polymer is mainly due to the self avoiding nature of the chain. In this region the molecule will create small non interacting coils along the channel, where the DNA in each blob behaves as an unconfined Flory coil with a radius of gyration equal to the channel diameter (figure 2.3B). This gives an even distribution of the polymer along the length of the channel, and as a consequence the DNA extension within the channel scales linearly with its contour length. The relative extension along the channel, L_z, can be determined from [40]

$$L_z \backsimeq L_C \frac{(P \mathrm{w}_{\mathrm{eff}})^{1/3}}{D^{2/3}} \tag{2.2}$$

Note that the ionic strength of the buffer affects the effective width of the DNA molecule as well as its persistence length, which will largely affect the chain extension [41].

In the Odijk regime, where the channel diameter is smaller than the persistence length of DNA, the molecule can no longer create coils inside the channel. Instead the polymer chain will be deflected back and forth between the channel walls, with a characteristic length scale, λ, given by $\lambda \backsimeq (D^2 P)^{1/3}$ (figure 2.3C). With the help of the angle, α, between the channel wall and the deflected segment the extension for each segment along the channels is given by $\lambda \cos \alpha$. According to [42] the relative extension of the entire DNA molecule in a square channel can be described as

$$\frac{r}{L_C} \backsimeq \left[1 - \epsilon \left[\left(\frac{h}{P} \right)^{\frac{2}{3}} + \left(\frac{d}{P} \right)^{\frac{2}{3}} \right] \right] \tag{2.3}$$

Where h is the channel height, d the channel width and ϵ a constant of proportionality that has been estimated in simulations to $\varepsilon = 0.09137 \pm 0.00007$ [43].

Both equation 2.2 and 2.3 above represents a mean value of the end-to-end distance of an extended polymer. Due to constant thermal fluctuations and conformational changes the length of an extended molecule is constantly changing around these mean values [11].

2.4.2 DNA relaxation in nano-channels

In order to introduce a DNA molecule into a confined space the resistance to entry, created from entropic forces and friction, must be overcome. Two main methods are used to overcome the resistance to entry. In the first method a voltage is applied across the nano-channel since that creates an electric force acting on the DNA molecules. The second method utilizes shear flow to drag the molecules into the confinement. The extra energy needed for the introduction into the nano-channels leads to an initial stretching of the molecules that is larger than the equilibrium stretching discussed above. As soon as the external force is removed entropic forces drives the DNA molecules to relax

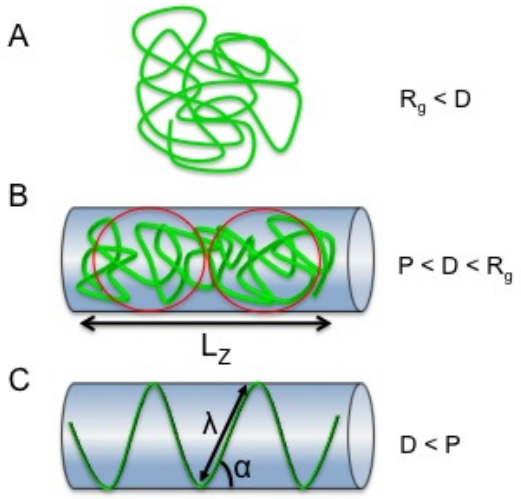

Figure 2.3: Schematic illustrations of DNA at different degrees of confinement. A. An unconfined DNA coil. B. Confinement in de DeGenne regime where the DNA molecule can be folded back on itself and therefore can be modeled as a series of blobs along the channel. C. Confinement in the Odjik regime where the DNA molecule cannot fold back on itself, but will instead be deflected back and forth between the walls.

towards their less stretched equilibrium state. The relaxation process has been studied experimentally for DNA molecules within pillar arrays, nano-slits, nano-channels as well as a numerically [44–46]. In this section the relaxation of DNA within nano-channels are discussed since that is the system used within the scope of this work.

An important parameter to study in order to better understand the relaxation behavior of DNA molecules is the relaxation time. The relaxation time for a DNA molecule relaxing within a nano-channel is dependent on the length and the initial stretching of the DNA molecule. Longer DNA chains leads to longer relaxation times. The end-to-end length, l, of a contracting molecule at time t in a nano-channel can roughly be characterized with an exponential fitting function:

$$l(t) = l_0 + (l_E - l_0)\exp(-t/\tau) \tag{2.4}$$

l_0 is the equilibrium length in the channel, l_E the measured initial extended length, and τ is the time constant of contraction [14].

In addition to driving the relaxation of DNA molecules entirely confined within a nano-channel, entropic forces also drive the relaxation (or recoil) of partly confined DNA chains back into a larger space which allows an increased number of possible conformations. The relaxation time for this process is dependent on the degree of confinement, where a higher confinement leads to increased entropic forces and thereby shorter relaxation times. When a molecule is only partly introduced into a nano-channel and then immediately allowed to recoil out into the unconfined space, the molecule will undergo contraction to its equilibrium stretching and recoiling into un confinement simultaneously. In order to follow the length changes of the DNA within the nano-channel a stretching factor, $\gamma(t)$, describing the degree of stretching of the inserted part compared to its equilibrium state is introduced. This factor is dependent on the size of the channel, since this affects the equilibrium extension as described above. With this stretching factor the

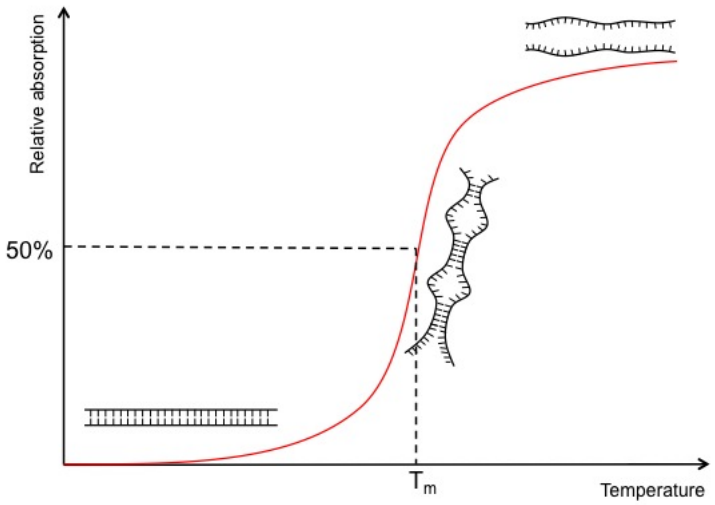

Figure 2.4: Typical melting curve from bulk measurements of DNA denaturation, together with schematic illustrations of the DNA molecule at different temperatures. Melting of a DNA molecule is initiated with the creation of small bubbles along the DNA chain. At increasing temperatures these bubbles grows larger until complete denaturation of the DNA molecule is reached.

length of the DNA part within the nano-channel at each time, t, can be determined from

$$l(t) = \gamma(t)\sqrt{-\frac{f}{\rho}(t - t_0)} \tag{2.5}$$

In equation 2.5 f is the entropic force, ρ the drag coefficient and t_0 the starting time [14]. In this model the two relaxation processes are treated as being independent of each other, which is a valid assumption due to their different relaxation time constants.

2.5 DNA denaturation

DNA denaturation (or melting) describes the process where the hydrogen bonds between the bases in the complementary chains are broken and the two chains separated. DNA melts over a range of temperatures and the melting temperature is defined as the temperature where half the DNA is melted (in its single-stranded form) (see figure 2.4). The melting temperature depends on the GC content of the chain, in such a way that a higher GC content gives a higher melting temperature [47]. A DNA molecule in physiological salt concentrations is in its double-stranded state at 37 °C, which is stabilized not only by the hydrogen bonding but also and mainly by the stacking of the planar aromatic bases [48, 49]. The stacking of the bases contributes to the stability of the helical structure by hydrophobic interactions between the adjacent base-pairs. Although, even at physiological conditions small (from a few to a few hundred base-pairs) single stranded domains, so called DNA-bubbles, open up intermittent along the DNA molecules and are immediately closed up again. At room temperature (around 25 °C) the relaxation time for such bubbles was shown to be around 50 μs [50]. This process is called DNA breathing and most often occurs at AT rich areas along the DNA strand, for example

the TATA box [51]. Furthermore it was shown that at melting conditions the relaxation time for bubble formation scales with N^2, where N is the number of base pairs in the unzipped bubble [52].

Despite the DNA breathing, additional energy is needed to separate larger domains along the two DNA strands in order to read the code. Inside the cells, during for example DNA replication and transcription, enzymes are used for the strand separation, whereas several other methods are used for DNA denaturation *in vitro*. The stability of the dsDNA (double-stranded DNA) is affected by for example ionic strength, chemical composition of the environment, pH and temperature [47]. For *in vitro* denaturation, usually a combination of altering the buffer chemistry and increasing the temperature is used, since the high temperatures otherwise needed can be difficult to handle and often causes strand breakage and depurination of DNA [53]. The buffer chemistry can either be altered by the addition of denaturation agents (chemicals that lowers the stability of the double helix) or by altering the ionic strength of the buffer. A lower ionic strength lowers the melting temperature since this decreases the number of cations around the DNA chain. The cations shields the negative charged phosphate groups along the DNA strands to suppress the electrostatic repulsion between the two strands. In complete deionized water a DNA chain would melt already at room temperature [47]. Despite the fact that a changed ionic strength will lead to DNA denaturation, a chemical agent such as formamide (discussed below) or urea is most often used in order to lower the melting temperature.

Traditionally, DNA melting has been performed in bulk and monitored by observing the UV-absorption of light in the 260 nm wavelength region [47]. Monitoring a single wavelength is possible due to a phenomena termed hyperchromicity, which describes the effect of a constant absorbance wavelength during an increasing absorbance. The increased absorbance arises from a decrease in hydrophobic interactions between the bases in the single stranded parts of the DNA chain. Within a dsDNA molecule the stacked bases interact with each other through their π-electron clouds, which are also responsible for the UV-absorption. The base-base interaction hinders the π-electron clouds from absorbing light in a dsDNA, but when the bases are separated due to melting the bases interaction with each other decreases and the π-electrons are free to absorb light [47].

During DNA melting, the weaker AT-rich areas melt first since the bases A and T are only connected by two hydrogen bonds, whereas the bases C and G are connected by three hydrogen bonds. This sequence dependence in melting behavior can be used to get sequence information as discussed later. When DNA melts, bubbles of ssDNA are within seconds created along the dsDNA chain. These bubbles then slowly grows and more bubbles are created until the two chains are completely separated (see figure 2.4). The melting probability for a base-pair is dependent on its environment. A base-pair adjacent to melted bases has a higher probability of melting than a base-pair within a double-stranded part of the chain, giving a cooperativity of the melting behavior [54].

2.5.1 Formamide as a denaturation agent

Formamide (CH_3NO) is a liquid in room temperature and is easily mixed with water. Addition of formamide to DNA solutions lowers the melting temperature of dsDNA by around 0.6 °C per percentage formamide being added, without affecting the cooperativity behavior of the melting [53]. Evidence of a two state interaction process between DNA and formamide has been shown. In the first step, water and ions associated with the

DNA chain is replaced by formamide, which effectively lowers the ionic strength in the proximity of the DNA and as a consequence the melting temperature is lowered. In the second step the formamide disrupts the hydrogen-bonds between the base-pairs [55]. With its capacity to form 4 hydrogen bonds, formamide is able to bind to the bases through hydrogen bonding and can thereby prevent the bases from binding to each other (figure 2.5).

The effect of formamide has been shown to depend on bp sequence where poly(dAdT) shows a higher affection than a mixed chain [55]. However, the total AT ratio within a DNA molecule does not seem to affect the decrease of melting temperature with increased formamide concentration [53].

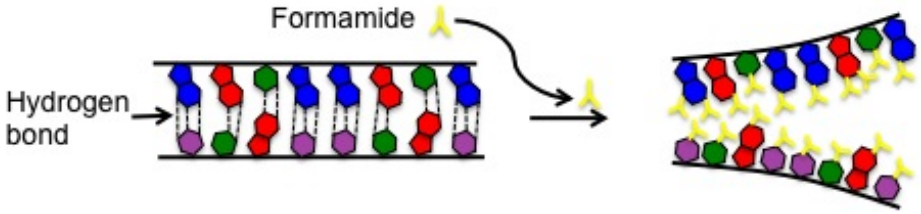

Figure 2.5: Schematic illustration of the interaction between DNA and formamide. Formamide interacts with DNA by forming new hydrogen bonds with the bases and thereby disrupting their internal binding.

3 DNA Sequencing

Since an error in the genetic code can lead to severe diseases or in worst cases death, major efforts have been put into developing methods to decode this information. A better understanding of the genetic code opens up for personalized medicine as well as an early detection of genetic disorders. In this chapter a short introduction to some of the most popular sequencing methods used today will be given.

3.1 Shotgun sequencing

Shotgun sequencing is a general term for the sequencing methods where the DNA is broken into random fragments that are sequenced separately. Specialized bioinformatic algorithms are used to assemble the pieces with the help of overlapping parts of the sequenced fragments. This assembly becomes increasingly complex with long DNA chains (> 1 kbp), prolonging the computational time. Furthermore it possesses a problem with highly repetitive or repeated parts, since it is hard to determine if two repetitive parts found on different pieces comes from separate parts of the genome or are just copies of the same part of the genome [6].

3.1.1 Chain termination sequencing

The most common chain termination sequencing method is the Sanger dideoxy method. This method was developed in 1977 by Frederick Sanger [56] and revolutionized molecular biology to such extent that it is still the source of inspiration for most new developments within sequencing technology. It has a base-pair resolution and can therefore be used for detecting SNPs. It is often used in a shotgun approach, and can be applied to DNA strands up to 1 kbp with extremely high accuracy.

Chain termination sequencing is today in general initiated with PCR (Polymerase chain reaction) amplification of the DNA followed by denaturation of the PCR products to create ssDNA molecules. A primer (a short single-stranded piece of DNA that is designed to pair with a specific part of the DNA to be sequenced) is bound to a known part at the end of the amplified DNA to create a starting point for the DNA polymerase. The ssDNA is divided into four different reaction tubes containing DNA polymerase and each of the four nucleotides. In addition, a small amount of the 2',3'-dideoxy analog of one of the four nucleotides is added to each tube. The analog lacks the 3'-hydroxyl terminus needed for the next nucleotide to be added to the chain. This means that the growth

of the complementary strand is terminated when the analog gets incorporated. During the reaction, the DNA polymerase will build the complementary strand to the unknown sequence until the analog gets incorporated and terminates the growth. The concentration of the analog is low in comparison to the normal nucleotides and therefore the chain termination will only happen occasionally, leading to complementary strands of different length. The chain terminated fragments can then be separated by gel-electrophoresis with one base represented in each lane and the sequence determined from the pattern on the gel [57].

3.1.2 Pyrosequencing

Pyrosequencing is a sequencing technique with single-base resolution based on enzyme-coupled reactions and bioluminescence detection [58]. Just as chain termination sequencing, the single base-pair resolution enables detection of SNPs. Due to the short read length (150 bp) the shot-gun approach is required for sequencing an entire genome [58].

Just as chain termination sequencing, the process is initiated by amplification of the unknown DNA by PCR. The PCR products are then denatured to create single-stranded substrates to which the sequencing primers can bind. With the primer as a starting point and the PCR product as a template, DNA polymerase builds a new strand base-by-base. The chain is extended by addition of one of the four nucleotides to the reaction buffer at the time. Before the next nucleotide is added the previous nucleotide is degraded to ensure that only one type of nucleotide is present in the solution at all times. Incorporation of the nucleotide into the growing chain is detected through the release of pyrophosphate. This pyrophosphate is converted by the enzyme sulfurylase into a flash of chemiluminescence, which is detected to determine if the added nucleotide was incorporated. The intensity of the detected light is used to determine if one or several nucleotides were incorporated in a row [58].

Due to the light based detection the chain growth can be followed in real time, eliminating the need for the electrophoresis step required in Sanger sequencing. This lowers the running costs and opens up for the possibility to make an automatic high-throughput tool working in a parallel manner.

3.1.3 Next generation sequencing

Over the last decade new array systems for sequencing going under the general term Next-generation sequencing has been developed [59, 60].

Most of the Next-generation sequencing tools are based on traditional pyro- or Sanger sequencing with the difference that the substrate is often surface bound and organized into ordered arrays. With the array systems a much higher degree of parallelism can be achieved, which strongly increases throughput while the small sizes of the systems used allows for a reduction of running costs. Recently two single molecule Next-generation methods were presented. They eliminate the need for DNA amplification and thereby further decrease time and cost for sequencing. Although, they suffer from the same major drawback that comes with all the Next-generation tools, namely the extremely short read length. The short read length leads to the requirement for sophisticated algorithms and much data power for sequence assembly in order to acquire useful sequencing data. In addition, highly repetitive sequences and homopolymers often posses a problem during

data acquisition and sequence assembly. Even though new improvements are constantly made on the data algorithms the short read length (10-100 bases) are still the "Achilles heel" of the Next-generation sequencing methods.

3.2 Single molecule sequence analysis

3.2.1 Chromosome banding

Banding can be used to identify individual chromosomes (karyotyping) in metaphase and to observe large genomic rearrangements such as translocations, inversions and deletions [61]. Even though the resolution varies between the different banding techniques none of them can be used to achieve a single base-pair resolution. If the conditions are right aberrations in the size of $1 - 10$ Mbp can be identified along the chromosomes [62].

During the banding procedure the DNA is stained, with for example Giemsa dye, at an early stage of mitosis to create a banding pattern (also sometimes referred to as a barcode or mapping pattern) of dark and bright stripes along the condensed chromosomes. Several banding techniques are available but they can be divided into two principal groups. The first group contains the methods where the banding pattern is distributed along the length of the whole chromosome such as G-banding (Giemsa banding) and R-banding (Reverse banding). In the second group the techniques resulting in a pattern on only a part of a chromosome are represented, such as C-banding (centromere banding) [63]. Different resolutions can be achieved by changing the condensation of the chromosomes, where less condensed chromosomes gives a better resolution.

G-banding is used to detect the chromatin structure and base composition along the chromosome [61]. There are several different methods for G-banding but the most widely used is the GTG-banding produced by staining protease treated chromosomes with Giemsa dye [61]. This creates a pattern of alternating dark and bright bands along the molecule where the light bands are GC-rich, early replicating, euchromatic and more active regions of the chromosome and therefore more biologically relevant [63].

Fluorescence dyes such as quinacrine, DAPI (4'-6- diamidino-2-phenylindole) and Hoechst 33258 has also successfully been used for chromosome banding. Both DAPI and Hoechst 33258 has a binding selectivity for AT whereas quinacrine binding is irrespective of sequence, although it fluoresces brighter in AT-rich regions. The advantage of fluorescence staining is the simplicity of the method compared to other staining methods, although the drawback is the tendency of photobleaching for fluorescent dyes [61].

3.2.2 Fluorescence in situ hybridization

Fluorescence in situ hybridization (FISH) is based on the hybridization of a fluorescently labelled probe (a short DNA strand with a well defined sequence) to a chromosome *in situ*. The hybridization is initiated by denaturation of both the chromosome target and the probe. Before the temperature is lowered the probe is added in large excess to ensure that it is annealed to the target chromosome. The probe will bind where the chromosome sequence is complementary to the probe sequence creating a double stranded hybrid molecule. After the removal of the unbound or loosely bound probes (due to not complete complementarity in the chromosome sequence) the remaining probes are detected. They can be labeled with either haptens (i.e. biotin, digoxygenin) or fluorochromes (i.e.

fluorescein isothiocyanate (FITC) , rhodamine). The FISH probes can in general be divided into three categories: repetitive sequence, whole chromosome, or specific sequence. Repetitive sequence probes are mostly used for studying centromeres, since they often contain many small repeated parts. Whole chromosome probes (chromosome painting) are composed of unique sequences from an entire chromosome or chromosome region. The most popular method is that of targeting a specific sequence along the DNA to detect translocations, copy number variations and deletions [63].

Many genetic diseases arise from genomic rearrangements in the size range $5-400\,\text{kbp}$ and can therefore not be detected by chromosome banding on metaphase chromosomes [7]. FISH can be performed on both metaphase and interphase cells and can reach a resolution of $10-50\,\text{kbp}$ [63]. To further increase the resolution, fiber-FISH with a resolution in the range of $1-300\,\text{kbp}$ was developed [64]. Fiber-FISH has been performed on both naked DNA strands and chromatin fibers among other things. The naked DNA strands gives a higher resolution but a lower coverage compared to FISH on chromatin strands. Even though fiber-FISH can be used to get a relatively high mapping resolution it still suffers from the drawback inherent in a FISH techniques, namely the improved mapping results gained by prior knowledge of the sample sequence.

3.2.3 Barcoding on stretched DNA

With new barcoding techniques it is possible to create barcodes on DNA strands with an unknown sequence with a resolution down to 1 kbp. Just as with fiber-FISH the high resolution barcodes are reached by stretching the DNA. Barcoding on elongated DNA molecules can basically be divided into two categories based on how the barcode is created. The first category includes methods based on specific cutting with restriction enzymes. When cutting with restriction enzymes, the size of the resulting DNA pieces will depend on where along the DNA strands the cutting takes place. If enzymes that only cut at a specific base-pair sequence is used the lateral placement of this sequence along the DNA can be determined [17, 65–67].

The second category includes methods based on the AT/GC ratio along the DNA. Within this category two main techniques are used to create the barcode. The first technique is based on competitive binding between a un fluorescent molecule with a strong binding and high base-pair selectivity (meaning it binds only to AT or GC base-pairs) and a standard unspecific nucleic acid stain such as YOYO-1. This creates a pattern of dark stripes where the non-fluorescent molecule binds and hinders the binding of the dye [18].

The second technique (often referred to as melting mapping) is based on partial melting of a DNA molecule stained with a dye that is equally distributed along the initial dsDNA. If a dye specific to dsDNA or with a large increase in fluorescence upon binding to dsDNA is used, dark areas will be created at the melted single stranded parts of the DNA molecule. Since AT are held together only by two hydrogen bonds a region containing a large amount of AT will be less stable than a region with a high GC content. During the right conditions only AT rich areas will melt and a barcode were AT rich areas are dark is created [19]. Melting mapping was the technique used during this work and as an example of a melting pattern kymographs (or time-traces) of two different T4GT7 DNA molecules is shown in figure 5.4 in section 5.3.

4

Handling Single DNA Molecules

Preparations for fluorescence imaging of single DNA molecules often includes stretching of the molecules as well as staining with a fluorescent dye. Today many different stretching methods exists, which can be used separately or in combination. Some examples are hydrodynamic stretching due to a buffer flow [21, 26, 27, 68, 69], elongation due to confinement in nano-channels [11, 13, 14, 37, 41, 44, 45], or by pulling on the ends of the DNA with tweezers or AFM [70, 71].

Optical and magnetic tweezers are versatile tools used to measure mechanical properties of biomolecules. Furthermore, tweezers can with success be used in combination with flow cells, in order to rapidly change the surrounding buffer conditions while simultaneously measuring the response from a biomolecule. With a setup including tweezers the stretching can be achieved either by pulling at both ends of the DNA molecule with two tweezers or by attaching one of the ends to a surface and pulling in the other end with the help of a tweezer. In addition, a single tweezer can be used to immobilize a DNA molecule while a hydrodynamic flow is used for the stretching.

Hydrodynamic flow can be used to stretch DNA molecules prior to absorption to a surface (used in DNA combing [72]) or to stretch molecules with one immobilized end. In this work one end of a DNA is attached directly to lipids within a supported lipid bilayer to created DNA arrays, which are discussed in more detail in section 4.1.4. When using hydrodynamic forces for the elongation the degree of stretching depends on the flow velocity in such a way that an increased flow velocity leads to an increased degree of stretching until a maximum stretching is reached [26].

Nano-channels provide a dynamic system in which DNA molecules can be imaged in their equilibrium state, and was therefore the method of choice throughout most of this work. DNA molecules can easily be moved around in the nano-channels with electrophoresis or pressure driven flow (as in this work) and with a clever design the buffer surrounding the DNA molecule can easily be exchanged without moving the DNA. The uniform stretching (as discussed in section 2.4.1) provides a correlation between features spatial position along the polymer and their position within the genome [11]. Since no external forces are required to extend the DNA molecule close to native conditions can be reached. Confinement of DNA molecules in nano-channels have been used to gain a deeper understanding of the physical behavior of semi-flexible polymers in confinement (see section 2.4.1) as well as mapping of DNA with several of different techniques as described in section 3.2.3.

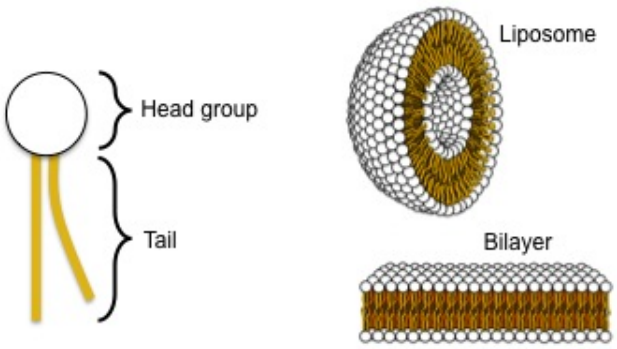

Figure 4.1: LEFT Schematic illustration of a phospholipid. RIGHT Drawings of different self-assembly structures for lipids in water-based solutions.

4.1 Surface functionalization

Ideally, anchoring enables easy visualization of the molecules while retaining their biological integrity. For easy visualization and analysis it is important to prevent unspecific absorption to the surface, which leads to the need for surface passivation. There are many different approaches used to passivate a surface, including nonspecific blocking agents (e.g., biotinylated bovine serum albumin (BSA), casein or streptavidin) or covalent modifications of the surface with for example polyethylene glycol (PEG) [26, 27]. In addition, supported lipid bilayers have successfully been used for surface passivation and were proven to prevent nonspecific absorption of both DNA and several different proteins at near-neutral pH ranges [26, 27, 73]. Recently, lipids were used to passivate nano-channels as a first step toward using nano-channels to investigate of protein-DNA interactions [74]. Lipid bilayers are advantageous for surface passivation since they provide a micro environment that mimics the inside of a cell, are easy to create, are stable in a vide range of buffer conditions. Furthermore, its function can be varied by integration of lipids with modified head groups.

4.1.1 Structure and behavior of lipids

Lipid molecules are amphiphilic, which means that they posses both hydrophilic (i.e. water-loving) and hydrophobic (i.e. fat-loving) properties. The hydrophobic part consists of one or more (often two) acyl-chains. The hydrophilic part (the head group) shows a great chemical diversity and can be neutral, charged or zwitterionic (the charge depends on pH) [75]. The most common phospholipids are phosphatidylcholine (PC) and phosphatidylethanolamine (PE), which are neutral in the pH range of 3-10.

Different molecules can be attached to the head group in order to functionalize the lipid. For example can PE be modified with biotin to enable attachment of a biotin modified DNA through a biotin-neutravidin-biotin linkage [26, 27].

Due to their amphiphilic nature, lipids arrange themselves so that the head groups face outwards in water solutions and the tails face outwards in fatty solutions. In water they self assemble into for example liposomes/vesicle or bilayers in order to protect their hydrophobic tail groups (see figure 4.1). In a bilayer the head groups are exposed on each side and the tails are hidden within the membrane. A liposome consists of a bilayer

in a spherical shape with water inside as well as outside the sphere.

4.1.2 Vesicle preparation

Different methods can be used to create unilamellar vesicles (i.e vesicles surrounded by only a single bilayer) such as sonnication with a tip probe sonnicator, bulk sonnication or extrusion. During lipid vesicle extrusion (the method of choice during this work) the lipid solution is pressed back and forth through a polycarbonate extrusion membrane at least 11 times. This is done by connecting two 1 ml glass syringes (one which contained the lipid solution) to each side of a metal holder containing the membrane (as shown in figure 4.2). The lipid solution is then moved back and forth between the two syringes passing the filter each time. In order to minimize the concentration of unfiltered vesicles the final filtration is always done into the initially empty syringe. By using different pore sizes the final size of the unilamellar vesicles can be varied.

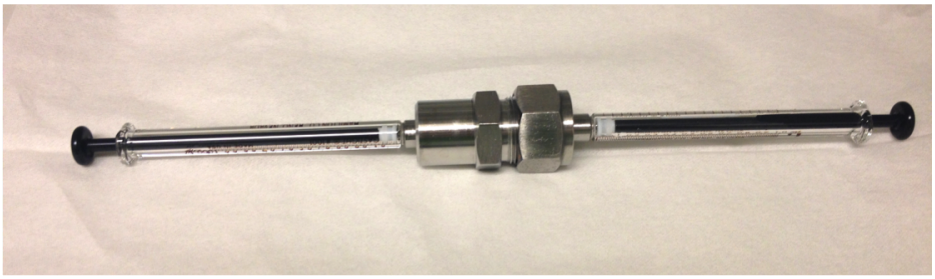

Figure 4.2: Image of the setup used for lipid vesicle extrusion. The solution containing the lipid vesicles are passed back and forth between the two syringes. Each time it passes a filter that is held in place by the metal holder.

4.1.3 Supported phospholipid bilayers (SLB)

Vesicles form planar bilayers on certain surfaces. When using POPC (1-palmitoyl-2-oleoyl-sn-glycero-3-phosphocholine) lipids, self-healing structures with a thickness of 4.5−5 nm are created [76]. The fluidic properties of a lipid bilayer enables molecules tethered to lipids within the bilayer to diffuse freely in two dimensions with diffusion constants around $\sim 1\ \mu m^2/s$ [77, 78]. SLBs are often formed by vesicle absorption followed by spontaneous vesicle rupture and self assembly of the lipids into a bilayer [79, 80]. This process results in a high surface coverage and reproducibility, but are dependent on a clean and smooth surface as well as the correct buffer conditions (such as ionic strength and pH) [81].

4.1.4 Creating DNA arrays

In order to visualize a large amount of DNA molecules on a single molecule level a specific DNA array method was developed. The developed DNA array is a structure where DNA molecules are aligned next to each other and elongated with hydrodynamic forces (figure 4.3) [26]. To create a DNA array a SLB, that acts both as surface passivation and provides an anchoring point for the DNA molecules, is created within a micro-fluidic channel. The bilayer is made from unmodified POPC lipids and a small amount of lipids with a biotin molecule bound to their head group. After bilayer formation a buffer

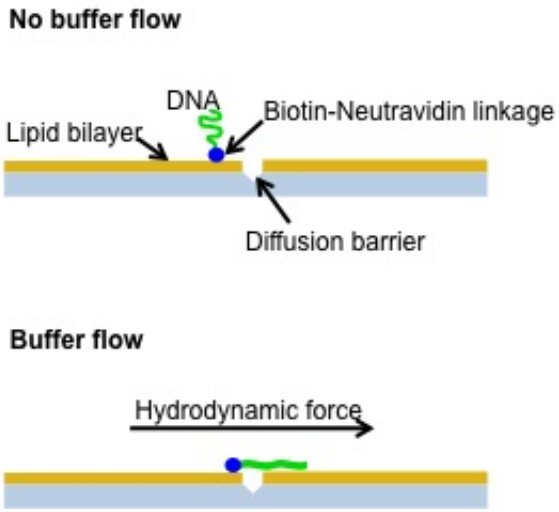

Figure 4.3: A cartoon illustration of how to create a DNA array by applying a hydrodynamic force to tethered molecules.

containing neutravidin is incubated in the micro-channel. The neutravidin binds to the biotin-modified lipids to create anchoring points on the lipid bilayer for biotin-modified DNA molecules. Hydrodynamic forces are then used to move tethered DNA molecules across the bilayer and organize them into closely packed arrays. The array pattern is defined by micro-scale mechanical diffusion barriers, which can be either in the form of a trench or a wall. Trenches can be created manually with a diamond drill (as in this work) or by using electron been lithography (EBL) to define the position and shape of the trench followed by an etching step. To create a wall the etching step is replaced with a deposition step where for example chromium can be deposited at the places defined during EBL [27]. During data collection hydrodynamic flow is used to elongate the DNA molecules to enable visualization of features along the DNA molecule.

5 Optical Imaging

Optical imaging was in this work used to study DNA molecules in a system of micro- and nano-channels. Light microscopy was used to follow the chip processing, whereas epi-fluorescence was used during measurements on the DNA molecules. A nice overview of standard light microscopy is given by Abramowitz in reference [82], wheres fluorescence imaging is well described by Lakowicz in reference [83].

5.1 Light microscopy

The first simple glass magnifiers were designed more than 500 years ago. They consisted of a convex lens that magnified the image of the object by increasing the visual angle on the retina. Today advanced microscopes with a system of aligned lenses enabling imaging of single cells or molecules exists. A microscope should not only produce a magnified image of the object but also be able to separate details in the image and render these details visible to the eye. In summary a microscope needs an excellent magnification, resolution and contrast. The magnification is often flexible in modern microscopes with a range of objectives and eyepieces to be combined. For a microscope the total magnification is the combined magnification of the objective and the eyepiece, meaning that a setup with a 20x objective and a 10x eyepiece will give 200x magnification.

Resolution quantifies the minimum distance, r, at which two objects can be imaged separately. As light passes through the system of lenses in the microscope and the sample it is diffracted and scattered slightly. This results in an image where each point of the specimen is portrayed as a disk (known as an Airy disk) and not a point. The criterion for the minimum separation between two resolved point sources states that the first diffraction minimum from one point source coincide with the diffraction maximum from the second point. This is called the Rayleigh criterion and can for a microscope be calculated using equation 5.1.

$$R = \frac{1.22\lambda}{(NA_{cond} + NA_{obj})} \tag{5.1}$$

Here R is the resolution, λ the wavelength of the illumination light, NA_{cond} the numerical aperture of the condenser and NA_{obj} the numerical aperture of the objective. Better lenses and an increased NA of the objective are ways to decrease the size of the Airy disks. NA is a dimensionless number characterizing the efficiency of the objective to

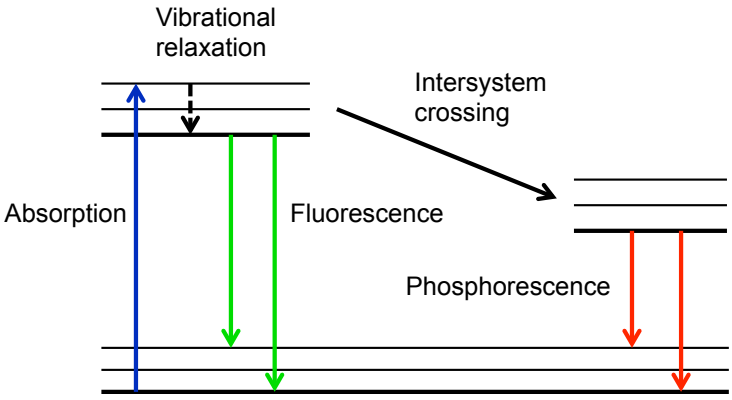

Figure 5.1: Jablonski diagram showing the transitions leading to fluorescence and phosphorescence.

collect light by describing over which angles the system can accept or emit light. Within the field of microscopy NA is often defined as:

$$NA = n \cdot sin\theta \tag{5.2}$$

Here n is the refractive index of the material between the objective and the sample and θ is the half-angle of the maximum cone of light that can enter or exit the objective. From equation 5.2 we conclude that an increased NA can be achieved by either increasing the angle of collection for the objective or choosing a material with a high refractive index between the objective and the sample. The critical angle for total internal reflection sets a limit for the collection angle creating the urge to change the medium between the objective and the sample. Immersion oil with a refractive index similar to that of glass ($n = 1.5$) is a popular choice of medium.

5.2 Fluorescence microscopy

Fluorescence microscopy is today an essential tool for studying biological processes and biomolecules. The family of fluorescence microscopy consists of several different techniques including TIRF, nanoscopy techniques (such as stimulated-emission-depletion (STED)) and epi-fluorescence.

The emission of light from a substrate is called luminescence and can be divided into fluorescence and phosphorescence. Both these phenomenas describe the excitation of a molecule by light absorption and subsequent relaxation by light emission. When a molecule absorbs a photon an electron within the molecule enters an excited state with a higher energy than the ground state. The absorption only occurs if the incoming photon has an energy that corresponds exactly to the energy gap between the ground state and the excited state as shown in the Jablonski diagram in figure 5.1.

If the excited state is a singlet state, meaning that the excited electron has an opposite spin compared to the electron in the ground state, the excitation leads to fluorescence. Due to the opposite spins of the electrons the excited molecule is allowed to return to the ground state, leading to fluorescent lifetimes in the nanosecond range. Phosphorescence occurs if the excited molecule has the same spin as the ground state molecule (i.e the

excited state is a triplet state). The relaxation back to the ground state is in this case a forbidden transition which leads to longer lifetimes, usually in the range from milliseconds to seconds.

The electron gets rid of the extra energy by radiation-less vibrational relaxation, internal conversion, photon emission or by transferring the extra energy to another molecule. Most molecules first relaxes through radiation-less vibration or internal conversions down to a lower state and then emits a photon to relax further down to its ground state. The initial vibrational relaxation leads to a longer wavelength for the emission light compared to the excitation light. This shift in wavelength between the excitation and the emission light was first described by Sir George G. Stokes and is therefore called the Stoke's shift or Stoke's law.

When an excited molecule collides with another molecule it can potentially transfer its extra energy to this molecule. During this transition the molecular structure of the excited molecule can be irreversible changed causing the molecule to loose its fluorescent properties. This phenomena is called photobleaching and is in general unwanted during fluorescent imaging, although some techniques for example FRAP (fluorescence recovery after photobleaching) make use of this phenomena. During the FRAP measurements a small area of for example a fluorescently labeled lipid bilayer is bleached and the recovery of fluorescence in that bleached area is measured and used to determine the fluidity of the bilayer.

Oxygen is a good candidate for intermolecular energy transfers and it is therefore important to keep the oxygen concentration to a minimum within the sample during imaging to minimize the photobleaching. In addition, the negative oxygen ion is a radical and extremely reactive which can lead to damage of the sample.

The excitation light can be both un isotropically and isotropically distributed, but the emitted light is always isotropically distributed meaning that only a small amount of the emitted light will reach the detector. Together with the lower intensities of the emitted light compared to the excitation light this creates the need for filtering out the excitation light before detection. Luckily, this is possible due to the wavelength shift described above and the fact that all molecules have their own characteristic absorption and emission wavelengths. This allows for imaging of samples with low quantum yields, which is the ratio of photon absorption to emission. A filter cube containing two filters and a dichroic mirror is used to filter out the emission light for detection (see figure 5.2). The first component in the light path is the excitation filter, which is a bandpass filter only transparent to wavelengths in the vicinity of the excitation wavelength. The second component in the light path is the dichroic mirror built to reflect the light passing through the excitation filter and to be transparent to the emitted light. The excitation light is reflected towards the sample, which after excitation emits light with a longer wavelength than the excitation light. The longer wavelength is passed through the dichroic mirror to the emission filter, which is a bandpass filter ensuring that only the emitted light reach the detector. To further increase the image quality an objective with a high NA can be used. Since a higher NA objective is created by increasing the maximum cone of light that can enter the objective a higher N.A means more light collected from the sample.

Strong illumination light can potentially damage a biological sample. To avoid this, neutral density (ND) filters can be placed in the light path before the sample. Neutral density filters equally reduces the light intensity of all visible wavelength. The two most common ND filters on the market are the ND4 and ND8 filters, which transmits 25%

and 12.5% of the incident light respectively.

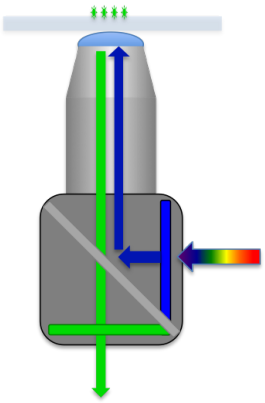

Figure 5.2: Schematic illustration of the light path through a filter cube. The incoming light first hits the excitation filter (blue rectangle) which is only transparent to the excitation wavelength. Secondly the light is reflected by the dichroic mirror (gray tilted rectangle). The emitted light passes the dichroic mirror and is then filtered through the emission filter (green rectangle) that is only transparent to the emitted wavelength.

5.2.1 Nucleic acid stains

Many samples are stained with fluorochromes (also termed fluorophores) prior to imaging. A wide range of different fluorochromes with different excitation and emission wavelengths and that binds to different objects are today available on the market. Fluorochromes often have a high quantum yield and are very specific in their attachment targeting. During single molecule studies of DNA with fluorescence microscopy fluorochromes are always used it stain the molecule. As a result a vide range of nucleic acid stains including cyanine dyes, DAPI and Hoechst 33258 have been developed. The group of cyanine dyes includes YOYO (491/509) and TOTO (642/660) which are the homodimers of oxazole yellow (YO) and thiazole orange (TO) respectively [84]. The strongly positively charged homodimers are created by linking the two monomers together with a bis-cationic linker to form a structure that is optimal for a bis-intercalating binding mode in which two aromatic moieties intercalates between the base-pairs (figure 5.3) [84]. Bis-intercalation is the main binding mode for YOYO until all the intercalation binding-sites are filled up, after which YOYO can bind externally in a grove binding fashion [84]. Due to the intercalating binding of the YOYO molecule the dsDNA-YOYO complex is extremely stable with a binding constant that has been estimated to $10^{10} - 10^{12}\, M^{-1}$ [84, 85]. Furthermore, YOYO shows a high fluorescence enhancement (1000 fold) upon binding makes it a perfect candidate for both single molecule studies of DNA [11, 13, 14, 18–20, 27, 41, 45, 65, 86, 87] and gel electrophoresis [84, 85]. Free YOYO gets rid of extra energy by rotating its ring structures. This is not possible when the rings are tucked in between the base pairs and therefore YOYO will get rid of excess energy by fluorescence instead.

Staining with YOYO will affect the properties of a DNA molecule in several ways. The intercalation of the aromatic rings between the base pairs leads an increase in the contour length of the DNA molecule, with a total increase around 30% at 100 nM [87].

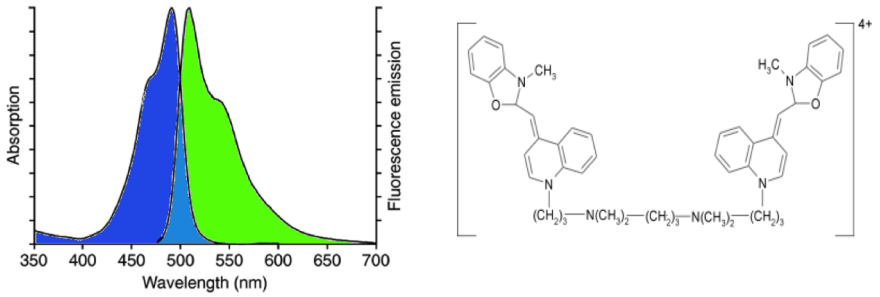

Figure 5.3: LEFT The absorption (blue) and admission (green) spectra of YOYO-1. The absorption shows a peak value at 490 nm whereas the emission spectra shows a peak value at 510 nm. RIGHT Chemical structure of a YOYO-1 molecule.

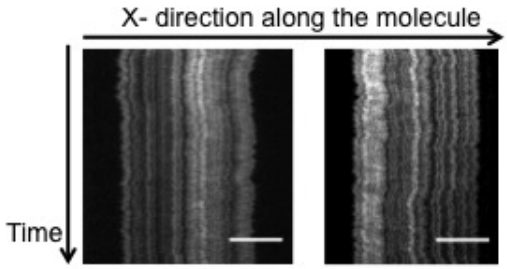

Figure 5.4: Kymographs visualizing the melting pattern along two T4GT7 molecules stretched in 150 x 150 nm grooves. The scale bars are 10 μm.

In addition, YOYO has been shown to increase the melting temperature of DNA by stabilizing the double stranded state [88]. Despite its affect on melting temperature YOYO is ideal for creating a barcode pattern along the DNA by partially melting of the DNA [19]. The reason for this is its extremely low binding affinity for ssDNA together with the large fluorescence enhancement upon binding to dsDNA. When partially melting YOYO stained DNA the dye loosens from the melted single stranded bubbles creating dark areas at the melted parts.

5.3 Image analysis

The movies were analyzed with the help of the free software ImageJ (http://rsbweb.nih.gov/ij/). To create a kymograph/time-trace a region of interest was positioned around each DNA molecule or molecule part to be analyzed. The region was then re-sliced to create a stack where each image represents a row/column in the original image. In the new stack the rows represents time (so each row represents one frame of the original movie). Lastly the kymograph was created by creating a single image showing the average intensity of all the images from the stack. Each row in the kymograph represents a new time and each column a new place along the molecule as is illustrated in figure 5.4.

6 Fluidics

6.1 Fluid mechanics

Newtons second law (eq 6.1) is used to describe the net force on an object.

$$F = ma \tag{6.1}$$

Within classical mechanics the force is assumed to act on the center of gravity of the object and the object is seen as a discrete mass, which gives accurate solutions when studying the overall movement of large objects. However, when studying the internal movement of a fluid (for example the movement of water within a raindrop) Newtons second law needs to be modified since fluids should be seen as a continuos medium. The fluid analog to Newtons second law is called Navier-Stokes equation (here presented in equation 6.2) and describes the velocity fields within a newtonian fluid. A fluid is newtonian if the density, ρ, of the fluid is independent of pressure and the fluids dynamic viscosity, η, is independent of the flow velocity.

$$\rho\left[\frac{d\mathbf{v}}{dt} + (\mathbf{v}\cdot\nabla)\mathbf{v}\right] = -\nabla p + \eta\nabla^2\mathbf{v} + \mathbf{f} \tag{6.2}$$

$\mathbf{v}$ the velocity and $\mathbf{f}$ represents body force densities such as gravity or centrifugal forces. The right hand side of the equation describes the applied force density whereas the left hand side describes the internal acceleration [89]. Due to the nonlinear term Navier-Stokes equation is difficult to solve analytically, but can be simplified under specific conditions [89]. A parameter called Reynolds number, Re, is used to determine if this simplification is possible. Reynolds number is the ratio between the viscous and inertial forces, which can be calculated from equations 6.3 and 6.4 respectively. Here l and v is the characteristic length-scale[1] and velocity of the system, respectively.

$$F_{viscous} = \eta l v \tag{6.3}$$

$$F_{inertial} = \rho l^2 v^2 \tag{6.4}$$

The calculated forces are then combined into a dimensionless ratio to determine Reynolds number [90]

[1] The characteristic length-scale is often defined as the smallest length scale of the system.

$$\frac{F_{internal}}{F_{viscous}} = \frac{\rho l v}{\eta} = Re$$

For $Re \ll 1$ viscous effects dominate over inertial effects and the flow is completely laminar (i.e parallel streamlines) and for $Re \gg 1$ inertial effect are dominating and turbulence occurs [90]. In the macro-world internal forces plays a large roll and we easily get turbulent flow, whereas in the micro world viscous forces are dominating due to the large surface to volume ratio. In situations with completely laminar flow (i.e low Reynolds number) the internal forces can be neglected and Navies-Stokes equation can be simplified into Stokes equation [89]

$$\rho \frac{d\mathbf{v}}{dt} = -\nabla p + \eta \nabla^2 \mathbf{v} + \mathbf{f}$$

This equation is easier to solve than its mother equation and is time-independent meaning that laminar flows are completely reversible. The mass conservation gives the incompressibility condition $\nabla \mathbf{v} = 0$, for incompressible fluids with nearly constant density, such as water [89].

6.2 Flow in a micro-channel

Due to the high surface to volume ratio in micro-channels viscous forces dominates, giving a laminar flow. As in many other fluidic systems the flow velocity is often of interest when working with micro-channels. The flow velocity can be calculated by dividing the flow rate, Q, with the cross sectional area, A, of the tube [90]. The flow rate is in turn determined by dividing the pressure drop, $\triangle P$, with the flow resistance, R [91]. The pressure drop is in general determined experimentally whereas the flow resistance needs to be calculated for each new channel design. It is intuitively clear that the flow resistance increases with decreasing channels diameter and increasing channel length, but what is often less intuitive is how it changes with the shape of the cross-section. For a circular and rectangular cross sections the calculations for determining R are straight forward using equations 6.5 and 6.6 respectively. Here a is the tube radius, w the tube with, h the tube height, L the length of the tube and η the dynamic viscosity of the fluid [91].

$$R = \frac{8\eta L}{\pi a^4} \tag{6.5}$$

$$R = \frac{12\eta L}{w h^3} \tag{6.6}$$

For square cross sections the expression becomes slightly more difficult as is apparent from equation 6.7 presented in reference [91].

$$R = \frac{12\mu L}{w h^3} \left[1 - \frac{h}{w} \left(\frac{192}{\pi^5} \sum_{n=1,3,5}^{\infty} \frac{1}{n^5} \tanh\left(\frac{n\pi w}{2h} \right) \right) \right]^{-1} \tag{6.7}$$

Since micro-channels can have many different shapes on their cross sections a way to approximate the diameter called the hydraulic diameter, D_h, has been developed. This

is calculated with the help of equation 6.8 and is then used in equation 6.5 to get an approximation for the resistance of the channel.

$$D_h = \frac{4 \times \text{cross section area}}{\text{wetted perimeter}} = \frac{4A}{P_{wet}} \tag{6.8}$$

The wetted perimeter, P_{wet} is the part of the inner channel wall in direct contact with the fluid, which for a completely filled channel is simply the inner circumference of the channel [90]. In addition to the resistance calculations the hydraulic diameter is often used as the characteristic length scale for a micro-fluidic channel.

6.3 Mixing in micro-channels

In laminar flow conditions diffusion is the only source of mixing. Therefore, the mixing rate in micro-channels is determined by the flux of particles, **J**, from a higher to a lower concentration through Fick's law:

$$\mathbf{J} = -D\frac{dC}{dx}, \tag{6.9}$$

where C is the concentration of the species and D the diffusion coefficient [90]. For a spherical particle the diffusion coefficient can be determined from Einstein- Stokes equation

$$D = \frac{k_B T}{6\pi r \eta}, \tag{6.10}$$

where k_B is Boltzmann's constant, T the temperature and r the radius of the particle [92]. From equation 6.10 it is clear that small particles diffuse faster than large particles. The average distance, x, traveled by a diffusing particle can be determined from $x = \sqrt{2Dt}$, where t is the travel time [91]. Different micro-fluidic designs for mixing two samples have been presented including long meandering channels for increasing the diffusion time and channels with obstacles forcing the flow into a turbulent state [89].

Mixing by diffusion can be used to create concentration gradients, which can for example be used to determine how the binding behavior of a ligand depends on the concentration of the ligand in the buffer. A Y-shaped channel can be used to create a concentration gradient along the width of the combined channel since the two flows will continue to flow next to each other. The concentration profile for two parallel solutions within a micro-channel can be determined by

$$C(x,y) = \frac{C_0}{2}\left(1 - erf\left(-\frac{y\sqrt{U}}{2\sqrt{Dx}}\right)\right) \tag{6.11}$$

where x is the downstream distance from the converging point, y the transverse coordinate, C_0 is the initial concentration of the solute and U the flow rate [70]. From equation 6.11 it can be concluded that for a given substance an increase in flow rate will cause a steeper concentration profile and a narrower gradient at a certain position along the channel. In addition, it can be seen that a smaller and thereby faster diffusing molecule will lead to a wider gradient and a faster mixing for a specific flow rate.

7 Experimental Details

In this chapter an overview of the experimental setups used in this work are given, for a more detailed description the reader is advised to read reference [37] and chapter 9 in reference [93].

7.1 Microscope setup

For the imaging a custom designed microscope based on a inverted Nikon Eclipse TE2000 was used together with a 100x oil objective with a NA of 1.4. The microscope setup included a motorized xy-stage, motorized shutters, ND filters and two side lamps (one for fluorescence and one for bright filed imaging). Two separate but similar light paths were used to guide the light from the two side lamps towards the sample as shown in figure 7.1. For the epi-fluorescence measurements a mercury short arc lamp (100 W) was used to enable a strong and even illumination and for the bright light illumination a standard halogen lamp was used.

A back-illuminated electron multiplying CCD camera (Andor iXon DV-897) with the capacity to run in a frame-transfer mode was used for light detection and data recording. Frame transfer mode refers to the capacity to acquire data simultaneously as data from the previous frame is read out from the camera. In this way an almost continuos recording is made possible. During this work a frame transfer of 100ms was most commonly used to maximize the light intensity in each frame without getting a blurry image due to thermal fluctuations and conformational changes of the DNA molecule. To minimize thermal noise from the camera it was cooled to $-50°C$ during data collection.

7.2 Buffer solutions

During the melting experiments the buffer solution used was Tris-Borate-EDTA (TBE) in a concentration of 0.05xTBE (4.5 mM Tris, 4.5 mM boric acid and 0.1 mM EDTA). TBE buffer consists of three different parts each with their special function. The first part Tris (tris(hydroxymethyl)aminomethane) is a buffering agent in the pH range between 7.1 and 9.0. Boric acid (H_3BO_3) is a weak acid that improves Tris buffering capabilities. The last ingredient is the chelating agent EDTA (Ethylenedinitrilotetraacetic acid), which is there to suppress DNA damage by scavenging multivalent ions. Scavenging multivalent

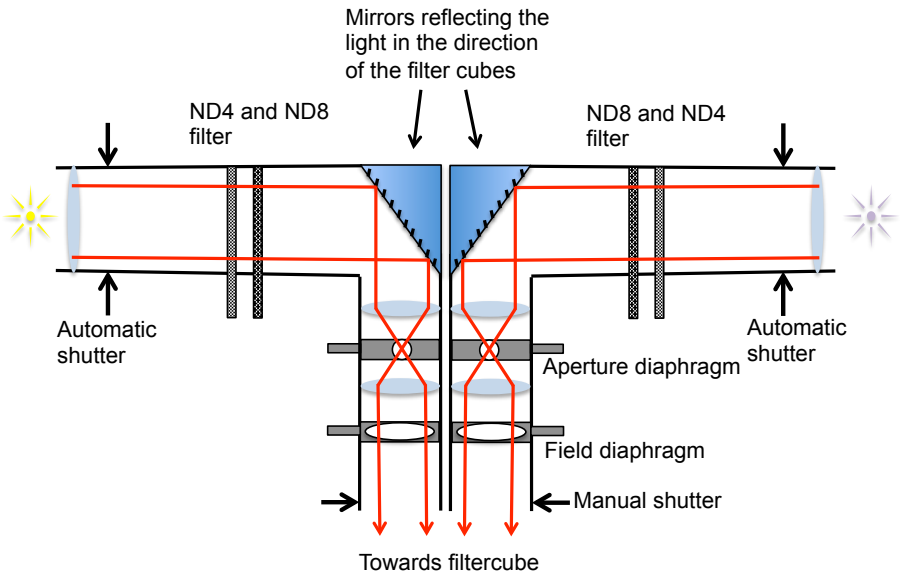

Figure 7.1: Schematic illustration of the light path through the microscope setup used in this study. The ND-filters were used to lower the intensity of the incoming light in order to minimize photo-damage and photo-bleaching of the sample.

ions (such as Ca^{2+} and Mg^{2+}) will deactivate metal-dependent enzymes, for example nucleases, and therefore removing these ions will prevent enzymatic degradation of DNA.

During fluorescence imaging with the cyanine dye YOYO-1, photo damage is often induced in DNA molecules. To prevent this β- mercaptoethanol (BME, $HOCH_2CH_2SH$) is added to the buffer solution before imaging. BME is a reducing agent used to prevent high levels of oxygen radicals, which are often responsible for DNA damage during imaging.

When creating DNA arrays a buffer containing 10 mM Tris pH 8.0 and 100 mM NaCl was used during bilayer creation whereas a buffer consisting 40 mM Tris pH 7.8, 1 mM DTT, 1 mM $MgCl_2$ and 0.2 mg/ml BSA was used after bilayer formation. DTT (dithiothreitol, $C_4H_{10}O_2S_2$) is a redox agent commonly used to reduce disulfide bonds between proteins and thereby prevent intramolecular interactions leading to aggregation of the proteins. BSA is a protein (66,000 Da) with a high stability and low reactivity that here was used for unspecific blocking of the parts of the channel where no bilayer had formed.

7.3 Handling DNA molecules

7.3.1 Handling DNA in nano-channels

For the studies of DNA confined in nano-channels $25x25$ mm^2 big fused silica chips containing a system of micro- and nano-channels were produced as described in paper I. A single chip contained four $1x5$ μm^2 channels connected to reservoirs at the ends. An array of nano-channels (either straight or meandering) spanned between two of the micro-channels. In addition, the melting experiments on T4GT7 were performed in a chip with a nano-slit spanning between the two remaining nano-channels. The nano-slit

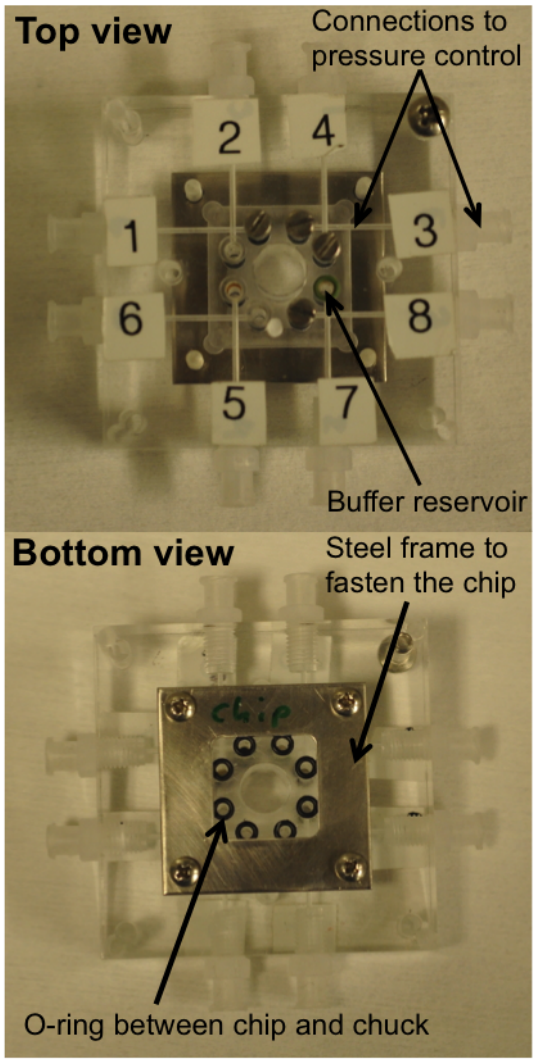

Figure 7.2: Images showing the chuck design.

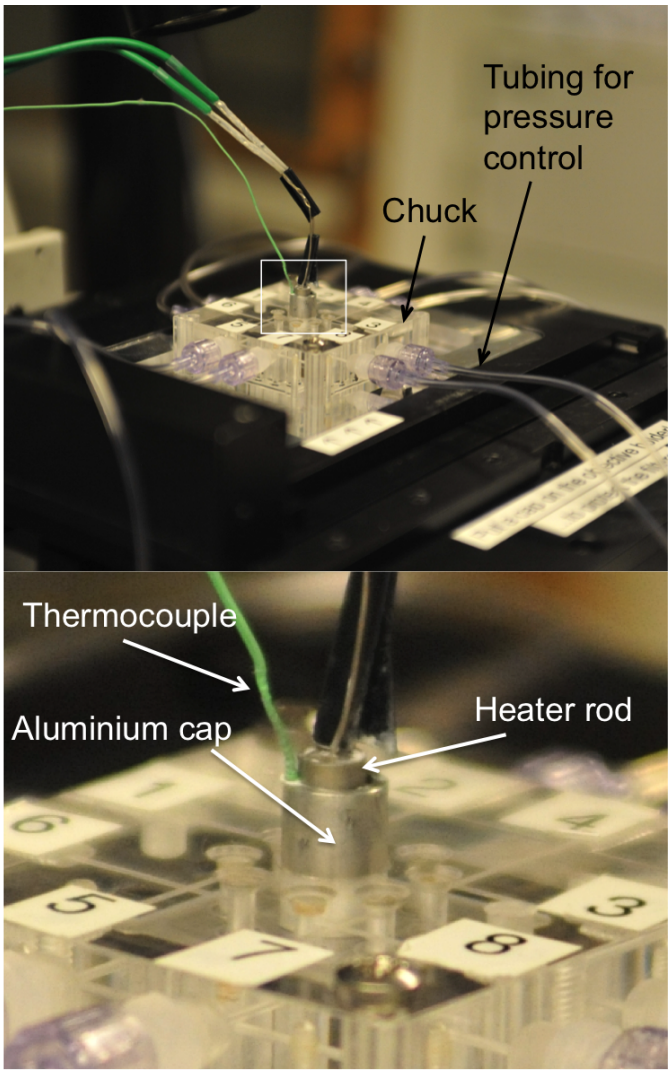

Figure 7.3: TOP Overview of setup for melting experiments. BOTTOM Zoom in of the part inside the white rectangle in the top image showing the heater setup.

spanned perpendicular across the nano-channels to create nano-grooves, which allowed for the free YOYO-1 molecules to diffuse away.

A chip holder (or chuck) was designed to enable manipulation of the DNA molecules within the fused silica chip as well as create a link between the microscope stage and the small chip (figures 7.2 and 7.3). The chuck was made in Zeonor 1060R (Sigolis AB) due to the plastic's low internal fluorescence, high resistance to chemicals and transparency. A transparent chuck eases the detection of unwanted bubbles within the channel system. Furthermore, the chuck was designed with eight separate reservoirs possible to align with the reservoirs on the chip and pipes connecting the top (the side facing away from the chip) of the reservoirs with a system used for pressure manipulation. A stainless steel frame that was carefully screwed into the chuck was used to fasten the chip to the bottom of the chuck. O-rings were placed at the reservoirs between the chip and the chuck to ensure a good connection and avoid leakage. The other end of the reservoirs in the chuck were sealed by screws and again o-rings were used to avoid leakage.

In addition, the chuck was designed with a hole spanning its center that held the heating system used for melting the confined DNA molecules. The heating system consisted of an aluminum cap in which the heater and a thermocouple was placed (figure 7.3). Thermal paste was used at all interfaces to ensure stable heat transfer throughout the system.

The flow within the micro- and nano-channels was controlled by controlling the pressure in each reservoir. In order to keep the oxygen in the sample buffer at a minimum, nitrogen gas was used to change the pressure within the reservoirs. Increasing the pressure in one of the reservoirs connected to a micro-channel lead to a flow in that channel. To force the buffer through the nano-channels or nano-slit the pressure in both of the reservoirs connected to a micro-channel in one end of the nano-channels was increased while the micro-channel in the other end was kept at atmospheric pressure (see figure 7.4). Before the chip was fastened to the chip holder the dry channels were wetted by placing a droplet of buffer on one of the inlet holes to each offimo the micro-channels and allowing the capillary forces to distribute the water within the channel system.

7.3.2 DNA locking

In this study DNA molecules were immobilized within a system of micro- and nano-channels by the introduction of low melting point agarose gel into the channels. Before introduction the agarose gel was melted and mixed with a solution of stained DNA molecules. For the experiments T4GT7 DNA (166 kbp, $L_C = 56.4\,\mu$m, Nippon Gene) stained with YOYO-1 to a ratio of 1 dye to 6 bp was used. The gel was kept melted during the introduction into the micro and nano-channels. Once the gel was equally distributed in the channel system it was quickly cooled to its solid state by placing a piece of ice in contact with backside of the chip. When agarose gel solidifies it creates a fine mesh that reduces the fluctuations of the DNA while still enabling movement of the DNA within the channel system. This gives a dynamic system with a possibility for immobile samples during data collection. Electrophoresis with platinum electrodes placed in two separate reservoirs were used to move the DNA molecules in the channels. The chip used for this study had a design as described above with $1x5\,\mu\text{m}^2$ micro-channels and $400x400\,\text{nm}^2$ nano-channels.

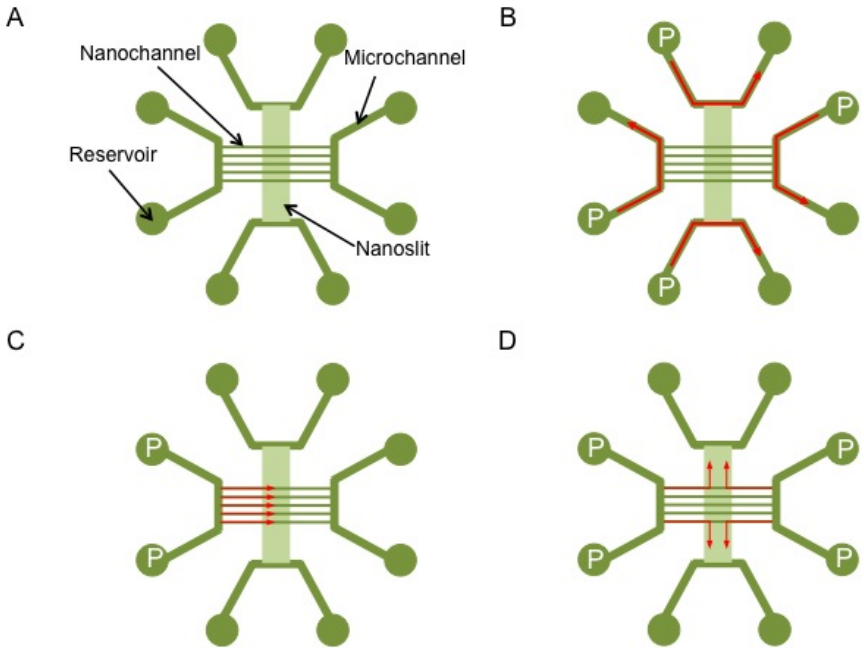

Figure 7.4: A. Schematic illustration of the chip design used in this study. Observe that the slit was only used during measurements on T4GT7. B. Illustration of how the pressure, P, is applied to produce a flow in the micro-channels. C. Illustration of how to create a flow through the nano-channel array. D. Illustration of how the pressure is applied in order to create a flow in the nano-slit. This flow profile was used to load DNA molecules into the nano-grooves (the interconnection between the nano-channels and nano-slit).

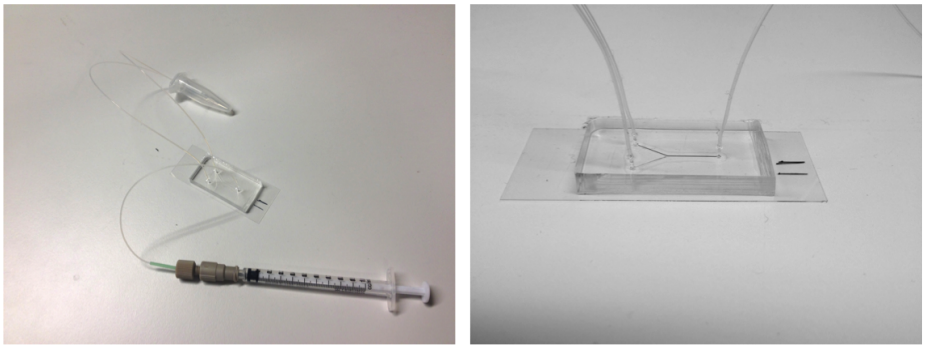

Figure 7.5: LEFT Image of the fluidic setup used for the protein-DNA studies. RIGHT Close up of the flow cell containing the Y-shaped channel used to create a concentration gradient at the measurement region.

7.3.3 DNA extraction from agarose gel

For the single molecule studies of long DNA molecules electrophoretic DNA size standards were purchased (see paper I for further details). Prior to imaging, the DNA molecules were extracted from the agarose gel in which they were purchased by placing a small piece of DNA containing agarose gel in a large volume of buffer. This mixture was left at room temperature (20°C) over night, during which the DNA molecules diffused out of the gel into the buffer. The extraction buffer also contained YOYO-1 molecules to enable simultaneous staining and extraction.

7.3.4 Handling DNA in micro-channels

For the DNA array measurements, flow-cells of polydimethylsiloxane (PDMS) (see figure 7.5) were made as described in paper III. The flow-cells consist of a molded PDMS part bound to a microscope cover slip with dimensions $24x60\,\mathrm{mm}^2$ and $0.13 - 0.19\,\mathrm{mm}$ thick (Mentzel Gläser). The channels had a Y-shape design with two $200\,\mu$m wide inlets and a combined channel with a width of $400\,\mu$m. The channel heigh was $200\,\mu$m all along the channel system.

To access the micro-channel, holes were made at each of the channel ends during molding of the PDMS part. Just prior to experiment PTFE tubings were inserted into inlet holes within the PDMS and syringes, which served as fluid reservoirs, were connected to the free ends of the PTFE tubings. During the sample preparation (including the lipid bilayer creation and attachment of the DNA molecules) the different solutions were pressed directly into the $400\,\mu$m channel by hand. For experiments including a concentration gradient the flow was inverted and syringes connected to the two arms of the Y just prior to imaging. Each of the syringes were connected to separate syringe pumps in order to individually manipulate the two inlet flows.

Before the channel system was used for any DNA experiments FRAP measurements were performed to verify the quality (i.e surface coverage and fluidity) of the bilayer created within our system.

8
Results & Discussion

In this work a new meandering nano-channel design was used to image a 5.7 Mbp long chromosome from *Schizosaccharomyces pombe* (*S.pombe*). A barcode pattern was experimentally created along the elongated chromosomes and part of this barcode matched to a theoretical barcode for the *S.pombe* genome. Melting mapping was brought one step closer to commercialization through the optimization of the time the molecules spent in confinement at a raised temperature. Furthermore, DNA arrays were integrated with Y-shaped micro-channels to create a versatile tool to study DNA behavior and protein-DNA interactions. In a short study it was shown that agarose gel can be used to decrease the fluctuations of a DNA molecule in a nano-channel.

8.1 Paper I: Mapping of intact chromosomes in meandering nano-channels

During fluorescence imaging of stretched DNA molecules, the field of view used (around $82x82\ \mu m^2$ with 100x magnification with our camera) sets a limit to the length of the DNA molecules that can be imaged continuously. For molecules longer than the field of view used, several images are needed to collect data from entire molecule. These images are then stitched together during data analysis, which prevents continuous imaging and therefore processes with short time scales can be difficult to detect.

To solve this problem a channel design including an array of meandering nano-channels spanning between two micro-channels were created. The meandering part of these channels were designed to be 1 mm long and could therefore hold up to 10 Mbp long DNA molecules stretched to 30% extension within one field of view. To minimize stress on the DNA molecules as well as simplify the analysis the meandering part of the nano-channel was designed with 50 μm long straight parallel parts that were connected with soft bends. The bends were in turn designed with a 1 μm long straight part connected to two 90-degree turns.

The increased length of the nano-channels leads to a higher flow resistance of the channels (as described in section 6.2), which leads to decreased flow rates unless the pressure drop across the channels is increased. Since a higher pressure increases the risk for chip breakage and shearing of the molecules the increased resistance was instead compensated for by keeping the inlets of the nano-channels in close proximity to each other.

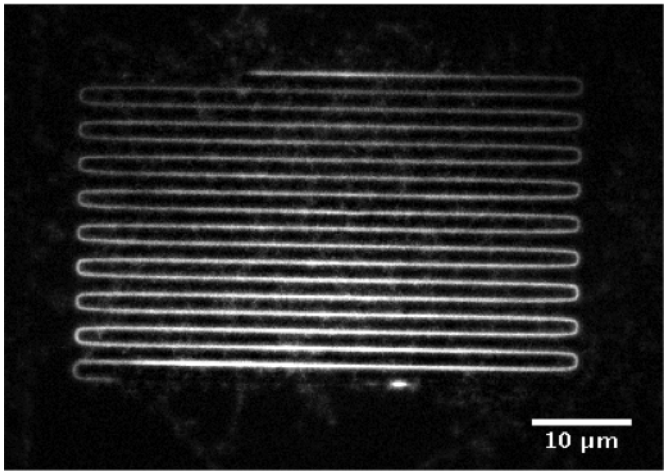

Figure 8.1: The entire 5.7 Mbp long chromosome from *S.Pombe* imaged in a $250x250$ nm meander-channel. The DNA was stained with YOYO-1 to a ratio of 6 bp to 1 dye molecule.

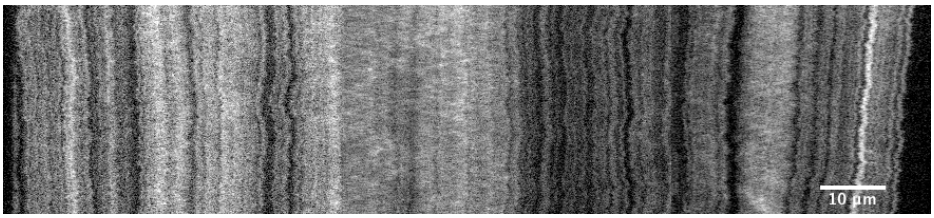

Figure 8.2: Kymograph visualizing the melting pattern along part of a *S.pombe* chromosome stretched in a $250x250$ nm channel. The DNA was stained to a ratio of 1 dye to 6 bp prior to experiments.

Initially, the chips were created with pillar arrays designed to pre-stretch the DNA at the inlets to the meander-channels. However, due to their large size the DNA molecules were already pre-stretched by the flow in the micro-channels, which eliminated the need for a pillar array.

During this work meandering nano-channels were successfully used to image a 5.7Mbp long chromosome from *S.pombe* (figure 8.1). At the time of imaging the molecule has not yet reached the equilibrium elongation and is therefore extended to 50% instead of its equilibrium stretching of 30%. The slow relaxation of long DNA molecules enables imaging of features along the DNA chain before an equilibrium state is reached. Due to the long relaxation time the molecules does not move considerably during the capture of a single frame, a movement that serves to unfocus images of shorter molecules with faster relaxation times.

To show the biological relevance of this chip design a mapping pattern was created along the elongated chromosomes (as shown in figure 8.2) and part of this barcode was matched to a theoretical barcode for the *S.pombe* genome.

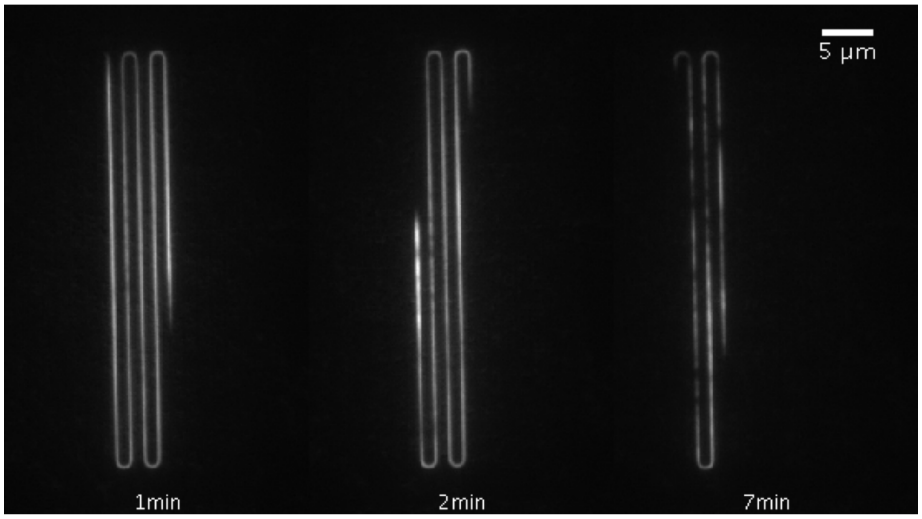

Figure 8.3: Time evolution of part of a *S.pombe* chromosome. It is clear that the pattern develops during the first 7 minutes after introduced into an area with increased temperature.

8.2 Paper II: Time dependence of DNA melting mapping

An optimization of melting mapping (described in section 3.2.3) was performed with respect to the occupation time of the DNA molecules in the nano-grooves and thereby their time at a higher temperature. T4GT7 DNA molecules were introduced into the nano-grooves, which were constantly held at 31 °C, and imaged at 5 min intervals during 15 min. In this way the evolution of the melting pattern was followed together with the total intensity of the molecules. The total intensity of the molecules was observed to decrease both in the absence and in the presence of light and in room temperature as well as at higher temperatures. At raised temperatures the rate of intensity decrease was observed to decrease with time, but at room temperature the intensity decrease was constant with time. At higher temperatures unbinding of the dye due to melting will contribute to the decrease in intensity, although this does not explain the intensity drops observed at room temperature. It will however explain the change in the rate of intensity decrease at raised temperatures. One theory to explain the bleaching phenomena is the close proximity to the negatively charged walls which attracts the dye molecules. A clear increase in background fluorescence observed from the channel walls when the molecules were flushed away after completing the measurements supports the theory. In addition, the mapping pattern, due to partial melting of the DNA molecule, developed during a time period of at least 10 min before settling into a steady state. These long melting times were observed for T4GT7 in nano-grooves as well as for long DNA molecules in meandering channels (figure 8.3). Since the breathing dynamics has been shown to occur within seconds, our theory is that the extended melting times could be due to electrostatic interactions between YOYO-1 and the single strands of the DNA molecule.

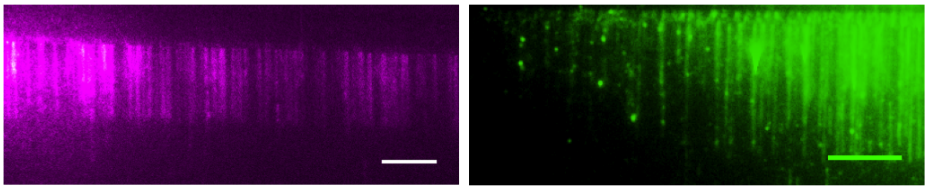

Figure 8.4: LEFT DNA array of λ-DNA molecules stained with YOYO-1 to a ratio of 1 dye to 100 bases. RIGHT An array after introduction of Rad51 in a concentration gradient. It is clear that the low Rad51 concentrations have lead to individual nucleation sited along the molecules in the array. The scale bars are 10 μm.

8.3 Paper III: Probing concentration-dependent behavior of DNA-binding proteins on a single molecule level illustrated by repair protein Rad51

DNA arrays were integrated with Y-shaped micro-channels to create a versatile tool to study DNA-protein interactions or DNA molecules response to environmental changes.

A gradient of the fluorescent dye fluorescein was used to visualize the robustness and stability of the concentration gradient within the measurement channel, whereas YOYO-1 were used to show the effects of a concentration gradient across a dense DNA array. As expected, the molecules exposed to higher YOYO-1 concentrations in the buffer showed a higher intensity and increased lengths compared to molecules exposed to lower concentrations of YOYO-1.

In addition, a concentration gradient of Rad51 was used to study how the concentration affect its binding to DNA. At low Rad51 concentrations only individual nucleation sites of Rad51 could be seen along the DNA molecules, whereas continuos filaments of Rad51 was completely dominating at higher concentrations. The complete protein coverage at higher concentrations lead to an elongation around 36% of the DNA molecules. By correlating the concentration of Rad51 on the DNA molecules with the Rad51 concentration in the buffer it is possible to directly probe the binding behavior of Rad51 to DNA. This correlation showed a linear behavior, meaning that no cooperativity of the binding was observed at the Rad51 concentrations used in this study (figure 8.4).

8.4 DNA locking

Agarose gel was used to decrease the fluctuations of a DNA molecule within a micro- and nano-channel system, while keeping the mobility of the molecules. As long as the gel was molten no clear reduction of the DNA movements (due to thermal fluctuations and conformational changes) could be seen (figure 8.5a). Although as soon as the gel was cooled into a solid state a reduction of the movements was clearly observed for DNA molecules in both micro- and nano-channels (figure 8.5b and c). The fine mesh created during gel solidification increases the confinement of the DNA leading to a decrease in conformational changes. Also, the low temperatures achieved by cooling with ice slightly lowers the thermal fluctuations.

To prove that the molecules were still mobile within the channel system a voltage was applied across the nano-channel array. The voltage gave rise to an electrophoretic

movement of the DNA molecules along the nano-channels as shown in figure 8.5d.

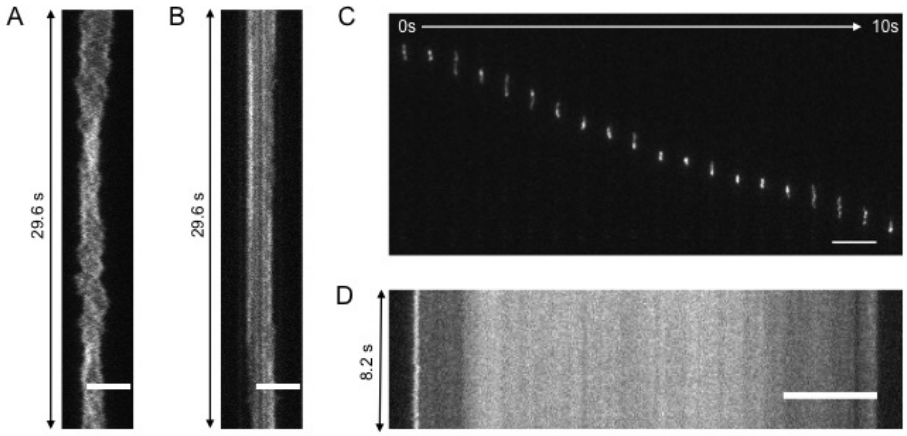

Figure 8.5: DNA immobilization by agarose gel in micro- and nano-channels. Experiments were performed with T4GT7 DNA molecules stained with YOYO-1 to a ratio of 1 dye to 6 bp. A. Kymograph visualizing part of a T4GT7 DNA molecule inside a $400x400$ nm large channel containing molten agarose gel. B. Kymograph of the same molecule as in A after rapid solidification of the agarose gel. C. Electrophoretic movement of a DNA molecule inside a $400x400$ nm nano-channel containing solid agarose gel. D. Kymograph of a hydrodynamically stretched molecule immobilized within a microchannel by solid agarose gel. In A and B the scale bars are 5 μm, whereas in C and D the scale bars are 10 μm.

9
Conclusions & Outlook

A meandering nano-channel design extensively eases the imaging of DNA molecules in the Mbp range. Due to the slow relaxation of longer DNA molecules it is possible to image such long molecules with a high resolution before they are fully relaxed. This can be utilized to increase the resolution of for example a mapping pattern created along the elongated DNA molecules. Furthermore, we show that a a DNA molecule in the Mbp range is stretched by the shear forces from the flow in the micro-channels, which eliminates the need for pre-stretching prior to introduction into the nano-channels.

It was shown that a barcode pattern could be created by local melting of YOYO-1 stained molecules confined in a meandering nano-channel. A mapping pattern with a resolution of around 1 kbp along un interrupted elongated chromosomes allows for determination of the the number and placement of repetitive parts along the chromosome. Something that is impossible with existing mapping methods with lower resolution or in methods where only shorter sequences are analyzed. Furthermore, the high resolution mapping that can be achieved on stretched DNA molecules can be used for identification of microorganisms as well as large genomic rearrangements. With the appropriate surface passivation, this new handling method could potentially be used to study DNA protein interactions along entire eukaryotic chromosomes and in the future lead to automated microfluidic systems for analysis of DNA from individual microorganisms with applications in diagnostics of infectious disease and characterization of the human micro-biome. However, before the system can be automated more studies are needed to gain a deeper understanding about the dynamic behavior of Mbp long DNA molecules in confinement. Studies would include measurements of the relaxation times of DNA molecules extended by shear forces upon entry into the nano-channels, recoil times for molecules only partially introduced into a nano-channel as well as the size of the fluctuations around the mean polymer extension.

Imaging of single molecules with an acceptable signal to noise ratio requires a high fluorescence intensity from the molecules. Here we show that the intensity of YOYO-1 stained molecules elongated in nano-grooves decreases in the absence as well as in the presence of illumination, and therefore bleaching is not the only source working to decrease the total intensity of the DNA. Furthermore, it was shown that the equilibrium time for a melting pattern along elongated DNA molecules lies in the minute time scale. These results can be used to achieve a higher correlation to theoretical calculations of the barcode, and thereby more reliable results, which is a prerecuisit for commercialization.

Additional studies are needed in order to fully understand the kinetics of DNA-YOYO

interactions in a confined space with negative walls. Future studies would include longer time series as well additional temperatures to gain a broader view of the process. It would also most likely be necessary to improve the way used to determine the number of YOYO molecules bound to the DNA molecule, since the background fluorescence can cause difficulties during analysis.

The Y-shaped microfluidic channel design used in combination with a DNA array provides a dynamic and yet stable system for investigations of DNA-protein interactions and dynamics. With this high throughput system it is possible to simultaneously follow time and concentration trajectories. As a proof of concept, the binding behavior for Rad51 was investigated as function of its buffer concentration. These studies points at an uncooperative binding behavior for Rad51 at the concentrations used. Additional investigations would include a higher range of concentrations as well as investigations with longer single stranded DNA parts. In the future this method can be used to answer a wide range of biologically relevant questions about DNA-protein or interaction kinetics or the reaction of DNA molecules to environmental changes.

With the correct surface passivation nano-channels can potentially be used to study DNA protein interactions. For example, nano-channels have been coated with a lipid bilayer as a first step to study protein DNA interactions in these systems [74].

In this work we showed that introduction of agarose gel into nano-channels can be used to decrease the fluctuations of the DNA molecules. The molecules were still mobile within the system and buffer could be flushed through the solidified gel. This sets the basics for a dynamic system that can be used to study the reaction of a DNA molecule to changes in buffer conditions as well as for imaging DNA molecules elongated in nano-channels with nanoscopy methods [94, 95]. Although, more studies are needed in order to gain a better understanding of the system and to determine the optimal cooling rates and gel concentrations.

Bibliography

[1] R. Glaser, *Biophysics: An Introduction*. Springer Berlin Heidelberg, 2012.

[2] M. A. Ratner and D. Ratner, *Nanotechnology[: A Gentle Introduction to the Next Big Idea*. Safari Tech Books Online, Pearson Prentice-Hall Prof, 2003.

[3] A. M. van Oijen, "Cutting the forest to see a single tree?," *Nature chemical biology*, vol. 4, pp. 440–3, Aug. 2008.

[4] A. a. Deniz, S. Mukhopadhyay, and E. a. Lemke, "Single-molecule biophysics: at the interface of biology, physics and chemistry.," *Journal of the Royal Society, Interface / the Royal Society*, vol. 5, pp. 15–45, Jan. 2008.

[5] J. Watson and F. Crick, "Molecular structure of nucleic acids - A Structure for Deoxyribose Nucleic Acid," *Nature*, vol. 171, pp. 737–738, 1953.

[6] B. Alberts, D. Bray, K. Hopkin, A. Johnson, J. Lewis, M. Raff, K. Roberts, and P. Walter, *Essential cell biology*. No. v. 1, Garland Science Pub., 2004.

[7] P. Stankiewicz and J. R. Lupski, "Genome architecture, rearrangements and genomic disorders.," *Trends in genetics : TIG*, vol. 18, pp. 74–82, Feb. 2002.

[8] a. J. Cuticchia, "Future vision of the GDB human genome database.," *Human mutation*, vol. 15, pp. 62–7, Jan. 2000.

[9] E. S. Lander, L. M. Linton, B. Birren, C. Nusbaum, M. C. Zody, J. Baldwin, K. Devon, K. Dewar, M. Doyle, W. FitzHugh, R. Funke, D. Gage, K. Harris, a. Heaford, J. Howland, L. Kann, J. Lehoczky, R. LeVine, P. McEwan, K. McKernan, J. Meldrim, J. P. Mesirov, C. Miranda, W. Morris, J. Naylor, C. Raymond, M. Rosetti, R. Santos, a. Sheridan, C. Sougnez, N. Stange-Thomann, N. Stojanovic, a. Subramanian, D. Wyman, J. Rogers, J. Sulston, R. Ainscough, S. Beck, D. Bentley, J. Burton, C. Clee, N. Carter, a. Coulson, R. Deadman, P. Deloukas, a. Dunham, I. Dunham, R. Durbin, L. French, D. Grafham, S. Gregory, T. Hubbard, S. Humphray, a. Hunt, M. Jones, C. Lloyd, a. McMurray, L. Matthews, S. Mercer, S. Milne, J. C. Mullikin, a. Mungall, R. Plumb, M. Ross, R. Shownkeen, S. Sims, R. H. Waterston, R. K. Wilson, L. W. Hillier, J. D. McPherson, M. a. Marra, E. R. Mardis, L. a. Fulton, a. T. Chinwalla, K. H. Pepin, W. R. Gish, S. L. Chissoe, M. C. Wendl, K. D. Delehaunty, T. L. Miner, a. Delehaunty, J. B. Kramer, L. L. Cook, R. S. Fulton, D. L. Johnson, P. J. Minx, S. W. Clifton, T. Hawkins, E. Branscomb, P. Predki, P. Richardson, S. Wenning, T. Slezak, N. Doggett, J. F. Cheng, a. Olsen, S. Lucas, C. Elkin, E. Uberbacher, M. Frazier, R. a. Gibbs, D. M. Muzny, S. E. Scherer, J. B. Bouck, E. J. Sodergren, K. C. Worley, C. M. Rives, J. H. Gorrell, M. L. Metzker, S. L. Naylor, R. S. Kucherlapati, D. L. Nelson, G. M. Weinstock, Y. Sakaki, a. Fujiyama, M. Hattori, T. Yada, a. Toyoda, T. Itoh, C. Kawagoe, H. Watanabe, Y. Totoki, T. Taylor, J. Weissenbach, R. Heilig, W. Saurin, F. Artiguenave, P. Brottier, T. Bruls, E. Pelletier, C. Robert, P. Wincker, D. R. Smith, L. Doucette-Stamm, M. Rubenfield, K. Weinstock, H. M. Lee, J. Dubois, a. Rosenthal, M. Platzer,

G. Nyakatura, S. Taudien, a. Rump, H. Yang, J. Yu, J. Wang, G. Huang, J. Gu, L. Hood, L. Rowen, a. Madan, S. Qin, R. W. Davis, N. a. Federspiel, a. P. Abola, M. J. Proctor, R. M. Myers, J. Schmutz, M. Dickson, J. Grimwood, D. R. Cox, M. V. Olson, R. Kaul, N. Shimizu, K. Kawasaki, S. Minoshima, G. a. Evans, M. Athanasiou, R. Schultz, B. a. Roe, F. Chen, H. Pan, J. Ramser, H. Lehrach, R. Reinhardt, W. R. McCombie, M. de la Bastide, N. Dedhia, H. Blöcker, K. Hornischer, G. Nordsiek, R. Agarwala, L. Aravind, J. a. Bailey, a. Bateman, S. Batzoglou, E. Birney, P. Bork, D. G. Brown, C. B. Burge, L. Cerutti, H. C. Chen, D. Church, M. Clamp, R. R. Copley, T. Doerks, S. R. Eddy, E. E. Eichler, T. S. Furey, J. Galagan, J. G. Gilbert, C. Harmon, Y. Hayashizaki, D. Haussler, H. Hermjakob, K. Hokamp, W. Jang, L. S. Johnson, T. a. Jones, S. Kasif, a. Kaspryzk, S. Kennedy, W. J. Kent, P. Kitts, E. V. Koonin, I. Korf, D. Kulp, D. Lancet, T. M. Lowe, a. McLysaght, T. Mikkelsen, J. V. Moran, N. Mulder, V. J. Pollara, C. P. Ponting, G. Schuler, J. Schultz, G. Slater, a. F. Smit, E. Stupka, J. Szustakowski, D. Thierry-Mieg, J. Thierry-Mieg, L. Wagner, J. Wallis, R. Wheeler, a. Williams, Y. I. Wolf, K. H. Wolfe, S. P. Yang, R. F. Yeh, F. Collins, M. S. Guyer, J. Peterson, a. Felsenfeld, K. a. Wetterstrand, a. Patrinos, M. J. Morgan, P. de Jong, J. J. Catanese, K. Osoegawa, H. Shizuya, S. Choi, Y. J. Chen, and J. Szustakowki, "Initial sequencing and analysis of the human genome.," *Nature*, vol. 409, pp. 860–921, Feb. 2001.

[10] D. a. Wheeler, M. Srinivasan, M. Egholm, Y. Shen, L. Chen, A. McGuire, W. He, Y.-J. Chen, V. Makhijani, G. T. Roth, X. Gomes, K. Tartaro, F. Niazi, C. L. Turcotte, G. P. Irzyk, J. R. Lupski, C. Chinault, X.-z. Song, Y. Liu, Y. Yuan, L. Nazareth, X. Qin, D. M. Muzny, M. Margulies, G. M. Weinstock, R. a. Gibbs, and J. M. Rothberg, "The complete genome of an individual by massively parallel DNA sequencing.," *Nature*, vol. 452, pp. 872–6, Apr. 2008.

[11] J. O. J. Tegenfeldt, C. Prinz, H. Cao, S. Chou, W. W. W. Reisner, R. Riehn, Y. Y. M. Wang, E. E. C. Cox, J. J. C. Sturm, P. Silberzan, Others, and R. H. Austin, "The dynamics of genomic-length DNA molecules in 100-nm channels," *Proceedings of the National Academy of Sciences of the United States of America*, vol. 101, no. 30, p. 10979, 2004.

[12] T. Su, S. K. Das, M. Xiao, and P. K. Purohit, "Transition between two regimes describing internal fluctuation of DNA in a nanochannel.," *PloS one*, vol. 6, p. e16890, Jan. 2011.

[13] W. Reisner, K. Morton, R. Riehn, Y. Wang, Z. Yu, M. Rosen, J. Sturm, S. Chou, E. Frey, and R. Austin, "Statics and Dynamics of Single DNA Molecules Confined in Nanochannels," *Physical Review Letters*, vol. 94, p. 196101, May 2005.

[14] J. T. Mannion, C. H. Reccius, J. D. Cross, and H. G. Craighead, "Conformational analysis of single DNA molecules undergoing entropically induced motion in nanochannels.," *Biophysical journal*, vol. 90, pp. 4538–45, June 2006.

[15] Y. M. Wang, J. O. Tegenfeldt, W. Reisner, R. Riehn, X.-J. Guan, L. Guo, I. Golding, E. C. Cox, J. Sturm, and R. H. Austin, "Single-molecule studies of repressor-DNA interactions show long-range interactions.," *Proceedings of the National Academy of Sciences of the United States of America*, vol. 102, pp. 9796–801, July 2005.

[16] C. Zhang, P. G. Shao, J. a. van Kan, and J. R. C. van der Maarel, "Macromolecular crowding induced elongation and compaction of single DNA molecules confined in a nanochannel.," *Proceedings of the National Academy of Sciences of the United States of America*, vol. 106, pp. 16651–6, Sept. 2009.

[17] R. Riehn, M. Lu, Y.-M. Wang, S. F. Lim, E. C. Cox, and R. H. Austin, "Restriction mapping in nanofluidic devices.," *Proceedings of the National Academy of Sciences of the United States of America*, vol. 102, pp. 10012–6, July 2005.

[18] L. K. Nyberg, F. Persson, J. Berg, J. Bergström, E. Fransson, L. Olsson, M. Persson, A. Stå lnacke, J. Wigenius, J. O. Tegenfeldt, and F. Westerlund, "A single-step competitive binding assay for mapping of single DNA molecules.," *Biochemical and biophysical research communications*, vol. 417, pp. 404–8, Jan. 2012.

[19] W. Reisner, N. B. Larsen, A. Silahtaroglu, A. Kristensen, N. Tommerup, J. O. Tegenfeldt, and H. Flyvbjerg, "Single-molecule denaturation mapping of DNA in nanofluidic channels.," *Proceedings of the National Academy of Sciences of the United States of America*, vol. 107, pp. 13294–9, July 2010.

[20] E. T. Lam, A. Hastie, C. Lin, D. Ehrlich, S. K. Das, M. D. Austin, P. Deshpande, H. Cao, N. Nagarajan, M. Xiao, and P.-Y. Kwok, "Genome mapping on nanochannel arrays for structural variation analysis and sequence assembly.," *Nature biotechnology*, vol. 30, pp. 771–6, Aug. 2012.

[21] R. Marie and A. Kristensen, "Nanofluidic devices towards single DNA molecule sequence mapping.," *Journal of biophotonics*, 2012.

[22] J. P. Beech, S. H. Holm, K. Adolfsson, and J. O. Tegenfeldt, "Sorting cells by size, shape and deformability," *Lab on a Chip*, vol. 12, no. 6, pp. 1048–1051, 2012.

[23] E. Y. Chan, N. M. Goncalves, R. A. Haeusler, A. J. Hatch, J. W. Larson, A. M. Maletta, G. R. Yantz, E. D. Carstea, M. Fuchs, G. G. Wong, S. R. Gullans, and R. Gilmanshin, "DNA Mapping Using Microfluidic Stretching and Single-Molecule Detection of Fluorescent Site-Specific Tags," *Genome Research*, vol. 14, no. 6, pp. 1137–1146, 2004.

[24] C. S. Effenhauser, G. J. Bruin, a. Paulus, and M. Ehrat, "Integrated capillary electrophoresis on flexible silicone microdevices: analysis of DNA restriction fragments and detection of single DNA molecules on microchips.," *Analytical chemistry*, vol. 69, pp. 3451–7, Sept. 1997.

[25] P. Jönsson, A. Gunnarsson, and F. Höök, "Accumulation and separation of membrane-bound proteins using hydrodynamic forces.," *Analytical chemistry*, vol. 83, pp. 604–11, Jan. 2011.

[26] A. Granéli, C. C. Yeykal, T. K. Prasad, and E. C. Greene, "Organized arrays of individual DNA molecules tethered to supported lipid bilayers.," *Langmuir : the ACS journal of surfaces and colloids*, vol. 22, pp. 292–9, Jan. 2006.

[27] T. Fazio, M.-L. Visnapuu, S. Wind, and E. C. Greene, "DNA curtains and nanoscale curtain rods: high-throughput tools for single molecule imaging.," *Langmuir : the ACS journal of surfaces and colloids*, vol. 24, pp. 10524–31, Sept. 2008.

[28] A. Granéli, C. C. Yeykal, R. B. Robertson, and E. C. Greene, "Long-distance lateral diffusion of human Rad51 on double-stranded DNA.," *Proceedings of the National Academy of Sciences of the United States of America*, vol. 103, pp. 1221–6, Jan. 2006.

[29] T. K. Prasad, C. C. Yeykal, and E. C. Greene, "Visualizing the assembly of human Rad51 filaments on double-stranded DNA.," *Journal of molecular biology*, vol. 363, pp. 713–28, Oct. 2006.

[30] J. M. Berg, J. L. Tymoczko, and L. Stryer, *Biochemistry.* W. H. Freeman, 2010.

[31] R. T. Gregory, "Animal Genome Size Database," 2013. http://www.genomesize.com/.

[32] A. Link and M. Olson, "Physical Map of the Saccharomyces cerevisiae Genome at 110-Kilobase Resolution," *Genetics Society of America*, vol. 127, pp. 681–698, 1991.

[33] F. R. Blattner, "The Complete Genome Sequence of Escherichia coli K-12," *Science*, vol. 277, pp. 1453–1462, Sept. 1997.

[34] J. Miné, L. Disseau, M. Takahashi, G. Cappello, M. Dutreix, and J.-L. Viovy, "Real-time measurements of the nucleation, growth and dissociation of single Rad51-DNA nucleoprotein filaments.," *Nucleic acids research*, vol. 35, pp. 7171–87, Jan. 2007.

[35] J. Hilario, I. Amitani, R. J. Baskin, and S. C. Kowalczykowski, "Direct imaging of human Rad51 nucleoprotein dynamics on individual DNA molecules.," *Proceedings of the National Academy of Sciences of the United States of America*, vol. 106, pp. 361–8, Jan. 2009.

[36] E. M. Zaitseva, E. N. Zaitsev, and S. C. Kowalczykowski, "The DNA binding properties of Saccharomyces cerevisiae Rad51 protein.," *The Journal of biological chemistry*, vol. 274, pp. 2907–15, Jan. 1999.

[37] F. Persson and J. O. Tegenfeldt, "DNA in nanochannels–directly visualizing genomic information.," *Chemical Society reviews*, vol. 39, pp. 985–99, Mar. 2010.

[38] W. Reisner, J. N. Pedersen, and R. H. Austin, "DNA confinement in nanochannels: physics and biological applications.," *Reports on progress in physics. Physical Society (Great Britain)*, vol. 75, Oct. 2012.

[39] V. A. Bloomfield, D. M. Crothers, and J. Ignacio Tinoco, *Nucleic Acids: Structures, Properties, and Functions.* Univ. Science Books, 2000.

[40] P. G. de Gennes, *Scaling concepts in polymer physics.* CORNELL University Press, 1979.

[41] W. Reisner, J. Beech, N. Larsen, H. Flyvbjerg, A. Kristensen, and J. Tegenfeldt, "Nanoconfinement-Enhanced Conformational Response of Single DNA Molecules to Changes in Ionic Environment," *Physical Review Letters*, vol. 99, p. 058302, Aug. 2007.

[42] T. W. Burkhardt, "Free energy of a semiflexible polymer in a tube and statistics of a randomly-accelerated particle," *Journal of Physics A: Mathematical and General*, vol. 30, no. 7, p. L167, 1997.

[43] Y. Yang, T. W. Burkhardt, and G. Gompper, "Free energy and extension of a semiflexible polymer in cylindrical confining geometries," *Physical Review E*, vol. 76, p. 11804, July 2007.

[44] D. Stigter, "Wall effects on DNA stretch and relaxation.," *Biophysical chemistry*, vol. 101-102, pp. 447–59, Dec. 2002.

[45] S. Turner, M. Cabodi, and H. Craighead, "Confinement-Induced Entropic Recoil of Single DNA Molecules in a Nanofluidic Structure," *Physical Review Letters*, vol. 88, p. 128103, Mar. 2002.

[46] O. Bakajin, T. Duke, C. Chou, S. Chan, R. Austin, and E. Cox, "Electrohydrodynamic Stretching of DNA in Confined Environments," *Physical Review Letters*, vol. 80, pp. 2737–2740, Mar. 1998.

[47] R. H. Garrett and C. M. Grisham, *Biochemistry*. Available Titles CengageNOW Series, Brooks/Cole Publishing Company, 2010.

[48] J. D. Watson and F. H. C. Crick, "the Structure of Dna," *Cold Spring Harbor Symposia on Quantitative Biology*, vol. 18, pp. 123–131, Jan. 1953.

[49] S. G. Delcourt and R. D. Blake, "Stacking energies in DNA.," *The Journal of biological chemistry*, vol. 266, pp. 15160–9, Aug. 1991.

[50] G. Altan-Bonnet, A. Libchaber, and O. Krichevsky, "Bubble Dynamics in Double-Stranded DNA," *Physical Review Letters*, vol. 90, p. 138101, Apr. 2003.

[51] T. Ambjörnsson, S. K. Banik, O. Krichevsky, and R. Metzler, "Breathing dynamics in heteropolymer DNA.," *Biophysical journal*, vol. 92, pp. 2674–84, Apr. 2007.

[52] K. P. N. Murthy and G. M. Schütz, "Mean bubble formation time in DNA denaturation," *EPL (Europhysics Letters)*, vol. 96, p. 68003, Dec. 2011.

[53] C. Sadhu, S. Dutta, and K. P. Gopinathan, "Influence of formamide on the thermal stability of DNA," *Journal of Biosciences*, vol. 6, pp. 817–821, Dec. 1984.

[54] R. Metzler, T. Ambjörnsson, A. Hanke, and H. C. Fogedby, "Single DNA denaturation and bubble dynamics.," *Journal of physics. Condensed matter : an Institute of Physics journal*, vol. 21, p. 034111, Jan. 2009.

[55] R. D. Blake and S. G. Delcourt, "Thermodynamic effects of formamide on DNA stability.," *Nucleic acids research*, vol. 24, pp. 2095–103, June 1996.

[56] F. Sanger, "DNA sequencing with chain-terminating inhibitors," *Proceedings of the ...*, vol. 74, no. 12, pp. 5463–5467, 1977.

[57] K. M. Wilson and J. M. Walker, *Principles and techniques of biochemistry and molecular biology*. Principles and Techniques of Biochemistry and Molecular Biology, CAMBRIDGE University Press, 2010.

[58] S. Marsh, *Pyrosequencing protocols*. Methods in Molecular Biology Series, Humana Press, 2007.

[59] J. Shendure and H. Ji, "Next-generation DNA sequencing.," *Nature Biotechnology*, vol. 26, no. 10, pp. 1135–1145, 2008.

[60] E. R. Mardis, "Next-generation DNA sequencing methods.," *Annual review of genomics and human genetics*, vol. 9, pp. 387–402, Jan. 2008.

[61] W. Bickmore, "Karyotype Analysis and Chromosome Banding," *eLS*, 2001.

[62] T. Strachan and A. P. Read, *Human Molecular Genetics Three*. Garland Publishing, Incorporated, 2004.

[63] M. B. Keagle and S. L. Gersen, *The principles of clinical cytogenetics*. Humana Press Incorporated, 2005.

[64] M. Heiskanen, O. Kallioniemi, and a. Palotie, "Fiber-FISH: experiences and a refined protocol.," *Genetic analysis : biomolecular engineering*, vol. 12, pp. 179–84, Mar. 1996.

[65] J. Jing, J. Reed, J. Huang, X. Hu, V. Clarke, J. Edington, D. Housman, T. S. Anantharaman, E. J. Huff, B. Mishra, B. Porter, a. Shenker, E. Wolfson, C. Hiort, R. Kantor, C. Aston, and D. C. Schwartz, "Automated high resolution optical mapping using arrayed, fluid-fixed DNA molecules.," *Proceedings of the National Academy of Sciences of the United States of America*, vol. 95, pp. 8046–51, July 1998.

[66] M. Xiao, A. Phong, C. Ha, T.-F. Chan, D. Cai, L. Leung, E. Wan, A. L. Kistler, J. L. DeRisi, P. R. Selvin, and P.-Y. Kwok, "Rapid DNA mapping by fluorescent single molecule detection.," *Nucleic acids research*, vol. 35, p. e16, Jan. 2007.

[67] B. Teague, M. S. Waterman, S. Goldstein, K. Potamousis, S. Zhou, S. Reslewic, D. Sarkar, A. Valouev, C. Churas, J. M. Kidd, S. Kohn, R. Runnheim, C. Lamers, D. Forrest, M. a. Newton, E. E. Eichler, M. Kent-First, U. Surti, M. Livny, and D. C. Schwartz, "High-resolution human genome structure by single-molecule analysis.," *Proceedings of the National Academy of Sciences of the United States of America*, vol. 107, pp. 10848–53, June 2010.

[68] T. T. Perkins, S. R. Quake, D. E. Smith, and S. Chu, "Relaxation of a single DNA molecule observed by optical microscopy.," *Science (New York, N.Y.)*, vol. 264, pp. 822–6, May 1994.

[69] R. G. Larson, T. T. Perkins, D. E. Smith, and S. Chu, "Hydrodynamics of DNA molecule in a flow field," vol. 55, no. 2, pp. 1794–1797, 1997.

[70] E. Eriksson, J. Enger, B. Nordlander, N. Erjavec, K. Ramser, M. Goksör, S. Hohmann, T. Nyström, and D. Hanstorp, "A microfluidic system in combination with optical tweezers for analyzing rapid and reversible cytological alterations in single cells upon environmental changes.," *Lab on a chip*, vol. 7, pp. 71–6, Jan. 2007.

[71] a. J. Bhattacharyya and M. Feingold, "Single molecule study of the reaction between DNA and formamide.," *Talanta*, vol. 55, pp. 943–9, Dec. 2001.

[72] T.-F. Chan, C. Ha, A. Phong, D. Cai, E. Wan, L. Leung, P.-Y. Kwok, and M. Xiao, "A simple DNA stretching method for fluorescence imaging of single DNA molecules.," *Nucleic acids research*, vol. 34, p. e113, Jan. 2006.

[73] K. Glasmästar, C. Larsson, F. Höök, and B. Kasemo, "Protein adsorption on supported phospholipid bilayers.," *Journal of colloid and interface science*, vol. 246, pp. 40–7, Feb. 2002.

[74] F. Persson, J. Fritzsche, K. U. Mir, M. Modesti, F. Westerlund, and J. O. Tegenfeldt, "Lipid-Based Passivation in Nanofluidics.," *Nano letters*, Apr. 2012.

[75] R. Prasad, *Manual on membrane lipids*. Springer lab manual, Springer, 1996.

[76] R. B. Gennis, *Biomembranes: Molecular structure and function*. Springer advanced texts in chemistry, Springer-Verlag, 1989.

[77] C. Yoshina-Ishii and S. G. Boxer, "Arrays of mobile tethered vesicles on supported lipid bilayers.," *Journal of the American Chemical Society*, vol. 125, pp. 3696–7, Apr. 2003.

[78] B. C. Stevens and T. Ha, "Discrete and heterogeneous rotational dynamics of single membrane probe dyes in gel phase supported lipid bilayer.," *The Journal of chemical physics*, vol. 120, pp. 3030–9, Feb. 2004.

[79] R. P. Richter, R. Bérat, and A. R. Brisson, "Formation of solid-supported lipid bilayers: an integrated view.," *Langmuir : the ACS journal of surfaces and colloids*, vol. 22, pp. 3497–505, Apr. 2006.

[80] C. a. Keller, K. Glasmästar, V. P. Zhdanov, and B. Kasemo, "Formation of supported membranes from vesicles.," *Physical review letters*, vol. 84, pp. 5443–6, June 2000.

[81] E. Sackmann, "Supported Membranes : Scientific and Practical Applications," *Science*, vol. 271, no. 5245, pp. 43–48, 1996.

[82] M. Abramowitz, *Microscope Basics and Beyond*, vol. 1. 2003.

[83] J. R. Lakowicz, *Principles of fluorescence spectroscopy*. Springer London, Limited, 2006.

[84] A. Larsson, C. Carlsson, M. Jonsson, and B. Albinssont, "Characterization of the Binding of the Fluorescent Dyes YO and YOYO to DNA by Polarized Light Spectroscopy," *Journal of the American Chemical Society*, no. 6, pp. 8459–8465, 1994.

[85] C. Carlsson, M. Jonsson, and B. Akerman, "Double bands in DNA gel electrophoresis caused by bis-intercalating dyes.," *Nucleic acids research*, vol. 23, pp. 2413–20, July 1995.

[86] K. Günther, M. Mertig, and R. Seidel, "Mechanical and structural properties of YOYO-1 complexed DNA.," *Nucleic Acids research*, vol. 38, pp. 6526–6532, Oct. 2010.

[87] C. U. Murade, V. Subramaniam, C. Otto, and M. L. Bennink, "Interaction of oxazole yellow dyes with DNA studied with hybrid optical tweezers and fluorescence microscopy.," *Biophysical journal*, vol. 97, pp. 835–43, Aug. 2009.

[88] M. T. Bjorndal and D. K. Fygenson, "DNA melting in the presence of fluorescent intercalating oxazole yellow dyes measured with a gel-based assay.," *Biopolymers*, vol. 65, pp. 40–4, Oct. 2002.

[89] T. Squires and S. Quake, "Microfluidics: Fluid physics at the nanoliter scale," *Reviews of modern physics*, vol. 77, 2005.

[90] N. T. Nguyen and S. T. Wereley, *Fundamentals and applications of microfluidics*. Artech House integrated microsystems series, Artech House, Incorporated, 2002.

[91] D. J. Beebe, G. a. Mensing, and G. M. Walker, "Physics and applications of microfluidics in biology.," *Annual review of biomedical engineering*, vol. 4, pp. 261–86, Jan. 2002.

[92] E. L. Cussler, *Diffusion: Mass Transfer in Fluid Systems*. Cambridge Series in Chemical Engineering, Cambridge University Press, 1997.

[93] E. J. G. Peterman and G. J. L. Wuite, *Single Molecule Analysis: Methods and Protocols*. Methods in Molecular Biology, Humana Press, 2011.

[94] F. Persson, P. Bingen, T. Staudt, J. Engelhardt, J. O. Tegenfeldt, and S. W. Hell, "Fluorescence nanoscopy of single DNA molecules by using stimulated emission depletion (STED).," *Angewandte Chemie (International ed. in English)*, vol. 50, pp. 5581–3, June 2011.

[95] S. W. Hell, "Microscopy and its focal switch," *Nature Methods*, vol. 6, no. 1, 2009.

Mapping of intact chromosomes in meandering nano-channels

C. Freitag[2], *J. Fritzsche*[6], *F.Persson*[3], *T. Ambjörnsson*[4], *C. Noble*[5], *M. Reiter-Schad*[4], *K. U. Mir*, *A.Graneli*[2], *J. O. Tegenfeldt*[1]

affiliations:

1. Department of Physics Lund University, Lund, Sweden 2. Department of Physics, University of Gothenburg, Gothenburg, Sweden 3. Department of Cell and Molecular Biology, Computational and Systems Biology, Uppsala University, Uppsala, Sweden 4. Department of Theoretical Physics, Lund University, Lund, Sweden 5. The Wyss Institute, Harvard University, Cambridge, MA, USA 6. Department of Applied physics, Chalmers university of technology, Gothenburg 7. Wellcome Trust Centre for Human Genetics, University of Oxford, United Kingdom

* corresponding author, email: jonas.tegenfeldt@ftf.lth.se

Abstract

Using nano-channels for stretching and visualization of single DNA molecules have proven useful in several areas such as polymer physics and DNA mapping due to the flexibility of the channel design together with the uniform stretching of the confined DNA molecules. Direct visualization of single DNA molecules in nano-channels opens up exciting opportunities to obtain course-grained genomic information on the single-cell level of individual long intact DNA fragments. This may have important applications during the identification of microbial pathogens, sequence assembly or for direct diagnosis of large genomic rearrangements. An important problem in mapping whole chromosomes is their large size making them difficult to image efficiently. To solve this problem we have designed a long meandering nano-channel to image megabasepairs of DNA within a single frame of view. As a proof of principle a 5.7 Mbp long intact chromosome from *S. pombe* stretched to 50% of its contour length was imaged inside a meander-channel. The elongated *S.pombe* chromosomes were partially melted to create a barcode pattern. We developed an algorithm to extract a time-trace from a meandering nano-channel for easier analyzation of the pattern.

Introduction

Sequencing of human DNA is paramount for identification of genetic diseases, personalized medicine and cancer research among other things. Although, base-by-base sequencing gives the ultimate resolution of a single nucleotide all methods with this resolution (including Sanger and Next-generation sequencing)

available today are based on fragmenting the unknown DNA and sequencing each piece individually [1, 2]. Bioinformatic algorithms are subsequently used to assemble the fragments into a complete DNA sequence. Three main drawbacks accompanies this procedure. Firstly, long range contextual information is lost in the process. Secondly, longer DNA sequences (> 1 kbp) drastically increases the computing power needed for assembly. Thirdly, repetitive sequences (represented for example in heterochromatic regions of the genome [3]) possess a huge problem. The challenge with repetitive sequences creates gaps in the sequence coverage that together may constitute as much as 20% of the human genome [4]. Furthermore, most of the single nucleotide resolution techniques requires PCR amplification of the DNA prior to sequencing, which introduces the requirement of a prior knowledge of the unknown sequence and can potentially led to a bias where the more easily amplified parts are over represented within the assembled sequence. There are a few single molecule techniques within the next-generation family that does not require amplification of the DNA. However, they still possess the major drawback that accompanies all single nucleotide resolution techniques, namely the requirement of fragmenting the DNA prior to sequencing.

A mapping pattern (a barcode-like pattern of dark and bright stripes is created along the DNA), with a resolution of $1 - 10$ Mbp, has traditionally been created on metaphase chromosomes to detect chromosomal rearrangements (including translocations, inversions, duplications and deletions) responsible for many genetic diseases (including schizophrenia and mental retardation [5]). However, many genetic diseases arise from genomic rearrangements in the size range $5 - 400$kbp [5], and are therefore not detectable by mapping on metaphase chromosomes. Furthermore, the low mapping resolution prevents the identification of repetitive regions along the chromosomes. As a result, barcode patterns are today commonly created on stretched chromatin fibers (as in fiberFISH) or DNA strands and a resolution down to 1 kbp can be obtained [6].

Stretching of single DNA molecules can be achieved by different techniques such as immobilization of DNA on a surface [7, 8, 9, 10, 11, 12], shear flow in micro-channels [13, 14, 15, 16] and confinement in nano-channels [17, 18, 19, 20, 21]. Elongation due to confinement has several advantages over alternative techniques and has proven useful within both polymer physics [17, 22, 23] and DNA mapping [19, 20, 21, 7, 12]. It does not require any external forces to perform the stretching and after a short relaxation time a steady state, where the DNA molecule will remain elongated in its equilibrium configuration, is reached [24, 17]. This steady state configuration allows for continuos measurements of length during an extended period of time. In addition, the equilibrium configuration shows an extension of the DNA molecule that scales linearly with the contour length of the DNA molecule and thereby provides a correlation between features spatial position along the polymer and their position within the genome.

Single molecule studies eliminates the need for DNA amplification and thereby increases the efficiency of sequence analysis. In addition, single molecule studies removes the sample averaging that is inherent in all bulk-phase biochemical

assays. Since every molecule is individually investigated rare subpopulations, variations in genotype or molecular states can be identified [**?**, **?**].

Mapping using restriction enzymes to create specific patterns of digested DNA fragments have become popular and has proven to work on molecules extended both on surfaces and within nano-channels [21, 7, 9, 10]. However, the use of enzymes increases the complexity of this method and limits the resolution to the number of binding sites for the enzyme used. Furthermore, it has an inherent need for prior knowledge of the sequence in order to choose the optimal restriction enzymes for each sequence. Methods based on sequence specific labeling [25] opens up for the possibility to achieve a high resolution along a large DNA molecule by using carefully designed probes. It can also be used to accurately determine the distance between two specific sequences along a DNA strand, although prior knowledge of the sequence is beneficial in order to design useful probes. Methods based on the AT/GC ratio along the molecules and thereby eliminates the benefit from a prior knowledge of the sequence have been developed [19, 20]. One of the methods is based on competitive binding between a standard fluorescent DNA dye with no sequence specificity and a non-fluorescent molecule with exceptional sequence specificity and high binding constant. The fluorescent dye is replaced by the non-fluorescent molecule and as a result dark areas are created along the molecule. The barcode-pattern can be created with a single step in bulk before imaging [19]. A second method is based on local melting of a DNA molecule stained with a dye with a large enhancement in fluorescent intensity when bound to dsDNA (such as the commonly used dimeric intercalating cyanine dye YOYO-1) [20]. The melting can be performed by altering the buffer conditions (for example by adding formamide), by simply raising the temperature or a combination of both. In order to identify specific chromosomes within a mixture or find large genomic rearrangements along a DNA strand the experimental barcode is usually correlated to a theoretically calculated barcode for the sequence [20, 26].

Even though nano-channel systems exhibit a large potential they have so far only been used for elongation of relatively short DNA strands when compared to genome sizes of most organisms, limiting their usefulness for biologically relevant problems. One limitation with current designs is the use of straight nano-channels, only allowing limited segments of native genomic molecules to be observed in a single field of view.

In our work we drastically decrease the number of frames required to image large genomes by simply folding the nano-channels into a meandering pattern. This design was used to image DNA molecules in the Mbp range within a single field of view. We show that the new channel design can be used in combination with partial melting to create a high-resolution mapping pattern along an entire eukaryotic chromosome. This mapping pattern was used to determine the spatial position of repetitive regions along the chromosome. A barcode pattern along chromosomal length DNA can be used to obtain information about long-range genomic information as well as finding large genomic rearrangements and copy number variants associated with a number of medical conditions [5].

Materials and methods

Experimental setup

A fluorescence microscopy system incorporating a Nikon Eclipse TE2000 inverted microscope, a 100x N.A. 1.4 oil immersion objective, an EMCCD camera (Andor iXon DV-897) and a standard mercury short arc lamp (100 W) was used.

A setup similar to the one described in [20] was used to enable mounting of the chip to the microscope, heating of the DNA sample and control of the flow within the micro- and nano-channels. The setup included a fused-silica chip containing the channel system (created as explained below), a chip holder (or chuck), a heater system and a homebuilt pressure system for flow manipulation.

A single chip contained two $1x5\ \mu m^2$ channels for transporting the DNA to the array of nano-channels spanning between the micro-channels. Inlet holes at the ends of the micro-channels created a connection to the macro world.

The chuck (designed to support the chip) was made of Zeonor 1060R (Sigolis AB, Sweden), due to the plastics high resistance to chemicals, low internal fluorescence and transparency. Reservoirs in the chuck connected to the inlet holes on the chip enabled easy loading and manipulation of the sample during experiments. For managing the flow inside the chip nitrogen gas was used to create an overpressure at the appropriate reservoir. Nitrogen gas was used in order to keep oxygen concentration at a minimum and thereby minimizing the photo damaging of the molecules.

The heating system consisted of a temperature controller (336 Cryogenic Temperature Controller, Lake Shore, USA), an aluminum cap, a cartridge heater and a thermocouple. Both the cartridge heater and thermocouple were positioned inside the aluminum cap which was in turn placed in contact with the backside of the chip through a hole spanning the center of the chuck. As a result a reproducible thermal contact between the heater and the chip was achieved and a feedback loop created to ensure a stable temperature. To further increase the heat transfer thermally conductive grease (Omegatherm, Omega, USA) was applied at all interfaces in the heating system.

Chip production

The fabrication of the nanofluidic chip comprises the following processing steps, based on photolithography (PL), electron-beam lithography (EBL), reactive ion etching (RIE), sandblasting, fusion bonding and dicing: (1) Alignment marks for PL and EBL were etched 500 nm deep into a 4-inch fused silica wafer of 500 µm thickness (from HOYA Corporation, USA), using fluorine based (50 sccm Ar, 50 sccm CHF3, 30 m Torr, 150 W RF-power) RIE and a photo resist (S1813, Shipley, USA) etch mask. Subsequently, the wafer was cleaned in piranha acid (H_2SO_4 2:1 H_2O_2) at 120 ° C for 10 min, rinsed in DI-water and dried under nitrogen stream. (2) Aligned to the marks fabricated during the first precessing step, meandering grooves of 400 nm width were etched 200 nm into the substrate with fluorine based RIE (5 sccm Ar, 50 sccm CF_4, 10 sccm CHF_3,

8 mTorr, 100 W RF-power, 100 W ICP-power), using an electron-beam resist (ZEP520A, NIPPON ZEON CO. LTD., Japan) as an etch mask. After RIE, the resist was stripped under the same conditions as before. (3) Repeating the processing of the first step, 1 µm deep grooves were fabricated, overlapping with the ends of the meandering structures. After sealing the fluidic system, these grooves will form microfluidic channels that allow reagents to be brought to the nano-channels, which are formed by the sealed, meandering grooves etched during the previous step. (4) To fabricate inlet and outlet holes, Nitto SW-tape (Nitto Denko, Japan) was glued on both sides of the processed wafer. The tape served as a soft mask during sandblasting on the backside and as protection against contamination on the frontside. Small openings of approximately 1 mm diameter were cut into the tape at the desired position of the in/outlets, and through-holes were sandblasted using fused aluminum oxide powder of 50 µm particle size. (5) After removing the protective tape, the processed wafer was cleaned again in piranha etch (see above) and, together with a second unprocessed wafer of 175 µm thickness (from University Wafers, USA), immersed for 10 min first in RCA II (5:1:1 H_2O:HCl:H_2O_2) and then in RCA I solution (5:1:1 H_2O:NH_2OH:H_2O_2) at 80 ° C, rinsed in DI and dried under nitrogen stream. The two wafers were then brought together and covalently fusion bonded by annealing them at 1100 ° C in nitrogen atmosphere for 6 h. (7) Finally, nanofluidic chips of $25x25$ mm^2 were diced from the bonded wafers, using a 200 µm wide resin-bonded blade with 40 µm-diamonds (Dicing Blade Technology, USA).

Sample preparation

The experiments were performed with chromosomes from *Schizosaccharomyces pombe* (*S. pombe*) (CHEF DNA Size Marker, from Bio-Rad). The DNA was delivered in agarose gel as an electrophoresis size standard including DNA molecules with lengths 3.5 Mbp, 4.6 Mbp and 5.7 Mbp. To avoid degradation of the DNA molecules they were stored within the agarose gel at 8°C until use. Prior to experiments DNA was stained with YOYO-1 fluorescent dye (Invitrogen) at a ratio of 1 dye molecule per 6 base pairs. A simultaneous staining and gel-extraction process was performed in a buffer consisting of 10 mM NaCl in 0.05x TBE (4.5 mM Tris, 4.5 mM Boric acid and 0.1 mM EDTA) and YOYO-1. In this process small pieces of DNA containing agarose-gel were placed in a large volume staining buffer and left at room temperature (20°C) over night during which the DNA diffused out from the gel. The small pieces were created by careful cutting with a sharp knife. Just prior to experiments the running buffer was created by adding 2-mercaptoethanol (Sigma-Aldrich) and formamide (Sigma-Aldrich) directly to the staining solution to final concentrations of 3% and 50% respectively.

Experimental procedure

Prior to each new experiment a buffer consisting of 5 mM NaCl in 0.025x TBE, 3% (v/v) 2-mercaptoethanol and 50% formamide was flushed through the chan-

nels for at least 15 min to ensure correct buffer conditions before introducing the DNA. After DNA introduction of DNA the flow rate was kept as low as possible at all times to minimize shearing of the molecules. Once the DNA molecules reached the inlets to the nano-channels pressure was applied to both the reservoirs connected two the micro-channel containing the DNA. In this way the buffer is forced to flow through the nano-channels dragging the DNA with it. After introduction into the nano-channels the molecules were either imaged immediately to collect information about the relaxation times or heated during 10 min to create a barcode pattern before imaging.

Despite the use of thermally conducting grease the measured temperature vary slightly from the actual temperature in the channels. Also the temperature measured for DNA denaturation to be initiated can potentially vary from day to day. During the melting experiment the temperature was therefore slowly and step-wise increased from 29°C up to 45°C. Several different molecules were studied at each temperature to find the optimal melting conditions in each case. To ensure a stable temperature during data collection the system was equilibrated for 15 min at each new temperature before data collection was initiated.

Image analysis

Image analysis are required for extracting time-traces from the meandering nano-channels. To that end, our algorithm first rotates the image to have the linear parts vertical. Thereafter, a parametrized meander contour of the known nanolithography mask was placed on top of the picture with a scale-factor, up-down orientation and mean position as fitting parameters. This procedure allows for extraction of a time-trace for the melting map by walking along the parametrized meander contour. In this procedure a 7 pixel wide window was used in the direction perpendicular to the meander orientation. Finally, the different results for different times are aligned using the procedure in [20] and [26]. For the alignment a box-size of 25 pixels was used, and aligned to time-frame 50. Briefly, our algorithm performs local stretching operations and global translations to minimize the effect of center-of-mass and DNA conformational fluctuations in the channel. A simulated annealing algorithm was used for the associated global minimization problem. In order to not align "noise to noise" a moving average with a window-size of 5 pixels was applied to each time frame before using the approach in [20] and [26]. The resulting barcode shows "raw" aligned data, i.e. data without the moving average.

To achieve the aligned picture different regions of the melting map had to be aligned by only using the first 100 (out of 200) time frames. The time-frames 101-200 possibly includes a cutting event, which may cause problems for the standard alignment procedure. To deal with the possibility of cutting events of DNA a simple edge detection algorithm was performed along the aligned DNA. Note that this does not mean that in fact there is a cut in between those regions, but simple that we can reliably treat those regions as independent.

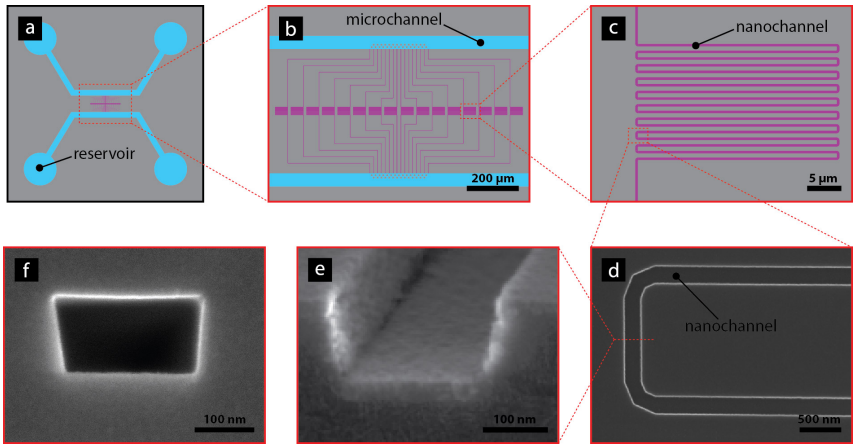

Fig. 1: a. Overview of chip design showing how the micro-channels (blue) connects the reservoirs to the meandering nano-channels (purple). b. Zoom in of the meander channel array. The pillar array initially placed at the inlets to the nano-channels are also visualized. c. Zoom in of the meandering part of the nano-channels. d. Image of one bend in meandering channel. e. Cross section of an open nano-channel prior to bonding. f. Cross section of nano-channel after closing of the channel.

Results & Discussion

Nano-channel design

Direct imaging of DNA molecules in the Mbp range was enabled by folding the nano-channels into a meandering pattern. Each meander could be imaged within a single field of view and was designed to hold up to 10 Mbp of DNA stretched to 30% extension (1 mm) (figure 1 and 4). To simplify the analysis the meandering part of the nano-channel was designed with 50 μm long straight parts parallel to each other and connected with soft bends. The bends were in turn designed with a 1 μm long straight part connected to two 90-degree turns to minimize stress on the DNA molecules in the meander-channels.

The higher resistance of longer channels together with the the high risk of shearing the molecules during entry into the nano-channels at high pressures lead to a design where the inlets of several meander-channels were kept in close proximity of each other. This increases the resulting bulk flow rate into the nano-channels decreasing the time needed for the introduction of DNA and ensures that the bulk flow rate exceeds the diffusional rate of the end of the molecule that is to be introduced.

A micro-post array spanning across half the micro-channel were initially placed at the inlets to the nano-channels inlets for pre-stretching of the molecules and thereby ease the introduction into the nano-channels (figure 2) [27]. However, for the long chromosomes used in this study the micro-post array turned

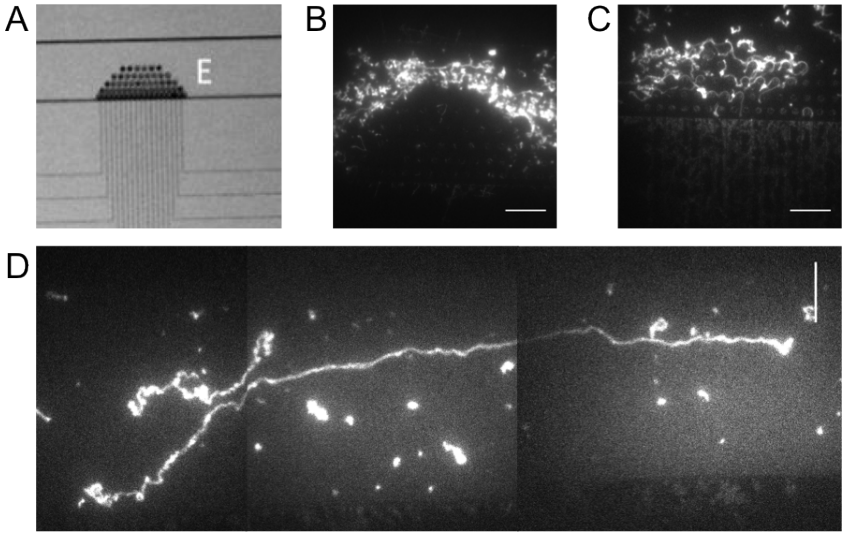

Fig. 2: DNA behavior with and without a micro-post array in the micro-channel. A. A bright field image showing the a micro-post array at the nano-channel inlets. B. A fluorescence microscopy image of long DNA molecules around the pillars in the micro-post array. Due to their large size the DNA molecules follow the flow lines around the pillars along the micro-channel rather than entering the array. C. During the introduction into the nano-channels the DNA molecules gets entangled around the pillars within the array which prevents then from entering the nano-channels. D. The parabolic velocity profile in the micro-channel pre-stretches the long DNA molecules rendering the pillar array unnecessary. The scale bars are 15 μm.

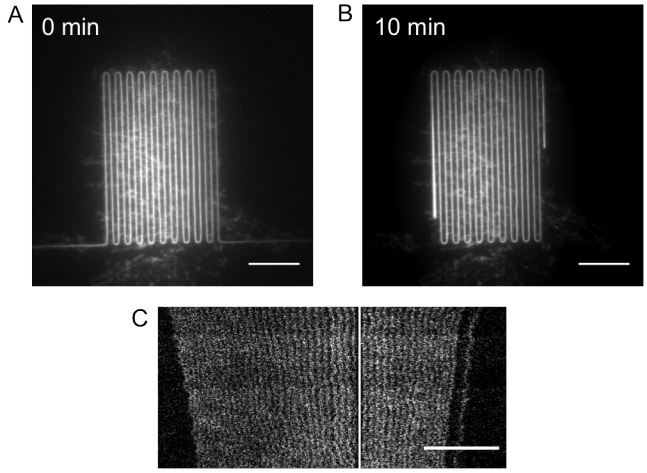

Fig. 3: Relaxation of long S.pombe DNA stained with YOYO-1 and imaged using a fluorescence microscope . The molecules were stretched in $250x250\ \mathrm{nm}^2$ meander channels. A. The image show a 5.7 Mbp long S. pombe chromosome highly extended due to the shear experienced during loading. B. The same molecule as in A but after 10 minutes in the meander-channel. It is clear that the molecule has relaxed considerably. C. Time-trace of a relaxing DNA molecule with a repetitive melting pattern along the molecule. The slow relaxation enables these high resolution images of relaxing molecules. The white vertical line represents a meander bend from which no data has been extracted. The scale bars represents 15 μm.

out to be more of an unneeded hinderance than an aid. The large DNA molecules followed the flow lines around the micro-post array and thereby ending up further from the inlets than they would have in the absence of the array. When forced to travel trough the array the DNA molecules got entangled around the pillars which prevented further movement towards the nano-channels.

DNA molecules in the Mbp range have a radius of gyration in the order of a micron and therefore a slight elongation due to confinement is apparent in the 1 μm deep micro-channel. Furthermore, the parabolic flow profile inside the channel serves to stretch the large DNA molecules since different parts of the molecule experience different flow rates.

Handling long DNA

As a proof of principle an entire chromosome (5.7 Mbp) from *S.pombe* was imaged in a $250x250\,\mathrm{nm}^2$ meander channel (figure 3A and B). Figure 3A shows the DNA molecule directly after the introduction into the meander-channel. Due to the shear experienced during introduction into the nano-channels the

molecule is highly extended. When the flow is stopped the molecule starts to relax towards its equilibrium state and after 10 min the molecule has relaxed considerably (3B). However, due to the slow relaxation for long molecules [24] it has still not reached its equilibrium state and is extended to 50%, compared to the expected 30% extension for a relaxed molecule.

Requirements for getting a sharp pattern structure in an image includes a movement of the sample that is slower than the exposure time used during imaging. The long relaxation times for chromosomal length DNA therefore enables imaging of fine structures on molecules that has not yet reached their equilibrium state and thereby gaining a higher resolution than would be possible for relaxed molecules in equal sized channels (figure 3C).

Mapping

Combining melting mapping with meandering nano-channels have lead to direct visualization of a barcode patten along DNA molecules in the Mbp range. As a proof of principle we show a melting mapping pattern along the 5.7Mbp *S. pombe* chromosome (figure 4). Our meander-finding algorithm correctly identified the meander in image 4 (top, left) as is visualized in figure 4(top, middle). The time-trace shown in figure 4middle was extracted with our tool by "walking along" the meander contour and successfully aligned (figure 4bottom).

Melting of whole chromosomes can be used to determine the number of repetitive parts as well as their lateral placement, something that can be difficult when only smaller parts are analyzed. The left end of the time-trace in figure 5 includes a repetitive part (magnified in the bottom image) whose lateral placement can be determined with the help of the un repetitive part of the barcode.

A common problem is photo-cutting of the DNA. In melting mapping it is not fully clear whether a dark area is DNA or just space in between two DNA strands. For small fragments diffusion would reveal a cut, but for long DNA it may be difficult to tell the difference. A simple edge detection algorithm along the aligned DNA identified three different regions (region I, II and III) along the barcode shown in figure 4. However, this does not mean that in fact there is a cut in between those regions, but simply that we can reliably treat those regions as independent.

Conclusions

We have shown that meandering nano-channels extensively ease direct imaging of DNA molecules in the Mbp range, by imaging 5.7 Mbp DNA molecule at 50% extension within a field of view. In the current design one of the meandering parts can almost hold the entire genome from *Saccaromyces cereviseae* (12.1 Mbp). With an optimized denser design we expect to be able to hold at least 20 mm of DNA per field of view. At 50% stretching, this would allow us to image the entire human genome with a mere 25 frames. Together with

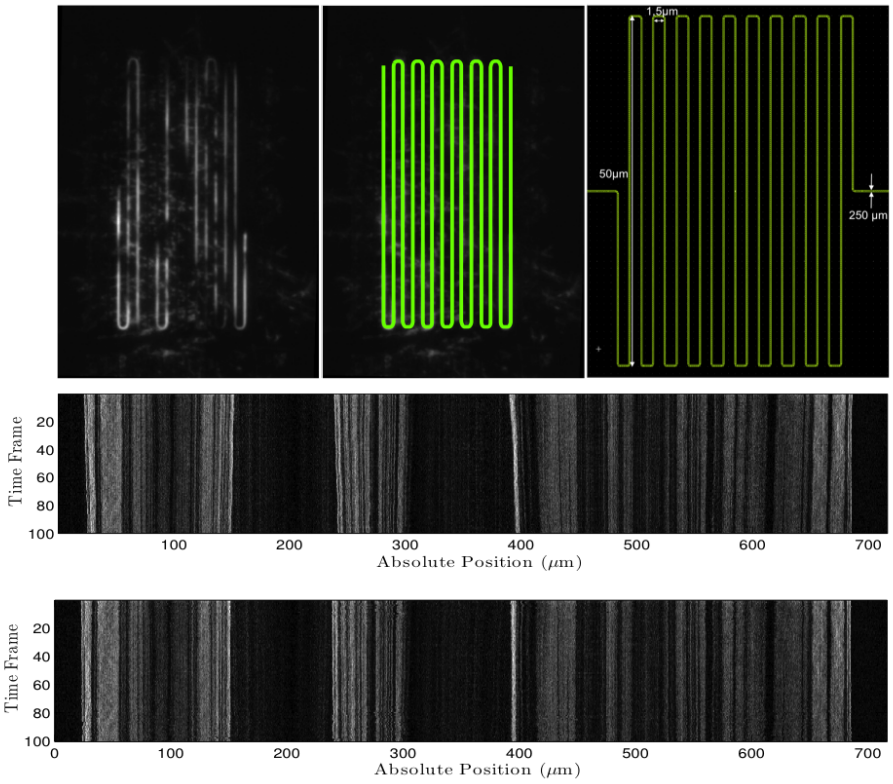

Fig. 4: (Top, left) Time-averaged raw fluorescence intensity image of a melted *S. pombe* chromosome. (Top, middle) The precise location of the meandering nano-channel was found and highlighted using our meander-finding algorithm. (Top, right) Nano- lithography mask. (Middle) Kymograph extracted by our tool by "walking along" the meander contour. In this procedure a 7 pixel wide window was used in the direction perpendicular to the meander orientation. (Bottom) The alignment procedure from [20] applied to the middle picture. For procedure a box-size of 25 pixels was used, and aligned to time-frame 50. Before applying this procedure a moving average with a window-size of 5 pixels was used to reduce noise. Final data shown is without the moving average.

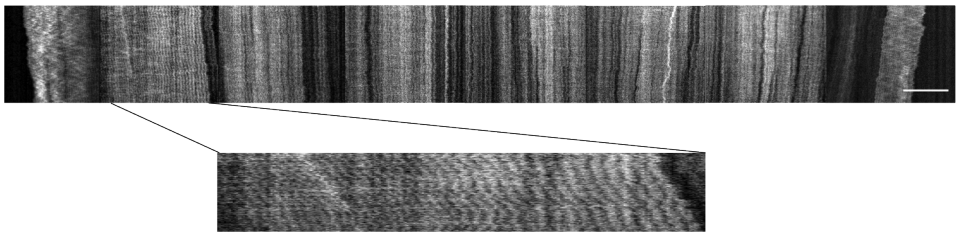

Fig. 5: TOP Time-trace of an S.pombe chromosome containing a clearly repetitive part in the left part of the image. BOTTOM A magnification of the repetitive part of the molecule. The scale bar is 15 μm.

our algorithm to extract barcodes from our meandering nano-channel the novel channel design is a first step towards an automated tool for whole chromosome analysis.

The biological relevance of this design was demonstrated by creating melting barcodes along the elongated molecules. A barcode pattern allowed us to identify a repetitive part in the genome and due to the long fragments analyzed the location of this repetitive part within the genome can be determined. Something that is difficult with existing mapping techniques, nor standard sequencing approaches due to the short DNA strands analyzed.

This technique opens up for the identification of single microorganisms, which will be important for rapid pathogen diagnosis and metagenomic studies without the need for culturing of the cells nor DNA amplification.

ACKNOWLEDGMENTS This work was supported by the Swedish Research Council (VR) grant nos. 2007-584 and 2007-4454, the EU's seventh Framework Programme (7RP/2007-2013) under grant agreement no. 201418 (READNA), and the Crafoord Foundation grant nos. 2008-0841 and 2005-1123. K.U.M. acknowledges support from the UK Royal Society Theo Murphy Blue Skies Award. VINNOVA (project number P35735-1).

References

[1] E. R. Mardis, *Annual review of genomics and human genetics*, 2008, **9**, 387–402.

[2] J. Shendure, H. Ji, *Nature Biotechnology*, 2008, **26**, 1135–1145.

[3] E. E. Eichler, R. a. Clark, X. She, *Nature reviews. Genetics*, 2004, **5**, 345–54.

[4] R. a. Hoskins, J. W. Carlson, C. Kennedy, D. Acevedo, M. Evans-Holm, E. Frise, K. H. Wan, S. Park, M. Mendez-Lago, F. Rossi, A. Villasante, P. Dimitri, G. H. Karpen, S. E. Celniker, *Science (New York, N.Y.)*, 2007, **316**, 1625–8.

[5] P. Stankiewicz, J. R. Lupski, *Trends in genetics : TIG*, 2002, **18**, 74–82.

[6] M. Heiskanen, O. Kallioniemi, a. Palotie, *Genetic analysis : biomolecular engineering*, 1996, **12**, 179–84.

[7] M. Xiao, A. Phong, C. Ha, T.-F. Chan, D. Cai, L. Leung, E. Wan, A. L. Kistler, J. L. DeRisi, P. R. Selvin, P.-Y. Kwok, *Nucleic acids research*, 2007, **35**, e16.

[8] T.-F. Chan, C. Ha, A. Phong, D. Cai, E. Wan, L. Leung, P.-Y. Kwok, M. Xiao, *Nucleic acids research*, 2006, **34**, e113.

[9] J. Jing, J. Reed, J. Huang, X. Hu, V. Clarke, J. Edington, D. Housman, T. S. Anantharaman, E. J. Huff, B. Mishra, B. Porter, a. Shenker, E. Wolfson, C. Hiort, R. Kantor, C. Aston, D. C. Schwartz, *Proceedings of the National Academy of Sciences of the United States of America*, 1998, **95**, 8046–51.

[10] B. Teague, M. S. Waterman, S. Goldstein, K. Potamousis, S. Zhou, S. Reslewic, D. Sarkar, A. Valouev, C. Churas, J. M. Kidd, S. Kohn, R. Runnheim, C. Lamers, D. Forrest, M. a. Newton, E. E. Eichler, M. Kent-First, U. Surti, M. Livny, D. C. Schwartz, *Proceedings of the National Academy of Sciences of the United States of America*, 2010, **107**, 10848–53.

[11] D. Bensimon, A. Simon, V. Croquette, A. Bensimon, *Physical review letters*, 1995, **74**.

[12] R. K. Neely, P. Dedecker, J.-i. Hotta, G. Urbanaviciute, S. Klimasauskas, J. Hofkens, *Chemical Science*, 2010, **1**, 453.

[13] E. Y. Chan, N. M. Goncalves, R. A. Haeusler, A. J. Hatch, J. W. Larson, A. M. Maletta, G. R. Yantz, E. D. Carstea, M. Fuchs, G. G. Wong, S. R. Gullans, R. Gilmanshin, *Genome Research*, 2004, **14**, 1137–1146.

[14] A. Granéli, C. C. Yeykal, T. K. Prasad, E. C. Greene, *Langmuir : the ACS journal of surfaces and colloids*, 2006, **22**, 292–9.

[15] R. Marie, J. N. Pedersen, D. L. V. Bauer, K. H. Rasmussen, M. Yusuf, E. Volpi, H. Flyvbjerg, A. Kristensen, K. U. Mir, *Proceedings of the National Academy of Sciences of the United States of America*, 2013, **10**, 4893–4898.

[16] T. T. Perkins, S. R. Quake, D. E. Smith, S. Chu, *Science (New York, N.Y.)*, 1994, **264**, 822–6.

[17] J. O. J. Tegenfeldt, C. Prinz, H. Cao, S. Chou, W. W. W. Reisner, R. Riehn, Y. Y. M. Wang, E. E. C. Cox, J. J. C. Sturm, P. Silberzan, Others, R. H. Austin, *Proceedings of the National Academy of Sciences of the United States of America*, 2004, **101**, 10979.

[18] J. O. Tegenfeldt, C. Prinz, H. Cao, R. L. Huang, R. H. Austin, S. Y. Chou, E. C. Cox, J. C. Sturm, *Analytical and bioanalytical chemistry*, 2004, **378**, 1678–92.

[19] L. K. Nyberg, F. Persson, J. Berg, J. Bergström, E. Fransson, L. Olsson, M. Persson, A. Stå lnacke, J. Wigenius, J. O. Tegenfeldt, F. Westerlund, *Biochemical and biophysical research communications*, 2012, **417**, 404–8.

[20] W. Reisner, N. B. Larsen, A. Silahtaroglu, A. Kristensen, N. Tommerup, J. O. Tegenfeldt, H. Flyvbjerg, *Proceedings of the National Academy of Sciences of the United States of America*, 2010, **107**, 13294–9.

[21] R. Riehn, M. Lu, Y.-M. Wang, S. F. Lim, E. C. Cox, R. H. Austin, *Proceedings of the National Academy of Sciences of the United States of America*, 2005, **102**, 10012–6.

[22] W. Reisner, K. Morton, R. Riehn, Y. Wang, Z. Yu, M. Rosen, J. Sturm, S. Chou, E. Frey, R. Austin, *Physical Review Letters*, 2005, **94**, 196101.

[23] E. Werner, F. Persson, F. Westerlund, J. O. Tegenfeldt, B. Mehlig, *Physical Review E*, 2012, **86**, 041802.

[24] J. T. Mannion, C. H. Reccius, J. D. Cross, H. G. Craighead, *Biophysical journal*, 2006, **90**, 4538–45.

[25] E. T. Lam, A. Hastie, C. Lin, D. Ehrlich, S. K. Das, M. D. Austin, P. Deshpande, H. Cao, N. Nagarajan, M. Xiao, P.-Y. Kwok, *Nature biotechnology*, 2012, **30**, 771–6.

[26] R. L. Welch, R. Sladek, K. Dewar, W. W. Reisner, *Lab on a Chip*, 2012, **12**, 3314–3321.

[27] H. Cao, J. O. Tegenfeldt, R. H. Austin, S. Y. Chou, *Applied Physics Letters*, 2002, **81**, 3058.

Time dependence of DNA melting mapping

C. Freitag[2], *J. Fritzsche*[3], *K. U. Mir*[4], *A.Graneli*[2], *J. O. Tegenfeldt*[1,*]

affiliations:

1. Department of Physics Lund University, Lund, Sweden 2. Department of Physics, University of Gothenburg, Gothenburg, Sweden 3. Department of Applied physics, Chalmers university of technology, Gothenburg, Sweden 4. Wellcome Trust Centre for Human Genetics, University of Oxford, United Kingdom

* corresponding author, email: jonas.tegenfeldt@ftf.lth.se

Abstract

Direct visualization of single DNA molecules elongated by confinement in nano-channels have proven useful in several areas such as polymer physics and DNA mapping. The flexibility of the channel design together with the even stretching of relaxed DNA molecules opens up for high resolution mapping on DNA in nano-channels. Mapping in nano-channels enables single molecules to be individually investigated and can therefore be used for the identification of single bacterias and yeast cells within a complex mixture of cells. Melting mapping is a promising method based on local melting along a DNA molecule stained with a strongly increased fluoresce when bound to ds-DNA. However, it possess a problem with reproducibility, which is a prerequisite for commercialization of the method. In this work we bring melting mapping one step closer to commercialization by optimizing the DNA molecules occupation time in the nano-groove and thereby their time at a raised temperature. We show an evolution of the melting barcode pattern over a time period of 10 min before a steady state is reached. Furthermore, we show that the molecules total intensity decreases with time in the absence as well as in the presence of illumination. This creates a time window for data collection where the pattern has reached equilibrium and the total intensity is still high.

Introduction

New highly parallel array based methods (referred to as next-generation sequencing methods) have increased the cost and efficiency of base-by-base sequencing compared to traditional methods such as Sanger sequencing. Just as traditional Sanger sequencing, most of the next-generation methods requires amplification of the DNA. However, a few single-molecule techniques (including the Helicos and Pacific Biosystems instruments) are available, but like other

techniques with a single nucleotide resolution they require shearing of the unknown DNA and individual sequencing of each fragment [1]. Highly sophisticated bioinformatics algorithms are used to assemble the DNA fragments into a complete sequence. Despite a vast development of the bioinformatics algorithms they possess problems with highly repetitive parts and DNA strands longer than 1 kbp. The limit in DNA length that can be analyzed prevents information about long range contextual information.

Instead a barcoding (or mapping) pattern can be used to detect chromosomal rearrangements (including translocations, inversions, duplications and deletions) which are responsible for many genetic diseases (including schizophrenia and mental retardation [2]). Traditionally this barcode pattern was created on metaphase chromosomes with a resolution of $1 - 10$ Mbp. However, today the patterns can be created on stretched chromatin fibers (as in fiberFISH) or naked DNA strands, on which a resolution down to 1 kbp can be obtained [3].

Several techniques are available for stretching single DNA molecules including stretching on surfaces [4, 5, 6, 7, 8, 9], with shear forces in micro-channels [10, 11, 12, 13] and confinement in nano-channels [14, 15, 16, 17, 18]. Using nano-channels for stretching and visualizing DNA molecules has several advantages over alternative stretching techniques and has proven useful within both polymer physics [17, 19, 20] and DNA mapping [14, 15, 5, 16, 8]. Stretching due to confinement does not require any external forces and after a short relaxation time an equilibrium elongation is reached [21, 17]. At equilibrium the DNA is evenly stretched with an elongation that scales linearly with its contour length, which provides a correlation between features spatial position along the polymer and their position within the genome. Furthermore, elongation due to confinement allows for continuos data collection during an extended period of time and is a better representation of the biological system than DNA immobilized on for example a surface.

Digestion of the DNA with restriction enzymes has become a popular mapping method and has been demonstrated on molecules extended both on surfaces and within nano-channels [16, 8, 7, 9]. With a high sequence specificity for the enzymes it is possible to create well defined DNA pieces, but this is is a complex method depending high yield of the enzymatic cutting. Furthermore, the resolution is limited by the number of binding sites for the enzymes used and a prior knowledge of the sequence is advantageous to choose the optimal enzymes. Methods based on sequence specific labeling gives a high resolution where the labels binds and a lateral distance between the probes but also benefits from a prior knowledge of the sequence when designing useful probes [22].

Methods based on the AT/GC ratio along the molecules eliminates the benefit from a prior knowledge of the sequence. The mapping pattern can be created either by local melting of a DNA molecule (melting mapping) or sequence specific competitive binding [14, 15]. Competitive binding between a standard fluorescent DNA dye with no sequence specificity and a non-fluorescent molecule with exceptional sequence specificity and high binding constant yields a barcode pattern with dark areas where the non-fluorescent molecule has bound to the DNA [14]. One advantage with this method is that the barcode-pattern can be

created with a single step in bulk before imaging. Melting mapping is based on the lower melting energies of AT-rich areas compared to GC-rich areas along the molecules. An increase in temperature or change in solution chemistry can be used to melt all AT-rich areas along a DNA molecule. If the DNA is evenly stained with a fluorescent dye with a large enhancement in fluorescent intensity when bound to dsDNA, a grayscale barcode pattern unique for each sequence will arise with lower intensities at the AT rich regions [15].

A dark part in a melting mapping barcode is created by an initial bubble formation to form a single stranded part along the DNA chain, followed by loosening of the fluorescent dye. Together these two steps comprises the total time needed for a dark area to appear. It has been shown that even at physiological conditions small bubbles (from a few to a few hundred base-pairs) single stranded domains, so called DNA-bubbles, opens up intermittent along the DNA molecules and are immediately closed up again. The relaxation times for such bubbles was shown to be around $50\,\mu s$ [23]. Furthermore it was shown that at melting conditions the time for bubble formation scales with N^2, where N is the number of base pairs in the unzipped bubble [24].

With a high selectivity for dsDNA together with a binding constant in the range of $10^{10} - 10^{12}\,\mathrm{M}^{-1}$ [25] for dsDNA YOYO-1 is commonly the dye of choice for melting mapping. To further strengthen its position as the dye of choice it is virtually non-fluorescent free in solution and has a 1000-fold fluorescent enhancement upon binding to dsDNA. YOYO-1 has been shown increase the melting temperature of DNA [26] and to increase the contour length of the DNA with up to 31% at high staining rations [27].

Although melting mapping shows a large potential, it still possesses a problem with reproducibility. A high reproducibility is a prerequisite for using this method to answer biological relevant questions and for commercialization. An important step towards reproducibility is to ensure that an equilibrium state of the barcode pattern is reached before data collection. In this work melting mapping in a micro- and nano-channel system has been optimized with regard to the DNA molecules occupation time at a raised temperature in order to determine the relaxation time for a barcode pattern.

Materials and methods

Sample preparation

The experiments were performed with T4GT7 DNA (166 kbp, $L_C = 56.4\,\mu m$, Nippon Gene). For long term storage the DNA was kept frozen at -20 °C, whereas the stained DNA molecules were stored at 8°C until use. Prior to the experiments the DNA was stained with YOYO-1 fluorescent dye (Invitrogen) at a ratio of 1 dye molecule per 6 base pairs. For this a staining buffer of 5 mM NaCl in 0.05x TBE (4.5 mM Tris, 4.5 mM boric acid and 0.1 mM EDTA) and YOYO-1 was used. The running buffer was created from 10 mM NaCl in 0.05x TBE to which BME (2-mercaptoethanol) was added to a final concentration of 3% and formamide added to a final concentration of 50%. During the staining

procedure the DNA dye mixture was heated to 50 °C for 2 h followed by a slow cooling in order to ensure an even staining [28].

Experimental setup

For imaging a fluorescence video-microscopy system incorporating a Nikon Eclipse TE2000 invented microscope, a 100x N.A. 1.4 oil immersion objective, an EM-CCD camera (Andor iXon DV-897) and a standard mercury short arc lamp (100 W) was used.

A setup similar to the one described in [15] was used to enable mounting of the chip to the microscope, heating of the DNA sample and control of the flow within the micro- and nano-channels. The setup included a fused-silica chip containing the channel system (created as explained below), a chip holder (or chuck), a heater system and a homebuilt pressure system for flow manipulation.

A single chip contained four $1x5\ \mu m^2$ channels with inlet holes at each end for transporting the DNA to the array of nano-channels or slit spanning between the micro-channels.

The chuck, which was designed to support the chip, was made of Zeonor 1060R (Sigolis AB, Sweden), due to the plastics high resistance to chemicals, low internal fluorescence and transparency. Reservoirs in the chuck connected to the chip inlet holes enabled easy loading and manipulation of the sample. Nitrogen gas was used to managing the flow inside the chip by creating an overpressure at the appropriate reservoir. Nitrogen gas was specifically chosen in order to keep oxygen concentration at a minimum and thereby minimizing the photo damaging of the molecules.

The heating system consisted of a temperature controller (336 Cryogenic Temperature Controller, Lake Shore, USA), an aluminum cap, a cartridge heater and a thermocouple. A reproducible thermal contact between the heater and the chip was achieved by positioning the cartridge heater and thermocouple inside the aluminum cap. The aluminum was in turn placed in contact with the backside of the chip through a hole spanning the center of the chuck. As a result a feedback loop was created to ensure a stable temperature. To further increase the heat transfer thermally conductive grease (Omegatherm, Omega, USA) was applied at all interfaces in the heating system.

Experimental procedure

To ensure the right conditions in the channels running buffer was flushed trough the chip for 15 min before the DNA solution was introduced. Data was collected by placing DNA molecules in the nano-grooves and taking a movie every 5 min, starting the first when the molecule just entered the nano-channel. During the 5 min waiting time there was no illumination of the sample and no flow in the channels. For image analysis a time-trace/kymograph was created from the movies at each time point and the amount melted as well as total intensity determined. To the determine the amount melted the image taken immediately after introduction into the nano-groove was assumed to be completely unmelted.

Despite the use of thermally conducting grease there is a slight difference between the measured temperature and the actual temperature in the channels. Furthermore, the temperature measured for DNA melting to be initiated can potentially vary from day to day, due to slight variations in the setup assembly. The temperature was therefore slowly and step-wise increased from 29°C up to 45°C during each melting experiment. Several different molecules were studied at each temperature to find the optimal melting conditions in each case. To ensure a stable temperature during imaging the system was equilibrated for 15 min at each new temperature before data collection was initiated.

Results & Discussion

In this work melting mapping in a micro- and nano-channel system was optimized with regard to the DNA molecules occupation time in the nano-grooves and thereby their time at a raised temperature. In order to determine the ideal conditions, T4GT7 DNA molecules were placed in a nano-groove under melting conditions and imaged every 5 min to collect information about the change in the barcode pattern and total intensity of the molecule with time.

Melting, dye bleaching and dissociation are the main phenomenas affecting the total intensity of a stained DNA molecule over time. These phenomenas will work to decrease the total intensity with time, and together create a time limit for melting experiments and a window of optimal S/N ratio. Ideally the experiment is performed in the time-span where melting is at its equilibrium and the overall intensity still high.

At 20 °C no melting occurs even with 50% formamide in the buffer and therefore dissociation is the sole contributor to the intensity decrease during the periods of no illumination. It is thereby clear from figure 1D that YOYO-1 dissociation from DNA is constant with time at the conditions used here. Dissociation of YOYO-1 from the DNA is potentially increased by the negatively charged walls attracting the DNA, ". In figure 1A we see a "ghost image" consisting of dye that moved from the DNA molecule to the negatively charged wall of the nano-channel.

As opposed to room temperature where the intensity decrease is constant with time, it seems to decrease towards a steady state at higher temperatures (figure 1C). At higher temperatures both melting and dissociation are working to lower the intensity of the molecule. However, the reduction in the rate of intensity decrease and average amount melted with time suggest a slowing of the melting towards a steady state (figure 2A). Furthermore, the last intensity drop for the higher temperature is only slightly larger than the drops at room temperature, which also points to the conclusion that dissociation is the main contributor to the intensity decrease after about 10 min. In addition, the time-trace and the plot in figure 2 clearly shows a development of the melting pattern with time, with larger pattern changes at earlier times. Only a slight change in the melting pattern is observed between 10 min and 15 min, indicating that a steady state is reached. We assume the steady state appears is due to an

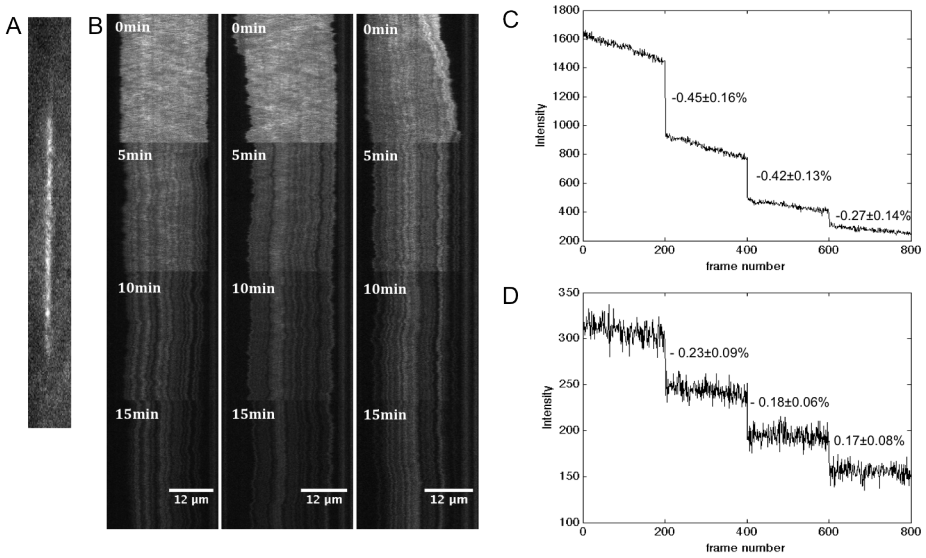

Fig. 1: Results showing total intensity decrease with time of a DNA molecule elongated in a nano-groove. **A.** "Ghost image" appearing due to YOYO-1 binding to the walls after occupation of a DNA molecule at that spot in the channel. **B.** Three different concatenated time-traces from 4 separate images of single T4GT7 molecules. The four time-traces (20 s each) all have the same brightness/contrast conditions in order to clearly show the intensity decrease with time. **C.** The mean intensity of the whole molecule plotted against frame number for the left molecule shown in fig 1B. Clear drops in intensity occurs during the 5 min dark waiting time between each movie. The average intensity decrease for 5 molecules is written next to each drop. **D.** The mean intensity of an entire molecule at room temperature (20 °C) plotted against frame number. Also here a decrease in intensity is apparent during the waiting periods. The average intensity decrease for 5 molecules is written next to each drop. In all cases the first image was taken as soon as the molecule entered the groove

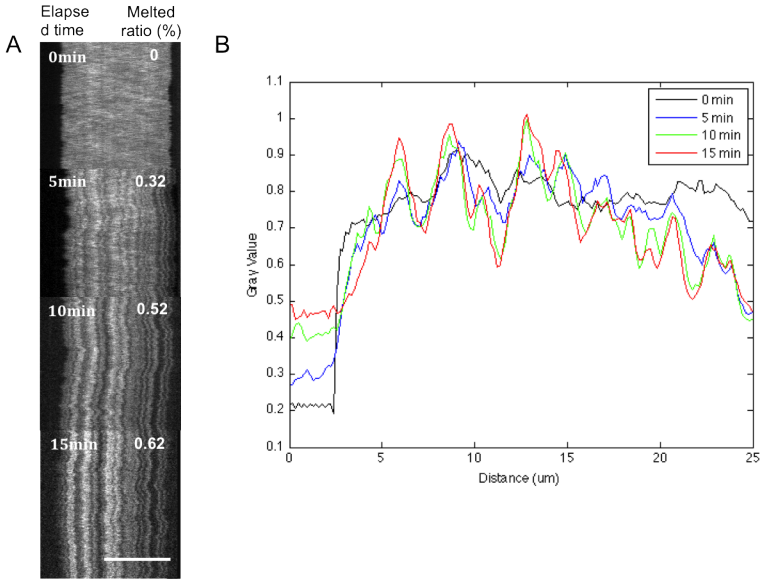

Fig. 2: Evolution of the melting pattern with time. **A**. Concatenated time-trace from 4 separate images of a single T4GT7 molecule kept at a temperature were melting occurs. The optimal brightness/contrast conditions was used for each of the four time-traces (20 s each). At the top of each new image the time and melted ratio is displayed. **B**. Intensity variation along the molecule after 0min (black), 5min (blue), 10min (green) and 15min (red). It is clear that the barcode develops with time during the first 10 min, after which the barcode is relatively stable.

equilibrium in the melting procedure and not due to saturation of the walls since we have a 40 times larger wall area than the total area of all the dye molecules bound to one T4GT7 DNA.

Barcoding of a DNA molecule includes loosening of the dye as well as the opening of the DNA strands. Both these processes contributes to the total patterning time. Due to the fast relaxation times of bubble formation in room temperature [23] it is assumed that the single-stranded melting bubbles are created within milliseconds after introduction into a higher temperature even though the relaxation time for bubble formation scales with N^2 [24] at denaturation conditions. We therefore believe that most of the time for pattern development is due to a slow loosening of YOYO-1 from the DNA molecule. Three physical effects can help stabilize the dsDNA-YOYO complex. Firstly, the strongly positive YOYO-1 molecules hold the two negative charged DNA strands together by electrostatic interactions. Secondly the stacking due to intercalation of the aromatic rings further stabilizes the double stranded state. Thirdly, the stretching and unwinding of the DNA chain by the YOYO-1 molecules lowers the charge density and thereby the repulsion of the two DNA strands from each other [29]. These effects have been shown to increase the melting temperature of DNA [26] and could potentially increase the melting times. On the other hand the YOYO-1 molecules feels an attraction to the negatively charged walls, which should serve to accelerate the loosening of dye molecules from the DNA especially from the melted parts, where dye molecules are responsible for holding the two DNA strands together.

Conclusions

High fluorescence intensity from the molecules of interest is a necessity for single molecule imaging with a high signal to noise ratio. In this work it is shown that the intensity of YOYO-1 stained molecules elongated in nano-grooves decreases in the absence as well as in the presence of illumination. This effect is apparent both at experimental conditions where melting occurs and during conditions where no melting is apparent and was attributed the close proximity of negative walls that attracted the positive dye molecules. Furthermore, the melting pattern along the DNA molecule was shown to develop during a time period around 10 min. The long melting times was explained by the dye's stabilization effects on the double stranded state of the DNA molecule. At higher temperatures these long melting times is a contributing factor to the reduction of the rate of intensity decrease with time in the absence of illumination. These results can be used to achieve a higher correlation to theoretical calculations of the barcode, and thereby more reliable results.

With our findings we increase the reproducibility of melting mapping and thereby bring it one step closer to commercialization. The next step in this work would be to design a way to better control and measure the temperature within the micro- and nano-channels. One way to do this could be to integrate temperature sensors in the fluidic chip and thereby bring the temperature sensors

closer to the nano-channels. Furthermore, it is necessary to improve the way used to determine the number of YOYO molecules bound to the DNA molecule in confinement, since the background fluorescence can cause difficulties during analysis. Future studies would include longer time series, additional temperatures and melting in micro-channels to gain a broader view of the process.

ACKNOWLEDGMENTS This work was supported by the Swedish Research Council (VR) grant nos. 2007-584 and 2007-4454, the EU's seventh Framework Programme (7RP/2007-2013) under grant agreement no. 201418 (READNA), and the Crafoord Foundation grant nos. 2008-0841 and 2005-1123. K.U.M. acknowledges support from the UK Royal Society Theo Murphy Blue Skies Award. VINNOVA (project number P35735-1).

References

[1] J. Shendure, H. Ji, *Nature Biotechnology*, 2008, **26**, 1135–1145.

[2] P. Stankiewicz, J. R. Lupski, *Trends in genetics : TIG*, 2002, **18**, 74–82.

[3] M. Heiskanen, O. Kallioniemi, a. Palotie, *Genetic analysis : biomolecular engineering*, 1996, **12**, 179–84.

[4] D. Bensimon, A. Simon, V. Croquette, A. Bensimon, *Physical review letters*, 1995, **74**.

[5] R. K. Neely, P. Dedecker, J.-i. Hotta, G. Urbanaviciute, S. Klimasauskas, J. Hofkens, *Chemical Science*, 2010, **1**, 453.

[6] T.-F. Chan, C. Ha, A. Phong, D. Cai, E. Wan, L. Leung, P.-Y. Kwok, M. Xiao, *Nucleic acids research*, 2006, **34**, e113.

[7] J. Jing, J. Reed, J. Huang, X. Hu, V. Clarke, J. Edington, D. Housman, T. S. Anantharaman, E. J. Huff, B. Mishra, B. Porter, a. Shenker, E. Wolfson, C. Hiort, R. Kantor, C. Aston, D. C. Schwartz, *Proceedings of the National Academy of Sciences of the United States of America*, 1998, **95**, 8046–51.

[8] M. Xiao, A. Phong, C. Ha, T.-F. Chan, D. Cai, L. Leung, E. Wan, A. L. Kistler, J. L. DeRisi, P. R. Selvin, P.-Y. Kwok, *Nucleic acids research*, 2007, **35**, e16.

[9] B. Teague, M. S. Waterman, S. Goldstein, K. Potamousis, S. Zhou, S. Reslewic, D. Sarkar, A. Valouev, C. Churas, J. M. Kidd, S. Kohn, R. Runnheim, C. Lamers, D. Forrest, M. a. Newton, E. E. Eichler, M. Kent-First, U. Surti, M. Livny, D. C. Schwartz, *Proceedings of the National Academy of Sciences of the United States of America*, 2010, **107**, 10848–53.

[10] E. Y. Chan, N. M. Goncalves, R. A. Haeusler, A. J. Hatch, J. W. Larson, A. M. Maletta, G. R. Yantz, E. D. Carstea, M. Fuchs, G. G. Wong, S. R. Gullans, R. Gilmanshin, *Genome Research*, 2004, **14**, 1137–1146.

[11] A. Granéli, C. C. Yeykal, T. K. Prasad, E. C. Greene, *Langmuir : the ACS journal of surfaces and colloids*, 2006, **22**, 292–9.

[12] R. Marie, J. N. Pedersen, D. L. V. Bauer, K. H. Rasmussen, M. Yusuf, E. Volpi, H. Flyvbjerg, A. Kristensen, K. U. Mir, *Proceedings of the National Academy of Sciences of the United States of America*, 2013, **10**, 4893–4898.

[13] T. T. Perkins, S. R. Quake, D. E. Smith, S. Chu, *Science (New York, N.Y.)*, 1994, **264**, 822–6.

[14] L. K. Nyberg, F. Persson, J. Berg, J. Bergström, E. Fransson, L. Olsson, M. Persson, A. Stå lnacke, J. Wigenius, J. O. Tegenfeldt, F. Westerlund, *Biochemical and biophysical research communications*, 2012, **417**, 404–8.

[15] W. Reisner, N. B. Larsen, A. Silahtaroglu, A. Kristensen, N. Tommerup, J. O. Tegenfeldt, H. Flyvbjerg, *Proceedings of the National Academy of Sciences of the United States of America*, 2010, **107**, 13294–9.

[16] R. Riehn, M. Lu, Y.-M. Wang, S. F. Lim, E. C. Cox, R. H. Austin, *Proceedings of the National Academy of Sciences of the United States of America*, 2005, **102**, 10012–6.

[17] J. O. J. Tegenfeldt, C. Prinz, H. Cao, S. Chou, W. W. W. Reisner, R. Riehn, Y. Y. M. Wang, E. E. C. Cox, J. J. C. Sturm, P. Silberzan, Others, R. H. Austin, *Proceedings of the National Academy of Sciences of the United States of America*, 2004, **101**, 10979.

[18] J. O. Tegenfeldt, C. Prinz, H. Cao, R. L. Huang, R. H. Austin, S. Y. Chou, E. C. Cox, J. C. Sturm, *Analytical and bioanalytical chemistry*, 2004, **378**, 1678–92.

[19] W. Reisner, K. Morton, R. Riehn, Y. Wang, Z. Yu, M. Rosen, J. Sturm, S. Chou, E. Frey, R. Austin, *Physical Review Letters*, 2005, **94**, 196101.

[20] E. Werner, F. Persson, F. Westerlund, J. O. Tegenfeldt, B. Mehlig, *Physical Review E*, 2012, **86**, 041802.

[21] J. T. Mannion, C. H. Reccius, J. D. Cross, H. G. Craighead, *Biophysical journal*, 2006, **90**, 4538–45.

[22] E. T. Lam, A. Hastie, C. Lin, D. Ehrlich, S. K. Das, M. D. Austin, P. Deshpande, H. Cao, N. Nagarajan, M. Xiao, P.-Y. Kwok, *Nature biotechnology*, 2012, **30**, 771–6.

[23] G. Altan-Bonnet, A. Libchaber, O. Krichevsky, *Physical Review Letters*, 2003, **90**, 138101.

[24] K. P. N. Murthy, G. M. Schütz, *EPL (Europhysics Letters)*, 2011, **96**, 68003.

[25] A. Glazer, H. Rye, *Nature*, 1992, **359**, 859–861.

[26] M. T. Bjorndal, D. K. Fygenson, *Biopolymers*, 2002, **65**, 40–4.

[27] K. Günther, M. Mertig, R. Seidel, *Nucleic Acids research*, 2010, **38**, 6526–6532.

[28] C. Carlsson, M. Jonsson, B. Akerman, *Nucleic acids research*, 1995, **23**, 2413–20.

[29] V. A. Bloomfield, D. M. Crothers, J. Ignacio Tinoco, *Nucleic Acids: Structures, Properties, and Functions*, Univ. Science Books, 2000.

[30] E. R. Mardis, *Annual review of genomics and human genetics*, 2008, **9**, 387–402.

[31] J. Lin, *Science*, 1999, **285**, 1558–1562.

[32] R. L. Welch, R. Sladek, K. Dewar, W. W. Reisner, *Lab on a Chip*, 2012, **12**, 3314–3321.

[33] D. Schwartz, X. Li, *Science (New York, ...*, 1993, **262**, 110.

Probing concentration-dependent behavior of DNA-binding proteins on a single molecule level illustrated by repair protein Rad51

*Karolin Frykholm,† Camilla Freitag,† Fredrik Persson,†,‡ Jonas Tegenfeldt,†, § and Annette Granéli *,†*

† Department of Physics, University of Gothenburg, Gothenburg, Sweden

‡ Department of Cell and Molecular Biology, Science for Life Laboratory, Uppsala University, Uppsala, Sweden

§ Division of Solid State Physics, Lund University, Lund, Sweden

KEYWORDS Single molecule, DNA, Rad51, microfluidics, supported lipid bilayer, fluorescence microscopy

ABSTRACT: We have developed a versatile tool for high-throughput analysis of DNA and DNA-binding molecules by combining microfluidics and dense DNA arrays. We use an easy-to-process microfluidic flow-channel system in which dense DNA arrays are prepared for simultaneous imaging of large amounts of DNA molecules, with single molecule resolution. The Y-shaped microfluidic design, where the two inlet channels can be separately and precisely controlled, enables the creation of a concentration gradient across the microfluidic channel, as

well as rapid and repeated addition and removal of substances from the measurement region. A DNA array stained in a gradient manner with YOYO-1 illustrates the method and serves as a proof of concept. We have applied the method to studies of the repair protein Rad51 and could directly probe the concentration dependent DNA-binding behavior of human Rad51 (HsRad51). In the low concentration regime used (100nM HsRad51 and below) we could not detect positive cooperative binding to double-stranded DNA (dsDNA).

INTRODUCTION

Single molecule investigations of biomolecular interactions have received increasing interest during the last decade; the approach offers the possibility to explore heterogeneous and dynamic behavior as well as deciphering new mechanisms and rare events at an unprecedentedly detailed level.[1,2]

The use of single molecule techniques thus puts new constraints on how to handle and manipulate the biomolecules of interest. Many applications require the molecules to be attached to a surface within a reaction chamber and the surface functionalization strategy must be carefully considered, fulfilling two requirements: 1) it must allow attachment of biomolecules in such a way that their function is retained and 2) it must strongly prevent non-specific interactions. One surface functionalization strategy that meets these requirements is the use of supported lipid bilayer (SLB) membranes.[3,4] SLBs are easily prepared on a glass or silica surface from small unilamellar lipid vesicles (SUVs) that, when exposed to the glass surface at a high enough surface concentration, spontaneously fuse and rupture, forming a continuous lipid bilayer. The SLB is fluid and allows lateral diffusion of lipids and the lipid motion can be directed by hydrodynamic forces from a bulk flow above the SLB.[5,6]

Single molecule techniques suffer from a few but important drawbacks; the experimental set-ups generally have a high technical complexity and a low throughput. To increase the throughput a DNA array technology has previously been developed, where DNA molecules are anchored to an SLB via a biotin-neutravidin-biotin coupling, using biotinylated DNA and lipids, allowing dense DNA arrays to be formed.[6] The DNA strands, tethered to the lipids, are dragged within the fluid lipid bilayer using the bulk flow. The lipids that anchor the DNA strands move in the direction of the flow until they encounter a diffusion barrier that they cannot traverse. This results in an array of DNA on the diffusion barrier, a "DNA curtain". Such a dense DNA array allows for simultaneous investigation of a large number of individual DNA molecules, thus increasing experimental throughput, and also offers the possibility of finding rare binding events.

In this study, we are combining the DNA array technology described above with an easy-to-use microfluidic diffusive mixer based on a flow-channel system with a Y-shaped design, which allows for the formation of a remarkably stable concentration gradient across the measurement channel as well as rapid switching between two different flows. A DNA-array stained with the fluorescent DNA-binding dye YOYO-1, applied to the array in a gradient manner, illustrates the method and serves as a proof of concept. Fluorescently labeled human Rad51 protein (HsRad51) bound to arrays of double-stranded DNA (dsDNA) confirms the applicability for studies of DNA-protein interactions.

Rad51 is a key protein in the DNA-repair pathway homologous recombination in eukaryotes.[7-9] It binds to single- or double-stranded DNA (ssDNA or dsDNA), forming a continuous helical filament and thereby elongating the DNA by approximately 50% compared to its normal B-DNA conformation.[10,11] At lower concentrations of Rad51 on DNA, patches of bound protein, so called nucleation sites, can be observed.[12,13] The elongated nucleoprotein filament is considered

to be the functioning assembly for DNA repair and the Rad51-DNA complex has, due to its important role in the mechanism of DNA repair, attracted great interest in single molecule studies.[14-16] Experimental techniques used in these studies include optical trapping and total internal reflection fluorescence (TIRF) microscopy, approaches that require specialized, and expensive, equipment. The microfluidic device presented here facilitates visualization of DNA-bound HsRad51 using a standard epi-fluorescence microscope, thanks to the possibility of rapid and convenient switching between the different flows in the measurement channel.

The here described method combines the investigation of single molecules in real-time with the concentration dependence of biomolecular interactions and offers a powerful tool for monitoring reaction dynamics and heterogeneity as well as the discovery of rare events and threshold behavior, as illustrated by studying the binding behavior of HsRad51 to dsDNA.

EXPERIMENTAL SECTION

Fabrication of microfluidic flow-channel systems. The microfluidic flow-channel system was made of polydimethylsiloxane (PDMS) using replica molding. An aluminum mold for the simultaneous fabrication of ten systems was custom made. The channel height was 200 μm, the widths of the inlet channels and combined channel were 200 μm and 400μm, respectively. Access holes were created by placing needles at the appropriate positions during molding. A PDMS replica was prepared from a mixture of Sylgard® 184 base and curing agent (Dow Corning) at a 10:1 weight ratio, which was allowed to cure at 90 °C for at least 2 hours. The PDMS replica was bonded to a microscope cover slip, 24x60 mm and 0.13-0.19 mm thick (Mentzel Gläser), that had been cleaned in a 2% (v/v) Hellmanex® (Hellma Analytics) solution for 30 minutes followed by thorough rinsing in MilliQ™ water and drying with N_2(g). For the subsequent preparation of DNA arrays in the flow-channels, diffusion barriers were

mechanically etched on the microscope cover glass using a diamond drill bit. The glass slide and the PDMS were place in a plasma cleaner (Harrick Plasma) for 30 seconds prior to bonding, which was accomplished by placing the surfaces in contact. The systems were then stored at room temperature. Prior to use, PTFE tubings (0.25x0.76 mm, inner and outer diameter, Cole Parmer) equipped with syringe connectors were fitted into the access holes in the PDMS.

Lipid vesicle preparation. Lipids, 1,2-dioleoyl-sn-glycero-3-phosphocholine (DOPC) and biotin-phosphatidylethanolamine (biotin-PE) (Avanti Polar Lipids), were stored in chloroform at -20 °C. Lipid vesicles were prepared from pure DOPC lipids or from 0.5% biotin-PE and 99.5% DOPC. The chloroform solution containing the appropriate lipid or lipid mixture was applied to a round bottom flask and the solvent was evaporated under a stream of nitrogen gas. The lipid film was further dried under nitrogen for at least 2 hours before it was resuspended in buffer A (10 mM Tris pH 8.0, 100 mM NaCl) at a concentration of 20 mg ml^{-1}, vortexed, left at 4 °C over night and then vortexed again. If not used directly for extrusion the lipid solutions were stored at -20 °C. The lipids were mixed and diluted with buffer A to obtain a final concentration of 10 mg ml^{-1} lipids and 0.05% biotin-PE before extrusion through a polycarbonate filter with 100 nm pores (Avanti Polar Lipids). The resulting lipid vesicles were stored at 4 °C and used within one week of preparation.

Biotinylation of DNA. A biotinylated oligonucleotide (5'-pAGGTCGCCGCCC-TEG-Biotin, Eurogentec S.A) was annealed to the 12-nucleotide overhang at the right end of the 48502 base pair long bacteriophage λ-DNA (Roche). A 20-fold molar excess of oligonucleotide was mixed with the λ-DNA in T4-DNA ligase buffer (Promega), heated to 80 °C for 10 minutes and then slowly cooled to room temperature (RT). The mixture was briefly (10-15 minutes) cooled on ice before the addition of T4 DNA ligase (Promega) and the reaction was then incubated at RT for at

least 2 hours. After completed reaction, the ligase was inactivated by heating to 70 °C for 10 minutes and excess oligonucleotide was removed by over-night dialysis against TE-buffer (10 mM Tris pH 8.0, 1 mM EDTA).

Surface functionalization and DNA arrays. The flow-cells were initially flushed with buffer A. During the surface functionalization procedure, all buffers and reagents were manually applied to the channel system through the combined (measurement) channel.

A supported lipid bilayer (SLB) was created in the flow-channel by applying lipid vesicles (0.5 mg ml^{-1}) containing 0.05% biotinylated lipids to the channel system in three injections, with 10 minutes between each injection and a total exposure time of at least 1 hour. Excess vesicles were then rinsed away using buffer A and the SLB was incubated for an additional 1 hour. To block potentially uncovered surface patches, buffer B (40 mM Tris pH 7.8, 1 mM DTT, 1 mM MgCl2, 0.2 mg ml^{-1} BSA) was added to the flow-channel and incubated for 30-45 minutes. Neutravidin (12 nM, Invitrogen) suspended in buffer B was then applied to the system and incubated for 30 minutes before rinsing with buffer B. Finally, biotinylated λ-DNA (24 pM) in buffer B was added to the flow-channel and incubated for 30 minutes, after which it was rinsed away with buffer B. In the experiments where HsRad51 was bound to the DNA arrays, the biotinylated λ-DNA was pre-incubated with YOYO-1 (at a staining ratio of 1 dye/100 base pairs) for 2 hours at RT prior to loading into the flow-channel.

Fluorescently labeled proteins. Fluorescent HsRad51 used in this study were labeled with either Alexa Fluor 555 or Atto 488. The fluorophore was attached to the protein at amino acid position 31, using HsRad51 C319S variant. The mutation scheme, protein expression and labeling protocol, as well as characterization of the fluorescently labeled proteins have been described in detail elsewhere.[13,17]

Instrumentation and experimental set-up. Flow into the branching channels of the microfluidic flow-channel system was controlled using two syringe pumps (CMA 400, CMA Microdialysis AB). Images overviewing the switching effect in the microfluidic flow-channel, was obtained on an epi-fluorescence video microscopy system consisting of a Nikon Eclipse TE2000-U inverted microscope with a 10× objective (NA 0.30, Nikon), with a 1.5× additional magnification lens for a total magnification of 15×, coupled to a cooled back-illuminated EMCCD camera (Andor Technology, iXon DV 897 BV) and a 100 W mercury lamp. Deionized water and a 10 μM solution of carboxyfluorescein, respectively, was applied to the microfluidic system through the two branching channels and inlet flows were varied to illustrate the switching effect. Characterization of the gradient width was performed using another microscope set-up, an inverted epi-fluorescence microscope, Leica DMI6000B, equipped with a 20× objective (NA 0.40, HCX PL FLUOTAR, Leica Microsystems), a 14 bit dynamic range EMCCD camera (C9100-12, Hamamatsu Photonics) and a fluorescence light-source, EL 6000 (Leica Microsystems). Either buffer A and a 1-10 μM solution of sodium fluorescein in buffer A, respectively, or buffer B and a 60 nM solution of HsRad51/Atto 488 in buffer B, respectively, was applied to the flow-channel system through the two inlet channels and images of the bulk flow in the combined channel was taken along the length of the channel and at different flow rates. When using protein the surfaces of the microfluidic system was rendered inert by creating an SLB in the channels and blocking with buffer B, as described above.

In experiments with YOYO-1 stained DNA arrays the Leica microscope set-up was used with a 100× oil immersion objective (NA1.3, HCX PL FLUOTAR, Leica Microsystems). The DNA arrays were exposed to a gradient of dye by applying YOYO-1 (Invitrogen) at 5 nM in buffer B (supplemented with 60 mM β-mercaptoethanol to suppress photobleaching and photodamage)

through one of the inlet channels at 20μl min^{-1} and buffer B (with 60 mM β-mercaptoethanol) at equal flow rate through the other. The successive binding of YOYO-1 to the DNA could be observed by following the increase in fluorescence intensity from the stained DNA. After approximately 15-20 minutes of exposure to YOYO-1, the dye flow was turned off and the buffer flow was subsequently increased to maintain a total flow rate of 40 μl min^{-1} in the measurement channel.

Binding of HsRad51 to the DNA arrays was visualized using the Nikon microscopy system, now equipped with a 100× oil immersion objective (NA 1.40, Nikon). HsRad51/Alexa Fluor 555 at 100 nM in buffer B, supplemented with 2 mM ATP, and buffer B with 2 mM ATP, respectively, was applied to the flow-channel system through the two inlet channels at equal flow rate (5 μl min^{-1} each) to create a gradient of protein over the DNA arrays. After 20 minutes of exposure, the protein solution flow was turned off and buffer flow was subsequently increased to 40 μl min^{-1} to ensure an adequate extension of the DNA.

Image analysis. Image analysis, including fluorescence intensity profiles and quantification of DNA extensions, were done using the public domain, Java-based image processing program ImageJ (version 1.46e).[18]

RESULTS AND DISCUSSION

Characterization of the microfluidic flow-channel system. The design of the microfluidic flow-channel system is schematically depicted in Figure 1a. The branching channels and the combined (measurement) channel were 200 μm and 400 μm, respectively, in width, 7 mm and 10 mm, respectively, in length and channel height was 200 μm (determined from the dimensions

of the channel relief in the mold). Fluid dynamics, in general, can be characterized by the dimensionless Reynolds number:

$$Re = UL\rho/\eta,$$

where U is the average flow velocity and L is the characteristic length scale.[19] For a channel with rectangular cross section, L can be estimated using the hydraulic diameter:

$$\frac{4A}{P},$$

where A is the cross-sectional area and P is the wetted perimeter.[20] Reynolds numbers below 2300 indicate laminar flow. The dimensions of the measurement channel in the here presented microfluidic flow-channel system result in a wetted perimeter of 1200 µm in the closed system. The highest flow rate that was used was 40 µl min^{-1}, corresponding to a flow velocity of 8 mm s^{-1} and the characteristic length scale is 0.32 mm. Using the density (ρ) and viscosity (η) of water a Reynolds number of 2.1 is obtained, thus orders of magnitude below the limit for laminar flow behavior and mixing in the microfluidic flow-cell will therefore be caused solely by diffusion.[19]

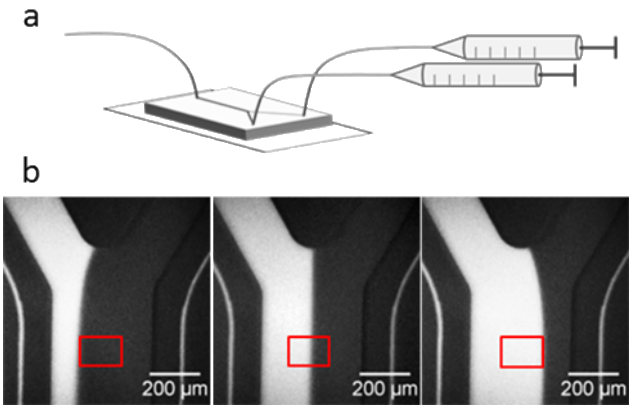

Figure 1. Design of the microfluidic flow-channel system. (a) The inlet channels can be separately and precisely controlled via two syringe pumps. (b) A fluorescein solution, applied to the flow-channel system through one of the inlet channels, illustrates how the Y-shaped design

enables switching between different sample conditions or creates a concentration gradient over the measurement region, indicated in red.

By using this Y-shaped microfluidic channel system two different flows, separately and precisely controlled via two syringe pumps, were introduced into a common flow stream to either create a concentration gradient, due to the diffusive mixing in the combined channel, or allow for easy switching between two different solutions. This is illustrated in Figure 1b, where one of the inlet channels contains a solution of the fluorescent dye fluorescein. A lower flow rate of the dye solution, compared to the buffer flow, results in a measurement region in the center of the combined channel experiencing only buffer conditions (Figure 1b, left), whereas a higher flow rate of dye, compared to buffer, exposes the measurement region to the dye solution (Figure 1b, right). Equal flow rates of the two solutions results in a concentration gradient over the measurement region (Figure 1b, center). Switching between the different measurement conditions can be done on the timescale of tens of seconds or less, depending on the flow rate and limited by the performance of the pumps.

The concentration gradient, caused by the diffusive mixing of the two flows from the inlet channels, was characterized in terms of its width, determined from fluorescence intensity profiles (assuming a linear relationship between fluorescence intensity and concentration of fluorescent dye), at different positions along the measurement channel. Flow rate, distance from the converging point and diffusion coefficient of the substance of interest are factors affecting the concentration profile, $C(x, y)$, of a solute in the diffusive mixing zone as described by the following expression:

$$C(x,y) = \frac{C_0}{2}\left(1 - erf\left(-\frac{y\sqrt{U}}{2\sqrt{Dx}}\right)\right),$$

where x is the downstream distance from the converging point, y is the transverse coordinate, C_0 is the initial concentration of the solute applied into the channel system and D is the diffusion coefficient of the solute.[19] For a given substance higher flow rates will cause a steeper concentration profile and a narrower gradient at a certain distance from the converging point, compared to lower flow rates. At a fixed flow rate, the gradient will be narrower close to the converging point and wider closer to the end of the combined channel.

The fluorescent dye fluorescein was used to illustrate the variations in gradient width at different position in the channel and fluorescence intensity profiles of fluorescein are shown in Figure 2a together with a theoretical calculation of the concentration profiles, using a diffusion coefficient of $6.4 \cdot 10^{-6}$ cm^2 s^{-1} for fluorescein.[21] The experimental data fits well with the theoretical predictions and can be repeated with high reproducibility, indicating a stable concentration gradient system (see Supporting Information). A small discrepancy between the experimental data and the theoretical expression is observed for short downstream distances from the converging point. This deviation can probably be ascribed to the rounded shape of the connection between the two branching channels, locally disturbing the flow profile of the merging flows from the inlets.

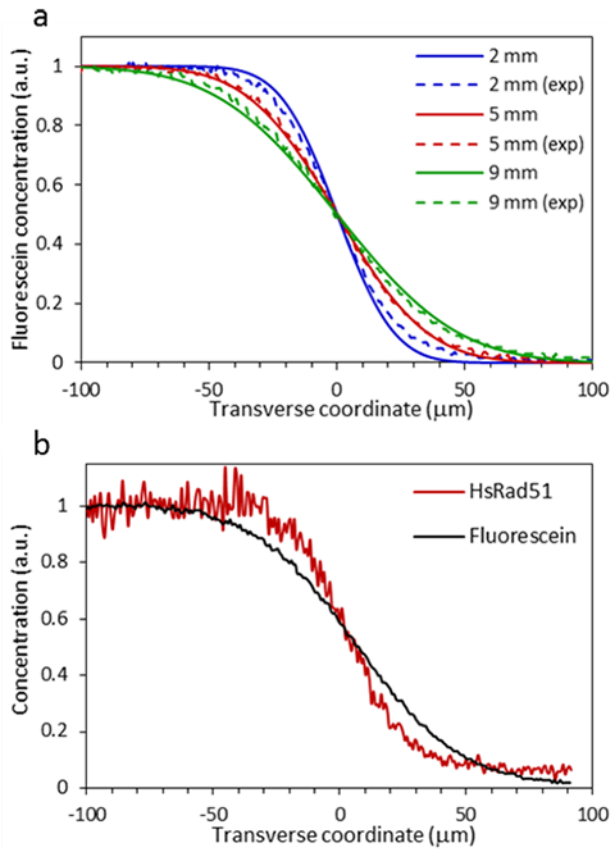

Figur 2. Characterization of the concentration gradient. (a) Theoretical (solid lines) and experimental (dotted lines) concentration profiles of fluorescein at different positions along the measurement channel. Flow rate was 40 µl min^{-1}. (b) A larger molecule (HsRad51) has a steeper concentration profile than a smaller molecule (fluorescein) at a given flow rate (20 µl min^{-1}) and position (5 mm) in the channel. The position is the measured distance from the converging point in the channel.

The concentration profile in the diffusive mixing zone of the microfluidic system was also characterized using fluorescent HsRad51. At a given flow rate, a larger molecule will result in a more narrow gradient than a smaller molecule at the same position in the channel, due to its slower diffusion. In Figure 2b, the effect of molecular size on the concentration gradient is

illustrated using measurements of the bulk fluorescence intensity from fluorescein and fluorescently labeled HsRad51, respectively.

Staining a DNA array with a gradient of YOYO-1. For the preparation of DNA arrays in the microfluidic channel, diffusion barriers were mechanically etched on the microscope cover glass using a diamond drill bit prior to flow-cell assembly. The surface of the flow-cell was functionalized with a SLB containing 0.05 % biotinylated lipids, to which biotinylated λ-DNA was tethered via a biotin-neutravidin-biotin coupling, in a similar way as previously described.[6] Arrays were formed by accumulation of DNA on the diffusion barriers, as DNA migrated within the SLB in the direction of the hydrodynamic force created by the buffer flow in the microfluidic flow-cell. The effect of a concentration gradient over such a DNA array is illustrated using the DNA binding dye YOYO-1 and shown in Figure 3a. YOYO-1 was applied to the flow-cell through one of the inlet channels, at a concentration of 5 nM and a flow rate of 20 μl min^{-1}, and buffer was applied through the other inlet channel at equal flow rate, thus giving rise to a concentration gradient of YOYO-1 in the measurement channel. The flow rate was chosen as it gives rise to a suitable width of the YOYO-1 gradient and an adequate degree of extension of DNA. The DNA array shown in Figure 3a is located approximately 5 mm from the converging point. At this position the width of the YOYO-1 gradient, equals the width of the field of view (80 μm), so that DNA at the both sides of the array are exposed to essentially 100% and 0%, respectively, of the YOYO-1 solution.

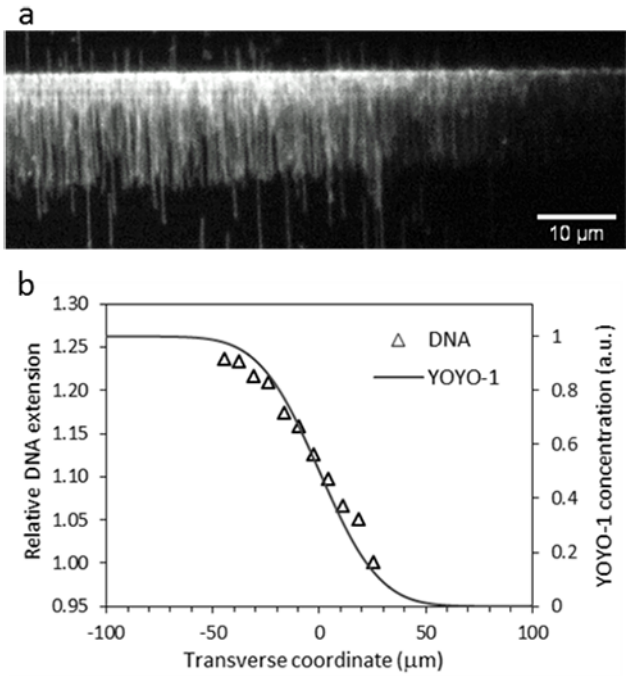

Figure 3. The effect of a concentration gradient over a DNA array. (a) The effect of increasing concentration of YOYO-1, from right to left, can be observed both as an increase in fluorescence intensity and as an elongation of DNA as the YOYO-1:DNA staining ratio increases. (b) The gradual elongation of DNA due to the increasing loading of YOYO-1 along the DNA array correlates well with the modeled intensity profile of the YOYO-1 gradient. DNA lengths were measured on 5 different arrays and ranged from 12.5 to 15.4 µm with a variation of ±0.5 µm.

Two effects of the gradually increasing concentration of YOYO-1 that the DNA array is exposed to can be seen in Figure 3a. Firstly, the fluorescence intensity increases as the staining ratio increases at higher YOYO-1 concentrations. Secondly, the extension of DNA is clearly increased from right to left in the array, with the DNA molecules to the left being more than 20% longer than those to the right. Elongation of DNA at high staining ratios is a well-known effect of the intercalating YOYO-1.[22,23] The successive elongation of the DNA due to the increased binding of YOYO-1 along the array was investigated and correlated to a calculated profile of the

YOYO-1 concentration gradient (Figure 3b). In absence of a determined value of the diffusion coefficient of free YOYO-1 in solution (due to it being non-fluorescent when not bound to DNA) an estimated value was used in the calculation. The two YO-chromophores in YOYO-1 stack in water,[24] giving the molecule (approximating spherical shape) a size similar to that of ethidium bromide, of which the diffusion coefficient has been determined to $4.15 \cdot 10^{-6}$ cm^2 s^1.[25] This value was used when modeling the gradient of YOYO-1 in Figure 3b.

Concentration dependence of HsRad51 binding to dsDNA. The presented method has been developed for the study of DNA-binding proteins and their interactions with DNA and we have used it to directly probe the concentration dependent binding behavior of HsRad51 to dsDNA. In contrast to YOYO-1, that is more or less non-fluorescent when not bound to DNA,[26] the fluorescently labeled protein cause a significant fluorescence signal in the bulk flow, interfering with the fluorescence from DNA-bound protein on the surface of the flow-channel. A requirement to be able to observe the Rad51-DNA complexes using epi-fluorescence microscopy is the possibility, offered by the microfluidic design, to fast and conveniently switch between flows and thereby remove unbound protein. Figure 4a shows an array of dsDNA, pre-stained at a low staining ratio with YOYO-1 (1 YOYO-1:100 base-pairs), exposed to a concentration gradient of HsRad51. A 100 nM solution of HsRad51 labeled with Alexa555 was applied to the flow-cell at 5 μl min^{-1} through one of the inlet channels, while buffer was applied at the same flow rate through the other inlet, creating a protein gradient with a width of ~70μm at a distance 5 mm downstream from the converging point. After 20 minutes of exposure to the protein solution, the protein flow was turned off and buffer flow was increased to 40 μl min^{-1}. Images of the DNA array were immediately taken to avoid protein dissociation. Across the DNA array the

successive assembly of HsRad51 on the DNA can be seen, from individual nucleation sites in the low concentration region (to the right in Figure 4a) to continuous nucleoprotein filaments at higher concentrations. In the high concentration region of the array, where DNA is completely coated with protein, the DNA is elongated compared to the uncoated DNA in the opposite end of the array. The typical extension of bare DNA at this flow rate is 12.5 μm, as seen in the low concentration region of the arrays in both Figures 3a and 4a, whereas the protein-covered DNA at the left side of the array in Figure 4a is extended up to 18 μm. When Rad51 proteins bind to YOYO-1 stained dsDNA the intercalating dye molecules are ejected, explaining why YOYO-1 fluorescence is only observed in the right side of Figure 4a where the protein concentration is low.[27]

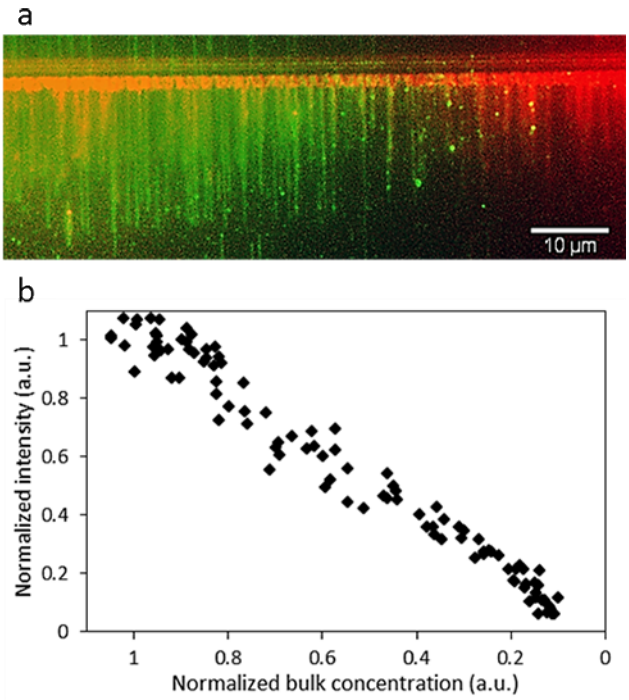

Figure 4. Binding of HsRad51 to a DNA array. (a) An overlay of two images of the same DNA array, where the images colored in red and green visualize DNA-bound YOYO-1 and fluorescently labeled HsRad51, respectively. (b) The normalized emission intensity from

HsRad51 across the DNA array, which corresponds to the concentration of DNA-bound protein, shows a nearly linear dependence on the normalized bulk concentration of HsRad51 (in a gradient from 0 to 100 nM). Intensity profiles over 4 different DNA arrays were analyzed and averaged, variation in pixel intensity between the individual arrays was in general less than 15%.

It has been suggested that binding of HsRad51 to dsDNA involves a rate-limiting step of nucleation followed by positive cooperative binding of HsRad51 to the nucleation site.[28] Using our method, we can directly probe the binding behavior of HsRad51 to dsDNA by correlating the intensity of the dsDNA-bound Rad51 to the bulk concentration (measured as the intensity of HsRad51 in the bulk across the concentration gradient). The emission intensity from the fluorescently labeled HsRad51bound to DNA was analyzed, in a 25 μm high image frame and pixel by pixel across the DNA array to obtain an intensity profile across the protein gradient. An intensity profile over the background emission, that can be seen in Figure 4a and that is arising from a small amount of protein binding non-specifically to the surface, was obtained by analyzing a 0.16 μm high image frame just below or above the DNA array. The background intensity profile was subtracted from the intensity profile obtained over the DNA array and the resulting intensity profiles from four different DNA arrays were averaged. The emission intensity corresponds directly to the concentration of DNA-bound protein and thus the intensity profile reflects the nucleoprotein assembly. Quenching of the labeling dye is not likely to occur since HsRad51 resides as multimeric rings off DNA and the protein is thus not crowded to a higher extend on DNA than off DNA.[29,30] Normalized emission intensity as a function of bulk concentration of HsRad51 is presented in Figure 4b. The intensity of DNA-bound HsRad51 shows a nearly linear correlation with the HsRad51 concentration in bulk, indicating that the protein assembly on DNA occurs without cooperativity.

If the binding of HsRad51 to dsDNA would be cooperative, the data in Figure 4b would be exponential or sigmoidal depending on the grade of saturation.[31] Since the data in Figure 4b shows a linear correlation it rather indicates that the binding is non-cooperative under the conditions and the concentration regime investigated. However, we cannot exclude that HsRad51 binds in a cooperative way to dsDNA under different conditions, or to ssDNA, which will be the target for future investigations using our experimental platform.

CONCLUSIONS

In the experimental set-up presented here we make use of microfluidics and DNA array technology. The DNA arrays shown in Figures 2a and 4a, stained with YOYO-1 and HsRad51, respectively, in a gradient fashion, clearly illustrates the additional gain from our combinational approach. With the DNA arrays comes the advantageous possibility of simultaneously observing a large number of individual DNA molecules, their dynamics over time and/or their interactions with a ligand in the surrounding buffer. The microfluidic design facilitates studies of DNA-ligand interactions at a range of concentrations in one field of view, which is important in screening experiments but also enables the discovery of threshold effects. Moreover, the Y-shaped microfluidic design facilitates easy addition and withdrawal of substances of interest to the DNA array, something that is impossible using traditional test-tube biochemistry. The microfluidic device is easy to fabricate, with no need of cleanroom lithography; it is convenient to use and shows a remarkable robustness in its performance. In combination with the DNA array technology it constitutes a sophisticated, but yet simple, tool for single molecule studies of DNA-protein interactions and dynamics, allowing time as well as concentration trajectories to be followed in one single measurement.

ASSOCIATED CONTENT

Supporting Information. Figure S1, illustrating the reproducibility of the concentration profile in the flow-channel system.

AUTHOR INFORMATION

Corresponding Author

* E-mail: Annette.Graneli@physics.gu.se

ACKNOWLEDGMENT

We are grateful to Prof. Mauro Modesti for providing the fluorescent HsRad51. Parts of this work have been performed at the bioimaging and PDMS facilities at Gothenburg University. The Swedish Foundation for Strategic Research (grant number I06-0240), the Olle Engkvist foundation, the Carl Trygger Foundation and the Swedish Research Council (VR) (grant numbers 2007-584 and 2007-4454) are acknowledged for financial supports.

REFERENCES

(1) Gorman, J.; Greene, E. C. *Nature Structural & Molecular Biology* **2008**, *15*, 768.
(2) Larson, M. H.; Landick, R.; Block, S. M. *Molecular Cell* **2011**, *41*, 249.
(3) Glasmastar, K.; Larsson, C.; Hook, F.; Kasemo, B. *J Colloid Interf Sci* **2002**, *246*, 40.
(4) Larsson, C.; Rodahl, M.; Hook, F. *Anal Chem* **2003**, *75*, 5080.
(5) Jonsson, P.; Beech, J. P.; Tegenfeldt, J. O.; Hook, F. *J Am Chem Soc* **2009**, *131*, 5294.
(6) Graneli, A.; Yeykal, C. C.; Prasad, T. K.; Greene, E. C. *Langmuir* **2006**, *22*, 292.
(7) Baumann, P.; West, S. C. *Trends in Biochemical Sciences* **1998**, *23*, 247.
(8) Bianco, P. R.; Tracy, R. B.; Kowalczykowski, S. C. *Front Biosci* **1998**, *3*.
(9) San Filippo, J.; Sung, P.; Klein, H. *Annu Rev Biochem* **2008**, *77*, 229.
(10) Ogawa, T.; Yu, X.; Shinohara, A.; Egelman, E. H. *Science* **1993**, *259*, 1896.
(11) Stasiak, A.; Di Capua, E.; Koller, T. *J Mol Biol* **1981**, *151*, 557.

(12) Hilario, J.; Amitani, I.; Baskin, R. J.; Kowalczykowski, S. C. *Proceedings of the National Academy of Sciences of the United States of America* **2009**, *106*, 361.
(13) Modesti, M.; Ristic, D.; van der Heijden, T.; Dekker, C.; van Mameren, J.; Peterman, E. J. G.; Wuite, G. J. L.; Kanaar, R.; Wyman, C. *Structure* **2007**, *15*, 599.
(14) Candelli, A.; Wuite, G. J. L.; Peterman, E. J. G. *Phys Chem Chem Phys* **2011**, *13*, 7263.
(15) Finkelstein, I. J.; Greene, E. C. *Mol Biosyst* **2008**, *4*, 1094.
(16) Forget, A. L.; Kowalczykowski, S. C. *Trends Cell Biol* **2010**, *20*, 269.
(17) Modesti, M. *Methods Mol Biol* **2011**, *783*, 101.
(18) Rasband, W. S.; U. S. National Institutes of Health: Bethesda, Maryland, USA, 1997-2012.
(19) Tabeling, P. *Introduction to microfluidics*; Oxford University Press: Oxford, U.K. ; New York, 2005.
(20) Eriksson, E.; Enger, J.; Nordlander, B.; Erjavec, N.; Ramser, K.; Goksor, M.; Hohmann, S.; Nystrom, T.; Hanstorp, D. *Lab Chip* **2007**, *7*, 71.
(21) Galambos, P.; Forster, F. K. In *Micro Total Analysis Systems '98, Proceedings from the MTAS 1998 Workshop*; Harrison, D. J., Van Den Berg, A., Eds.; Kluwer Academic Publishers: Banff, Canada, 1998, p 189.
(22) Gunther, K.; Mertig, M.; Seidel, R. *Nucleic Acids Research* **2010**, *38*, 6526.
(23) Sischka, A.; Toensing, K.; Eckel, R.; Wilking, S. D.; Sewald, N.; Ros, R.; Anselmetti, D. *Biophysical Journal* **2005**, *88*, 404.
(24) Carlsson, C.; Larsson, A.; Jonsson, M.; Albinsson, B.; Norden, B. *Journal of Physical Chemistry* **1994**, *98*, 10313.
(25) Gmeiner, W. H.; Hudalla, C. J.; Soto, A. M.; Marky, L. *FEBS Lett* **2000**, *465*, 148.
(26) Rye, H. S.; Yue, S.; Wemmer, D. E.; Quesada, M. A.; Haugland, R. P.; Mathies, R. A.; Glazer, A. N. *Nucleic Acids Research* **1992**, *20*, 2803.
(27) Zaitseva, E. M.; Zaitsev, E. N.; Kowalczykowski, S. C. *Journal of Biological Chemistry* **1999**, *274*, 2907.
(28) van der Heijden, T.; Seidel, R.; Modesti, M.; Kanaar, R.; Wyman, C.; Dekker, C. *Nucleic Acids Res* **2007**, *35*, 5646.
(29) Shin, D. S.; Pellegrini, L.; Daniels, D. S.; Yelent, B.; Craig, L.; Bates, D.; Yu, D. S.; Shivji, M. K.; Hitomi, C.; Arvai, A. S.; Volkmann, N.; Tsuruta, H.; Blundell, T. L.; Venkitaraman, A. R.; Tainer, J. A. *Embo J* **2003**, *22*, 4566.
(30) Yang, S. X.; Yu, X.; Seitz, E. M.; Kowalczykowski, S. C.; Egelman, E. H. *Journal of Molecular Biology* **2001**, *314*, 1077.
(31) De Zutter, J. K.; Knight, K. L. *J Mol Biol* **1999**, *293*, 769.

Supporting Information

Probing concentration-dependent behavior of DNA-binding proteins on a single molecule level illustrated by repair protein Rad51

Karolin Frykholm,[†] Camilla Freitag,[†] Fredrik Persson,[†,‡] Jonas Tegenfeldt,[†, §] and Annette Granéli [,†]*

[†] Department of Physics, University of Gothenburg, Gothenburg, Sweden

[‡] Department of Cell and Molecular Biology, Science for Life Laboratory, Uppsala University, Uppsala, Sweden

[§] Division of Solid State Physics, Lund University, Lund, Sweden

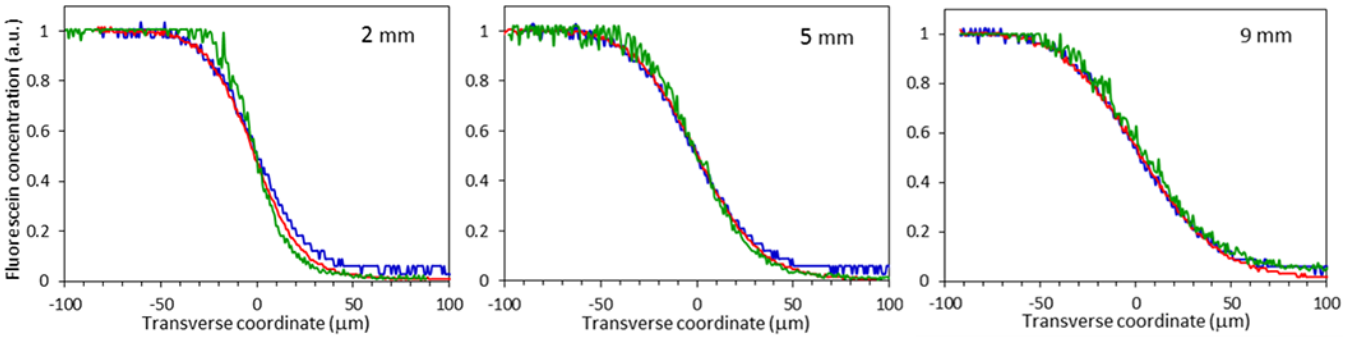

Figure S5. Typical concentration profiles, from fluorescence intensity data, for fluorescein in the measurement channel. Profiles at different downstream distances from the converging point in three individual microfluidic systems are shown. Flow rate was 40 ml min^{-1}. The variation between individual flow cells is small, indicating that fabrication of the microfluidic systems is a stable procedure.